Quantum Optical Control of Donor-bound Electron Spins in GaAs

Maksym Sladkov

University of Groningen
Zernike Institute
for Advanced Materials

Zernike Institute PhD thesis series 2011-09
ISSN: 1570-1530
ISBN: 978-90-367-4791-2 (PRINTED VERSION)
ISBN: 978-90-367-4790-5 (ELECTRONIC VERSION)

The work described in this thesis was performed in the research group Physics of Nanodevices of the Zernike Institute of Advanced Materials at the University of Groningen, the Netherlands. This work was supported by a Vidi grant by the Netherlands Organization for Scientific Research (NWO)

Printed by: Gildeprint Drukkerijen, Enschede, The Netherlands

Cover design: Kateryna Naumova, http://naumova.net

RIJKSUNIVERSITEIT GRONINGEN

Quantum Optical Control of Donor-bound Electron Spins in GaAs

Proefschrift

ter verkrijging van het doctoraat in de
Wiskunde en Natuurwetenschappen
aan de Rijksuniversiteit Groningen
op gezag van de
Rector Magnificus, dr. F. Zwarts,
in het openbaar te verdedigen op
vrijdag 11 februari 2011
om 11:00 uur

door

Maksym Sladkov

geboren op 10 september 1982
te Uzhgorod, Oekraïne

Promotor:	Prof. dr. ir. C. H. van der Wal
Beoordelingscommissie:	Prof. dr. M. Bayer Prof. dr. ir. L. M. K. Vandersypen Prof. dr. ir. P. H. M van Loosdrecht

Contents

Chapter 1

Introduction

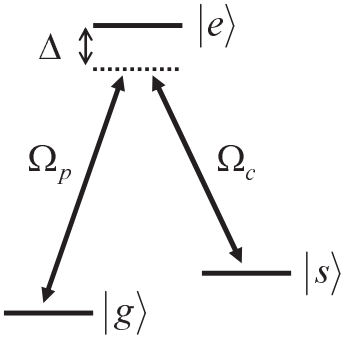

Figure 1.1: The 3-level Λ system. The two ground states $|g\rangle$ and $|s\rangle$ are optically coupled to the common excited state $|e\rangle$.

1.1 Quantum information science

Quantum information science (QIS) incorporates quantum principles into information processing and communication. The main driving force behind QIS are the ideas that quantum cryptography could enable secure communication through public channels [1], and quantum computing would efficiently solve certain computational problems that are believed to be intractable by conventional computing [2].

In the quantum information processing a bit of information is represented as a qubit, and the processing is realized by unitary quantum gates. The qubit is a single-particle state in a two-dimensional Hilbert space and can take a value of a $|0\rangle$ or a $|1\rangle$ and linear superpositions thereof. If the particle is a single photon, then the qubit can be encoded in several ways. For example, in polarization encoding, the logical zero state $|0\rangle$ can correspond to a single photon being left-circularly polarized and $|1\rangle$ to right-circularly polarized. In the case of the electron spin the $|0\rangle$ state could correspond to the spin $|\uparrow\rangle$ and the $|1\rangle$ state could be represented by the $|\downarrow\rangle$ spin.

Owing to the quantum mechanical properties of the qubit (e.g. electron spin states or optical photon states) the general qubit state can be expressed as a superposition of $|0\rangle$ and $|1\rangle$, and the general states of quantum information are superpositions of qubits.

1.2 Quantum memory

For quantum memory applications one needs to store the information carried by a qubit and to release it on demand. Photon states are often the preferred qubits for secure quantum communication because photons travel with the speed of light (and these are often referred to as the flying qubits), and because photons typically interact very weakly with the environment. In order to further utilize the information stored in quantum states of the photons, these states have to be stored in a quantum memory, where they can be processed and released afterwards as a new (or even the same) photonic quantum state. This sets two important criteria for a medium that is applicable for quantum memory.

First, quantum memory media need to have a long coherence time, as the states need to be stored long enough to perform the processing tasks at hand such as quantum gate operations.

Second, the media that are most suitable for quantum memory applications need to provide strong interactions with photons, for instance, a medium with high optical density or a medium inside a high finesse optical cavity. This criterion is needed if one needs to store the photon states effectively. The use of optical cavities is technically very demanding [3–5] therefore the search for optically dense media with good quantum coherence is of importance for developing successful QIS applications.

1.3 Electromagnetically Induced Transparency

One of the ways to incorporate quantum memory performance is to use a system where the phenomena related to Electromagnetically Induced Transparency (EIT) are possible [6]. EIT is a nonlinear optical effect that is observed in atoms with an energy-level structure resembling the letter Λ (Fig. 1.1). Two optical fields couple the excited level $|e\rangle$ to the respective ground state levels $|g\rangle$ and $|s\rangle$: the weak signal field Ω_p which may carry the quantum information and the strong control field Ω_c which is used to steer the atomic system. If the control field is absent, the signal field, which interacts with the resonant two-level system, undergoes partial or complete absorption as represented by the dashed line in the Fig.1.2(a). In the presence of the control field, the absorption of the signal is greatly reduced whenever the frequency difference of the two optical fields is close to the energy splitting between the $|g\rangle$ and $|s\rangle$ states, providing the condition that is known as *two-photon Raman resonance* (solid line in Fig.1.2(a)).

The transparency is observed when the fields are detuned from the two-photon

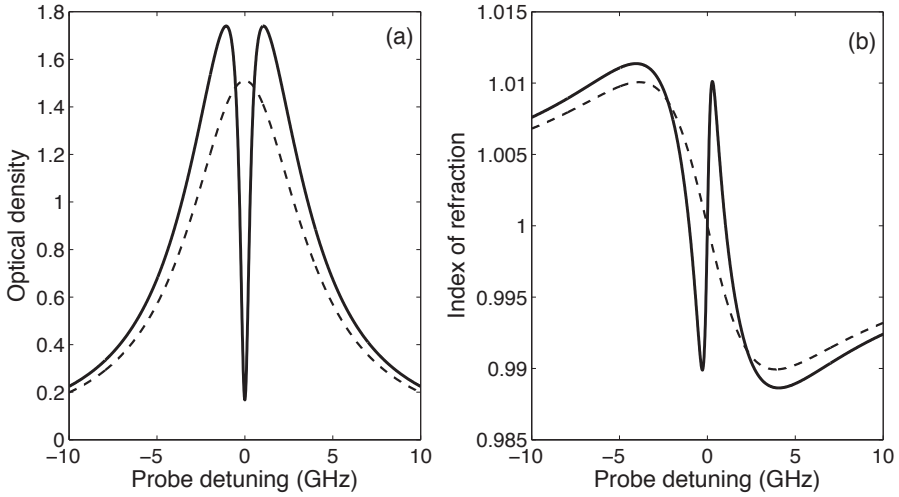

Figure 1.2: Example of optical spectra for a 10 μm long n-GaAs system with donor concentration $n_D = 10^{14}\text{cm}^{-3}$ and other parameters as in Chapter 6. (a) Optical density in the absence of the control field (dashed line) and with control field on (solid line). (b) Refractive index of the system with control field off (dashed line) and on (solid line).

resonance by no more than [6]:

$$\Delta_{EIT} \sim \frac{4}{\sqrt{\alpha L}} \frac{\Omega_c^2}{\gamma_{inh}} \tag{1.1}$$

where α is the absorbtion coefficient of the medium, L is the length of the medium, Ω_c is the Rabi frequency of the control field, and γ_{inh} is the inhomogeneous broadening of the optical transitions. The width of the EIT window is thus proportional to the intensity of the control field and can be much narrower than γ_{inh}. EIT is largely insensitive to the detuning Δ of the optical fields from their respective individual transitions. It can thus exist in the presence of inhomogeneous broadening for the optical transitions, as long as both optical transitions experience the same frequency shift.

Electromagnetically induced transparency was first observed in a vapor of Sr^+ ions [7]. Later work includes extensive studies with ensembles of alkali atoms [6], and work with a single atom in an optical cavity [3]. Observations of EIT (and the related effect of Coherent Population Trapping (CPT)) with solid state systems include an experiment with a single hole spin in GaAs quantum dot [8], rare-earth

doped crystals [9, 10] and the observation of CPT with donor-bound electron spins in GaAs [11], electron spins in GaAs quantum dots [12], and NV-centers in diamond [13].

1.4 EIT in an optically dense solid state medium

The quest for observing EIT in an optically dense solid state medium is mainly driven by the use of EIT media as a quantum memory. This is based on the fact that according to the Kramers-Kronig relations, an anomaly in the absorption spectrum always comes together with an anomaly in dispersion. A light field propagating under EIT conditions experiences a large positive dispersion (Fig. 1.2(b)), which implies a reduction of the group velocity by a factor of $n_g \sim \alpha c \gamma_{inh}/4\Omega_c^2$ with respect to the velocity of light in vacuum c [6]. The group velocity can in theory be arbitrarily reduced by lowering the intensity of the control field. Experimentally, a slowdown of the velocity of the photons by up to seven orders of magnitude has been demonstrated [14].

The effect of slow light provides a basis for the quantum memory application, which functions as follows [15, 16]: a light pulse, resonant with the EIT window, enters the EIT medium and slows down. The slowdown entails spatial compression, so the pulse, whose initial spatial extent by far exceeds L, will fit inside the medium. Once it is inside, we adiabatically reduce the control field intensity and bring the group velocity down to zero, thereby "collapsing" the EIT window and storing the pulse in the medium. When the pulse needs to be retrieved, the control field is turned back on. The pulse then resumes its propagation and leaves the EIT medium. The experimental demonstration of light storage using such an example of dynamical EIT includes storage of light in an atomic vapor [17] and in magnetically trapped sodium atoms [18].

Another application of EIT media builds on the ability to prepare quantum entanglement between an optical signal pulse and a quantum state of the medium. Work in this direction was strongly stimulated by the famous DLCZ proposal, which is a scalable scheme for long-distance quantum communication [19]. An elementary step of the DLCZ procedure consists of creating a stored collective excitation in an ensemble of Λ-type atoms. All the atoms are initially in the ground state (for the ensemble denoted as the state $|0_{atom}\rangle$). They are illuminated with a weak off-resonant optical control pulse (called the write pulse), resulting in a finite probability for Raman transfer of population from $|g\rangle$ into the metastable state $|s\rangle$ (Fig. 1.1). This is operated in the limit of very weak Raman scattering (less than one Raman photon on average). An event of this type is associated with scattering (emission) of a very weak optical Raman pulse, which is then a superposition

of the states with 0 and 1 photon, $|0_{pulse}\rangle$ and $|1_{pulse}\rangle$, and can be detected by a single photon counter. Upon the detection of a scattered photon, the quantum state of the matter system is projected onto a collective excitation with for the ensemble a total population of 1 in the state $|s\rangle$ (for the ensemble denoted as the state $|1_{atom}\rangle$). The initial emission of the optical pulse entangles the state of the optical pulse with the state of the matter system, resulting in the combined state: $|\Psi_{comb}\rangle = c_0|0_{atom}\rangle|0_{pulse}\rangle + c_1|1_{atom}\rangle|1_{pulse}\rangle$.
The use of an optically dense medium for such entanglement generation is beneficial since it will facilitate forward scattering of the Raman pulse owing to collective enhancement (gain for emission in the forward direction) [19].

The read-out of the quantum state of such collective excitations can be performed by driving the atomic ensemble with a classical field, resonant with the $|s\rangle - |e\rangle$ optical transition. This measurement will project the matter system back into the $|0_{atom}\rangle$ state, while detecting 0 or 1 Raman photon from the $|e\rangle - |g\rangle$. This effectively detects whether the ensemble was in the state $|0_{atom}\rangle$ or $|1_{atom}\rangle$, respectively. It is interesting to note, that the effect of electromagnetically induced transparency is essentially a simultaneous generation and readout of the DLCZ entangled state, since in the end it recovers an initially absorbed photon and thereby leads to an optically transparent medium.

The DLCZ scheme, which relies on a high probability for the absorption or emission of a single photon, and the slow-light based quantum-memory scheme both require an optically dense medium for efficient QIS application. We therefore focus on an experimental study of an ensemble of electron spins, that are bound at neutral donor sites in bulk GaAs. The density of the donors is such that the electronic orbits of neighboring donors do not overlap (thereby resulting in an ensemble of noninteracting electron spins). We demonstrate that the electron spin dephasing time is as long as $T_2^* = 2$ ns. This system was previously shown to be suitable for Coherent Population Trapping [11] with optical control fields. In this thesis we focus on the experimental realization and study of Electromagnetically Induced Transparency with this material system.

1.5 Outline of this thesis

In Chapter 2 of this thesis we give an in-depth overview of how electron spin ensembles in semiconductors can be used for entanglement generation through the DLCZ scheme. Chapter 3 presents the electronic structure and optical properties of the material system that is central in this work: the donor-bound electron spin in low-doped n-GaAs, and its excitations. This is our system of choice for the experimental study of EIT in a semiconductor. In Chapter 4 we introduce the theoretical

framework for treating the EIT phenomenon. This relies on solving the equation of motion for a density matrix operator under strong electromagnetic driving. Chapter 5 is devoted to the description of the experimental setup, which is essentially a cryogenic fiber-based confocal microscope that allows careful control of the light polarizations, even in the presence of a strong magnetic field. In Chapter 6 an experiment that demonstrates and studies EIT with donor-bound electron spins in GaAs is presented. Finally, Chapter 7 is devoted to an experiment that aims at coherent optical control of the quantum state of the electron spin ensembles with strong ultra-fast optical pulses. We have intentionally chosen to let the contents of some chapters to overlap in order to make it readable without the need to reference to the different parts of the thesis. This mainly concerns the optical spectroscopy data that are used for identification of the optical resonances and polarization selection rules associated with them.

References

[1] N. Gisin, G. Ribordy, W. Tittel, and H. Zbinden, *Quantum cryptography*, Reviews of Modern Physics **74**, 145 (2002), ISSN 0034-6861.

[2] N. D. Mermin, *Quantum Computer Science* (Cambridge University Press, 2007).

[3] M. Mücke, E. Figueroa, J. Bochmann, C. Hahn, K. Murr, S. Ritter, C. J. Villas-Boas, and G. Rempe, *Electromagnetically induced transparency with single atoms in a cavity.*, Nature **465**, 755 (2010), ISSN 1476-4687.

[4] J. McKeever, A. Boca, A. D. Boozer, R. Miller, J. R. Buck, A. Kuzmich, and H. J. Kimble, *Deterministic generation of single photons from one atom trapped in a cavity.*, Science (New York, N.Y.) **303**, 1992 (2004), ISSN 1095-9203.

[5] K. Hennessy, A. Badolato, M. Winger, D. Gerace, M. Atatüre, S. Gulde, S. Fält, E. L. Hu, and A. Imamoglu, *Quantum nature of a strongly coupled single quantum dot-cavity system.*, Nature **445**, 896 (2007), ISSN 1476-4687.

[6] M. Fleischhauer, A. Imamoglu, and J. Marangos, *Electromagnetically induced transparency: Optics in coherent media*, Reviews of Modern Physics **77**, 633 (2005), ISSN 0034-6861.

[7] K. J. Boller, A. Imamoglu, and S. E. Harris, *Observation of electromagnetically induced transparency*, Phys. Rev. Lett **66**, 2593 (1991).

[8] D. Brunner, B. D. Gerardot, P. A. Dalgarno, G. Wüst, K. Karrai, N. G. Stoltz, P. M. Petroff, and R. J. Warburton, *A coherent single-hole spin in a semiconductor.*, Science (New York, N.Y.) **325**, 70 (2009), ISSN 1095-9203.

[9] J. J. Longdell, E. Fraval, M. J. Sellars, and N. B. Manson, *Stopped Light with Storage Times Greater than One Second Using Electromagnetically Induced Transparency in a Solid*, Physical Review Letters **95**, 063601 (2005), ISSN 0031-9007.

[10] M. P. Hedges, J. J. Longdell, Y. Li, and M. J. Sellars, *Efficient quantum memory for light*, Nature **465**, 1052 (2010), ISSN 0028-0836.

[11] K.-M. Fu, C. Santori, C. Stanley, M. Holland, and Y. Yamamoto, *Coherent Population Trapping of Electron Spins in a High-Purity n-Type GaAs Semiconductor*, Physical Review Letters **95**, 187405 (2005), ISSN 0031-9007.

[12] X. Xu, Y. Wu, B. Sun, Q. Huang, J. Cheng, D. G. Steel, A. S. Bracker, D. Gammon, C. Emary, and L. J. Sham, *Fast Spin State Initialization in a Singly Charged InAs-GaAs Quantum Dot by Optical Cooling*, Physical Review Letters **99**, 97401 (2007), ISSN 0031-9007.

[13] C. Santori, P. Tamarat, P. Neumann, J. Wrachtrup, D. Fattal, R. Beausoleil, J. Rabeau, P. Olivero, A. Greentree, S. Prawer, et al., *Coherent Population Trapping of Single Spins in Diamond under Optical Excitation*, Physical Review Letters **97**, 247401 (2006), ISSN 0031-9007.

[14] L. Hau, S. Harris, Z. Dutton, and C. Behroozi, *Light speed reduction to 17 metres per second in an ultracold atomic gas*, Nature **397**, 594 (1999).

[15] A. Gorshkov, A. André, M. Fleischhauer, A. Sø rensen, and M. Lukin, *Universal Approach to Optimal Photon Storage in Atomic Media*, Physical Review Letters **98**, 123601 (2007), ISSN 0031-9007.

[16] A. Lvovsky, B. Sanders, and W. Tittel, *Optical quantum memory*, Nature Photonics **3**, 706 (2009).

[17] D. Phillips, A. Fleischhauer, A. Mair, R. Walsworth, and M. Lukin, *Storage of Light in Atomic Vapor*, Physical Review Letters **86**, 783 (2001), ISSN 0031-9007.

[18] C. Liu, Z. Dutton, C. H. Behroozi, and L. V. Hau, *Observation of coherent optical information storage in an atomic medium using halted light pulses.*, Nature **409**, 490 (2001), ISSN 0028-0836.

[19] L. M. Duan, M. D. Lukin, J. I. Cirac, and P. Zoller, *Long-distance quantum communication with atomic ensembles and linear optics.*, Nature **414**, 413 (2001), ISSN 0028-0836.

Chapter 2

Towards quantum optics and entanglement with electron spin ensembles in semiconductors

We review a technique that enables the controlled realization of quantum entanglement between collective excitations in electron spin ensembles in two spatially separated pieces of semiconductor material. The discussion assumes electron spin ensembles bound to neutral donors in GaAs, that are located inside optical waveguides. This material system has optical transitions that obey well-defined selection rules, which allows for selectively addressing the two electron spin states. Long-lived superpositions of these electron spin states can then be controlled with a pair of optical fields that form a resonant Raman system. Entangled states of collective spin excitations are prepared by applying quantum-optical measurement techniques to optical signal pulses that result from Raman transitions in the electron ensembles.

2.1 Introduction

Entanglement is the phenomenon that the quantum states of two (or more) degrees of freedom are inseparable, and is arguably the most distinct aspect of quantum theory [1]. It results in non-classical correlations between observable physical properties of the two subsystems. For *nonlocal entanglement* this concerns two degrees of freedom that are spatially separated over a large distance. The occurrence of such correlations has been thoroughly tested in several experiments, and the results leave little doubt that quantum theory provides the valid predictions. Experimental realizations were, until now, carried out with pairs of elementary particles or photons [2, 3], or with spins in very simple quantum systems as for example trapped ions [4] or alkali atoms [5, 6]. It is nevertheless interesting to continue research on the controlled realization of nonlocal entanglement with other material systems, in particular with degrees of freedom in solid state.

In part this interest is fundamental. Whether entangled states loose their coherence in a different manner than superposition states of individual degrees of freedom is still not fully understood [7, 8]. Recent developments here include an all-optical experiment that showed that entanglement can be lost much more rapidly than the loss of coherence in the two subsystems [9]. Another interesting result from work with entangled photon pairs showed that the relation between the amount of entanglement and the degree of mixedness of a two-particle state can only be represented by a plane of possibilities. Specific points in this plane depend on the nature of the environment that is decohering the initial maximally-entangled pure state [10, 11]. Furthermore, it is still not firmly established that quantum theory does not break down when applied to collective or macroscopic degrees of freedom [12, 13]. This justifies a study of how entangled states can be realized in solid state, and how these states loose their coherence: solid state can provide model systems with complex (collective) degrees of freedom, or systems with elementary degrees of freedom in a complex environment.

Research on the controlled realization of entanglement in solid state systems is also driven by the prospect that it may provide tools for quantum information technologies. Relevant to the discussion here is a proposal for long-distance quantum communication [14], that was until now mainly explored with ensembles of alkali atoms [5, 6], or alkali-atom-like impurities in solids [15–17]. However, widespread implementation favors a technique that can be implemented in micron-scale devices that fit inside optical fibers, which are compatible with high-speed optoelectronic operation[18]. Here, the electronic and optical properties of III-V semiconductors outperform the atomic or impurity-based systems. The coherence times of degrees of freedom in these materials, however, tend to be too short for

any realization of quantum information technology in the near future, but are long enough for initial experimental studies on entangled states.

We discuss here a technique that enables the controlled realization of nonlocal entanglement between collective spin excitations in ensembles of electrons bound to the neutral donors, which are located in two spatially separated pieces of GaAs semiconductor material. In Section 2.2 we review an approach where quantum-optical measurement techniques are used for preparing entangled states of spin degrees of freedom in ensembles of three-level quantum systems. Details on the GaAs material system that is suited for isolating and operating such three-level quantum systems are presented in Chapter 3.

2.2 Preparing and detecting entangled states via quantum optical measurement

We propose here to use the so-called DLCZ scheme [14] for preparing nonlocal entanglement with solid state devices. The main idea behind this approach is that spontaneous emission of a quantum optical pulse results in quantum correlations (entanglement) between the state of the optical pulse and the state of the system that emits. To illustrate this, consider a two-level system that is initially in its excited state $|s\rangle$. It is emitting a single photon while relaxing to its ground state $|g\rangle$. If we would be able to have control over this process such that it relaxes to a superposition of the states $|s\rangle$ and $|g\rangle$, the system would emit an optical pulse that is a superposition of the states with 0 and 1 photon, $|0_{pulse}\rangle$ and $|1_{pulse}\rangle$. The quantum state of the system and the optical pulse are then in fact entangled, and the only pure states that can describe the state of the combined system are of the form $|\Psi_{com}\rangle = c_0 |s\rangle|0_{pulse}\rangle + c_1 |g\rangle|1_{pulse}\rangle$.

Such control over spontaneous emission can be realized with a three-level Raman system (Fig. 2.1a). The states $|g\rangle$ and $|s\rangle$ are here typically the states of a spin, which both have an optical transition to a state $|e\rangle$. When this system is initially in the state $|g\rangle$, there will be only spontaneous emission of a Raman photon from the transition $|e\rangle - |s\rangle$ while a control field is driving the $|g\rangle - |e\rangle$ transition. Figure 2.1b illustrates how an extension of this scheme can be used to entangle the states of two three-level systems that are at different locations. Say Alice and Bob both have an identical version of such a three-level system prepared in the state $|g\rangle$. They both use a classical field to drive the $|g\rangle - |e\rangle$ transition, in order to get very weak spontaneous emission from the $|e\rangle - |s\rangle$ transition, such that each system emits an optical pulse that is a superposition of the photon-number states $|0_{pulse}\rangle$ and $|1_{pulse}\rangle$ (note that each of these pulses is then entangled with the system that emit-

ted it). The timing and propagation of these two pulses should be controlled such that they arrive at the same time at a measurement station, that consists of a 50/50 beam splitter with a photon counter at each of its two output channels. If the number of photons in the pulses are now measured after combining the two pulses on the beam splitter, there is some probability that one of the two detectors counts 1 photon and the other 0 photons. In that case, the total number of spin flips in the two three-level systems is 1, but it is impossible to tell which of the two emitted the photon. As a result, the systems of Alice and Bob have been projected onto an entangled state of the form $|\Psi_{AB}\rangle = \frac{1}{\sqrt{2}}\left(|\, s_A\rangle \,|\, g_B\rangle + \mathrm{e}^{i\varphi} \,|\, g_A\rangle \,|\, s_B\rangle\right)$ (where the phase φ can be derived from experimental conditions [14, 19].

Figure 2.1b depicts in fact emission from ensembles of three level systems. For weak (slightly detuned) driving of the $|\, g\rangle - |e\rangle$ transition, the expectation value for the total number of $|e\rangle - |\, s\rangle$ photons emitted by an ensemble of identical three-level systems can still be less than 1 photon. Notably, the spin excitation is then not stored on an individual three-level system. Instead, it is stored as a spin-wave mode (collective spin excitation) in this medium, with each three-level system having its spin flipped only by a very small amount. Thus, one can also use this approach for preparing entanglement between spin-wave modes in two different ensembles.

These ensembles should have a long elongated shape that is co-linear with the driving field. An important advantage of using such ensembles is that spontaneous emission becomes highly directional [14], with emission predominantly co-propagating with the driving field. In principle the system will emit very weak in all directions, but an initial spontaneous emission event (extremely weak, far below the single-photon level) is strongly amplified (gain) when it co-propagates with the driving field [20]. For very weak driving, the total energy in all of the spontaneous emission can still be at the single-photon level, and the gain then ensures that emission into the desired direction is exponentially stronger than into other directions. Thus, the collection efficiency for the total number of emitted photons by such ensembles can be near unity. This removes the need for using high-finesse optical cavities as in cavity-QED experiments, which is technically very demanding [21, 22].

One should also be able to confirm that entangled states have been prepared by reading out the states of each ensemble of a pair that has been entangled. Correlations between the spin excitations in the two ensembles (Fig. 2.1b) can be studied with an optical readout scheme that uses the inverse of the initial Raman transition. For each system separately, the number of flipped spins in its ensemble can be measured using a control field that is now driving the $|\, s\rangle - |e\rangle$ transition. This converts the spin state that is stored in an ensemble into the state of an highly-

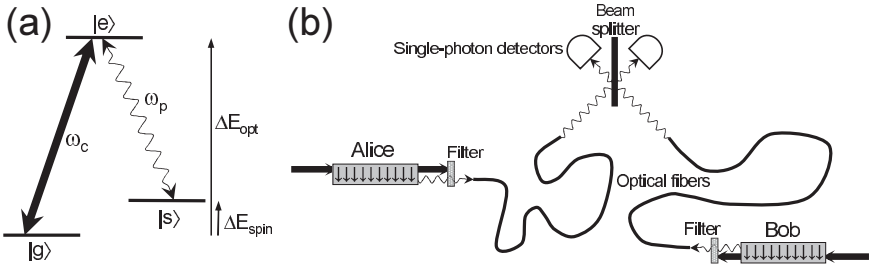

Figure 2.1: **a)** A three-level system with $\Delta E_{spin} << \Delta E_{opt}$. The transition between two low-energy spin states $|\,g\rangle$ and $|\,s\rangle$ under spontaneous emission of a signal photon from the transition $|e\rangle - |\,s\rangle$ (with energy $\hbar\omega_s$) can be controlled with an optical field (tuned to photon energy $\hbar\omega_c$) driving the transition $|\,g\rangle - |e\rangle$. The two legs can be selectively addressed using the optical frequency difference or their dependence on the polarization of the fields. **b)** Scheme for entangling the states of collective spin excitation modes in two different spin ensembles, see the text for details.

directional optical pulse (again a superposition of photon-number states $|0_{pulse}\rangle$ and $|1_{pulse}\rangle$) that results from a subsequent $|e\rangle - |\,g\rangle$ transition. This process fully returns the spin excitation into the $|\,g\rangle$ state. The detection should now directly count the number of photons in the emission from the ensemble that is measured (not using a configuration with a beam splitter). Each of the two ensembles should be measured separately in this manner. If the two ensembles were prepared in a state of the form $|\Psi_{AB}\rangle = \frac{1}{\sqrt{2}}\left(|\,s_A\rangle\,|\,g_B\rangle + e^{i\varphi}\,|\,g_A\rangle\,|\,s_B\rangle\right)$, the number of detected photons from the ensemble of Alice can be 0 or 1, each with probability $\frac{1}{2}$. However, for either measurement outcome, subsequent measurement of the number of photons emitted by Bob's ensemble must yield that it is perfectly anti-correlated with the result of Alice.

Such measurements can already provide evidence for the quantum nature of these correlations (in particular, the variance of these photon-count correlations should show strong sub-Poissonian statistics [20]). However, it does not yet allow for a formal test of Bell inequalities (testing for non-classical correlations), since this requires the ability to rotate the basis in which the state of each of the two-level systems is measured (with respect to the basis defined by $|0_{pulse}\rangle$ and $|1_{pulse}\rangle$). This cannot be performed directly with a readout technique based on photon-number measurements. To overcome this, the observation of entanglement between two ensembles of alkali atoms [5] used an approach where a local phase shift was applied to one of the two systems, either to the optical signal pulse

from readout [5] or to the stored spin excitation. However, the readout then requires once more to combine the signal pulses from readout of the two ensembles on a beam splitter, and to study the interference fringe that results from the local phase shift. A scheme that only relies on local readout of each ensemble can be realized when the states of both Alice and Bob are not stored in a single ensemble but in a pair of ensembles [14]. The photon-number readout can then be implemented with a certain setting for a phase difference between the states of these two ensembles. However, both of these approaches require that the path length between the ensembles and detector stations are stabilized with interferometric precision. An alternative more robust approach could be realized with alkali atom ensembles [6] and used the fact that in these systems the states $|g\rangle$ and $|s\rangle$ consist of multiple (degenerate) Zeeman sublevels. How a spin excitation is distributed over these Zeeman sublevels is then mapped onto two orthogonal polarizations of a signal field, and polarization selective readout then enables to rotate the basis in which signal fields are measured. Other solutions that are technically even less demanding are currently investigated [23–26].

Applying this quantum-optical measurement scheme for preparing entangled states in spatially separated electronic devices is an interesting alternative to related research that uses electronic control and measurement techniques. Activities here use for example electron spins in quantum Hall states [27] or quantum dots [28], or superconducting qubits [29]. A first advantage of this quantum optical approach is that it naturally allows for having the two devices separated by a large distance, whereas for electronic control coherent interactions are typically limited to short distances. More importantly, it allows one to use photon-number detection. This is a unique quantum measurement tool in the sense that projective measurement can be used for preparing states with very high fidelity. Tools for electronic readout have typically much higher noise levels, which results in a much weaker correlation between a measurement outcome and the state of the quantum system immediately after measurement.

2.3 Conclusions

The reasonably long coherence times for electron spin ensembles in n-doped GaAs materials allows for studies of how such ensembles can act as a medium for quantum optics. In turn, this allows for preparing entanglement between states of spin wave modes in two different ensembles. For initial studies, a low-doped n-GaAs system provides one of the most promising model systems. The electron ensembles are then addressed by placing the n-GaAs epi-layers inside optical waveguides, with in-plane propagation of optical control and signal fields. Realizing such

systems is compatible with standard epitaxial growth techniques for GaAs/$Al_xGa_{1-x}As$ heterostructures. In the following chapters we analyze that an optimal system is formed in n-GaAs with Si doping at 10^{14} cm^{-3}, since this gives access to studies in a medium with optical density $OD = 1$. In this system one can address electron spin degrees of freedom inside ensembles of three-level quantum systems with optical transitions that correspond to the excitation of donor-bound excitons D^0X, from the Zeeman-split spin states of donor-bound electrons D^0. Selective control over these two transitions is possible with polarization selection rules that naturally occur in this system. In addition, these transitions have very narrow lines and this allows for using spectral selectivity as well.

Progress towards the realization of entanglement with such a system first requires spectroscopy to confirm the optical selection rules. A crucial next step is then to demonstrate electromagnetically induced transparency (EIT) [30], as this provides evidence that a medium is suited for the quantum optical techniques that we discussed here. If these steps are successful, this clean material system is a very promising candidate for studies of entanglement with ensembles of electron spins in solid state. In particular, the observed long spin coherence times for electron spin ensembles imply that the Zeeman splittings are very homogeneous in these ensembles. This allows to generate Raman scattered fields from two different ensembles that are centered at identical optical frequencies, while their spectral width is tuned by the EIT bandwidth [30]. Consequently, the two signal pulses then have very good spectral overlap, and preparing entanglement by interfering these two pulses on a beam splitter should indeed be possible.

2.4 Acknowledgments

We thank X. Liu, D. Reuter, D. Gerace, H. E. Tureci and A. Imamoglu for help and stimulating discussions. This research is supported by the Netherlands Organization for Scientific Research (NWO).

References

[1] M. A. Nielsen and I. L. Chuang, *Quantum computation and quantum information* (Cambridge University Press, Cambridge UK, 2000).

[2] A. Aspect, J. Dalibard, and G. Roger, *Experimental test of Bell's inequalities using time-varying analyzers*, Physical Review Letters **49**, 1804 (1982).

[3] W. Tittel, J. Brendel, H. Zbinden, and N. Gisin, *Violation of Bell Inequalities by Photons More Than 10 km Apart*, Physical Review Letters **81**, 3563 (1998), ISSN 0031-9007.

[4] M. Rowe, D. Kielpinski, V. Meyer, C. Sackett, W. Itano, C. Monroe, and D. Wineland, *Experimental violation of a Bell's inequality with efficient detection*, Nature **409**, 791 (2001).

[5] C. W. Chou, H. de Riedmatten, D. Felinto, S. V. Polyakov, S. J. van Enk, and H. J. Kimble, *Measurement-induced entanglement for excitation stored in remote atomic ensembles.*, Nature **438**, 828 (2005), ISSN 1476-4687.

[6] D. N. Matsukevich, T. Chanelière, S. D. Jenkins, S.-Y. Lan, T. A. B. Kennedy, and A. Kuzmich, *Entanglement of Remote Atomic Qubits*, Physical Review Letters **96**, 030405 (2006), ISSN 0031-9007.

[7] T. Yu and J. H. Eberly, *Finite-Time Disentanglement Via Spontaneous Emission*, Physical Review Letters **93**, 140404 (2004), ISSN 0031-9007.

[8] P. Dodd and J. Halliwell, *Disentanglement and decoherence by open system dynamics*, Physical Review A **69**, 052105 (2004), ISSN 1050-2947.

[9] M. P. Almeida, F. de Melo, M. Hor-Meyll, A. Salles, S. P. Walborn, P. H. S. Ribeiro, and L. Davidovich, *Environment-induced sudden death of entanglement.*, Science (New York, N.Y.) **316**, 579 (2007), ISSN 1095-9203.

[10] G. Puentes, A. Aiello, D. Voigt, and J. Woerdman, *Entangled mixed-state generation by twin-photon scattering*, Physical Review A **75**, 032319 (2007), ISSN 1050-2947.

[11] A. Aiello, G. Puentes, D. Voigt, and J. Woerdman, *Maximally entangled mixed-state generation via local operations*, Physical Review A **75**, 062118 (2007), ISSN 1050-2947.

[12] A. Leggett and A. Garg, *Quantum mechanics versus macroscopic realism: Is the flux there when nobody looks?*, Physical Review Letters **54**, 857 (1985).

[13] A. J. Leggett and A. Shimony, *Quantum measurement: Beyond paradox* (University of Minnesota Press, Minneapolis, 1998).

[14] L. M. Duan, M. D. Lukin, J. I. Cirac, and P. Zoller, *Long-distance quantum communication with atomic ensembles and linear optics.*, Nature **414**, 413 (2001), ISSN 0028-0836.

[15] J. J. Longdell, E. Fraval, M. J. Sellars, and N. B. Manson, *Stopped Light with Storage Times Greater than One Second Using Electromagnetically Induced Transparency in a Solid*, Physical Review Letters **95**, 063601 (2005), ISSN 0031-9007.

[16] L. Rippe, M. Nilsson, S. Kröll, R. Klieber, and D. Suter, *Experimental demonstration of efficient and selective population transfer and qubit distillation in a rare-earth-metal-ion-doped crystal*, Physical Review A **71**, 062328 (2005), ISSN 1050-2947.

[17] M. V. G. Dutt, L. Childress, L. Jiang, E. Togan, J. Maze, F. Jelezko, A. S. Zibrov, P. R. Hemmer, and M. D. Lukin, *Quantum register based on individual electronic and nuclear spin qubits in diamond.*, Science (New York, N.Y.) **316**, 1312 (2007), ISSN 1095-9203.

[18] M. D. Lukin and A. Imamoglu, *Controlling photons using electromagnetically induced transparency.*, Nature **413**, 273 (2001), ISSN 0028-0836.

[19] C. Cabrillo, J. Cirac, P. García-Fernández, and P. Zoller, *Creation of entangled states of distant atoms by interference*, Physical Review A **59**, 1025 (1999), ISSN 1050-2947.

[20] C. H. van der Wal, M. D. Eisaman, A. André, R. L. Walsworth, D. F. Phillips, A. S. Zibrov, and M. D. Lukin, *Atomic memory for correlated photon states.*, Science (New York, N.Y.) **301**, 196 (2003), ISSN 1095-9203.

[21] J. McKeever, A. Boca, A. D. Boozer, R. Miller, J. R. Buck, A. Kuzmich, and H. J. Kimble, *Deterministic generation of single photons from one atom trapped in a cavity.*, Science (New York, N.Y.) **303**, 1992 (2004), ISSN 1095-9203.

[22] K. Hennessy, A. Badolato, M. Winger, D. Gerace, M. Atatüre, S. Gulde, S. Fält, E. L. Hu, and A. Imamoglu, *Quantum nature of a strongly coupled single quantum dot-cavity system.*, Nature **445**, 896 (2007), ISSN 1476-4687.

[23] S.-Y. Lan, S. Jenkins, T. Chanelière, D. Matsukevich, C. Campbell, R. Zhao, T. Kennedy, and a. Kuzmich, *Dual-Species Matter Qubit Entangled with Light*, Physical Review Letters **98**, 123602 (2007), ISSN 0031-9007.

[24] B. Zhao, Z.-B. Chen, Y.-A. Chen, J. Schmiedmayer, and J.-W. Pan, *Robust Creation of Entanglement between Remote Memory Qubits*, Physical Review Letters **98**, 240502 (2007), ISSN 0031-9007.

[25] L. Jiang, J. Taylor, and M. Lukin, *Fast and robust approach to long-distance quantum communication with atomic ensembles*, Physical Review A **76**, 012301 (2007), ISSN 1050-2947.

[26] S. Chen, Y.-A. Chen, B. Zhao, Z.-S. Yuan, J. Schmiedmayer, and J.-W. Pan, *Demonstration of a Stable Atom-Photon Entanglement Source for Quantum Repeaters*, Physical Review Letters **99**, 180505 (2007), ISSN 0031-9007.

[27] C. Beenakker, C. Emary, M. Kindermann, and J. van Velsen, *Proposal for Production and Detection of Entangled Electron-Hole Pairs in a Degenerate Electron Gas*, Physical Review Letters **91**, 147901 (2003), ISSN 0031-9007.

[28] J. R. Petta, A. C. Johnson, J. M. Taylor, E. A. Laird, A. Yacoby, M. D. Lukin, C. M. Marcus, M. P. Hanson, and A. C. Gossard, *Coherent manipulation of coupled electron spins in semiconductor quantum dots.*, Science (New York, N.Y.) **309**, 2180 (2005), ISSN 1095-9203.

[29] J. H. Plantenberg, P. C. de Groot, C. J. P. M. Harmans, and J. E. Mooij, *Demonstration of controlled-NOT quantum gates on a pair of superconducting quantum bits.*, Nature **447**, 836 (2007), ISSN 1476-4687.

[30] M. Fleischhauer, A. Imamoglu, and J. Marangos, *Electromagnetically induced transparency: Optics in coherent media*, Reviews of Modern Physics **77**, 633 (2005), ISSN 0034-6861.

Chapter 3

Optical transitions in the $D^0 - D^0X$ system in n-GaAs

This chapter provides an introduction into the variety of optical transition that exist for low-doped n-GaAs. The main focus is on excitation of free excitons (X) and donor-bound excitons (D^0-D^0X system), and their dependence on magnetic field.

3.1 Neutral donor D^0, free exciton X and donor-bound exciton D^0X

When it comes to the optical transitions in GaAs with donor or acceptor atoms at a low concentration, one can think of the following transitions:

- Excitation of the free electron-hole pairs. The minimal photon energy that is required is equal to the gap energy, $\hbar\omega = E_g$.
- Excitation of free excitons (X), which is an electron-hole pair bound together by the attractive Coulomb potential. The photon energy that is required for this transition is less than the gap energy by the amount of the exciton binding energy E_X, leading to $\hbar\omega = E_g - E_X$.
- Excitation of the neutral donor-bound exciton complex D^0X. This requires less energy than the excitation of free excitons by the amount the binding energy E_{D^0X} of the exciton to the donor. This yields $\hbar\omega = E_g - E_X - E_{D^0X}$.
- Excitation of an exciton bound to an ionized donor (D^+X) or acceptor-bound excitons (A^0X). These require even less photon energy due to the stronger binding for the exciton.

In this chapter we will focus on the optical properties of the donor-bound excitons D^0X since these will form the key object for the studies of coherent optical manipulation in this thesis.

3.1.1 Neutral donor: D^0

In GaAs doped with silicon, Si dopants usually play the role of donor by donating their excess electron to the electron ensemble in the conduction band. At low temperatures, however, the electron remains bound to the donor. If the concentration of dopants is sufficiently low the electron wave-functions of the neighboring donors do not overlap, and this results a system of localized non-interacting electrons in hydrogen-like orbitals. The temperature below which the donors are not ionized and the radius of the electron wavefunction can be found quite accurately with the effective mass theory [1]. This allows for writing the equation of motion for the electron's envelope wave-function $F_n(\vec{r})$ as:

$$\left(-\frac{\hbar^2\nabla^2}{2m_e^*} - \frac{e^2}{4\pi\varepsilon_0\varepsilon_r r}\right) F_n(\vec{r}) = E_n F_n(\vec{r}) \tag{3.1}$$

where $m_e^* = 0.067 m_e$ is the effective mass of the electron in the conduction band of GaAs, m_e is the free electron mass, e is the elementary charge, $\varepsilon_0 = 8.85 \cdot 10^{-12}$ F/m is the vacuum permittivity constant and $\varepsilon_r = 12.56$ is the relative permittivity constant for GaAs.

Equation 3.1 is a hydrogenic Schrödinger equation of motion in the Coulomb potential of the ionized donor, which results in following spectrum of eigenenergies:

$$E_n = -\frac{m_e^*}{m_e}\frac{1}{\varepsilon_r^2}\frac{R_H}{n^2} \tag{3.2}$$

where $R_H = 13.6$ eV is the Rydberg constant of the hydrogen atom and the energy E_n is defined with respect to the bottom of the conduction band.

The ground state ($n = 1$) of the D^0 electron lies 5.8 meV below the bandgap of the GaAs $E_g = 1.519$ eV (value for at 0 K). This means that donors are not ionized for temperatures well below ≈ 70 K.

The Bohr radius r_n of the n^{th} level can be approximated by:

$$r_n = \frac{m_e}{m_e^*}\varepsilon_r n^2 a_H \tag{3.3}$$

where $a_H = 5.29177 \times 10^{-11}$ m is the Bohr radius of the hydrogen atom. This gives $r_1 \approx 100$ Å. This size sets an upper limit of 10^{-14} cm^{-3} for the concentration of donors if one aims to work with an ensemble of non-interacting donor-bound electrons (this number is also supported by the experimental observations from Chapter 6 of this thesis).

The first excited state ($n = 2$) has a binding energy of 1.4 meV (again with respect to the bottom of conduction band) and a Bohr radius $r_2 = 396$ Å. The difference in energy between the ground $n = 1$ and the first excited $n = 2$ state is 4.4 meV. For the optical transitions of the D^0-D^0X system this translates into difference in wavelength of 20 Å. This is important to keep in mind since optical emission by a D^0X system from a transition to a D^0 state with $n = 2$ can be observed in luminescence experiments, and these luminescence side peaks are often referred to as two electron satellites (TES).

3.1.2 D^0 in a magnetic field

When no magnetic field is applied, the $n = 1$ ground state is two-fold degenerate due to the spin of the electron. When a magnetic field B is applied this degeneracy is lifted and a two-level system is formed. The energy of the spin-up state $|\uparrow\rangle$ is

lower than the energy of the spin-down state $|\downarrow\rangle$ by an amount:

$$\Delta E = g_e \mu_B B \tag{3.4}$$

where $g_e \approx -0.42 \pm 0.02$ [2, 3] is the g-factor for the electron of the GaAs D^0 system, and $\mu_B = 5.79 \cdot 10^{-5}$ eV/T is the Bohr magneton. In a magnetic field $B = 9$ T, $\Delta E = 0.23$ meV. For the optical transitions of the D^0-D^0X system this translates into a difference in wavelength $\Delta\lambda = 1.2$ Å. It would require a temperature below $T \simeq \Delta E / k_B = 2.7$ K, where k_B is the Boltzman constant, to thermally depopulate the $|\downarrow\rangle$ state. If one operates at liquid Helium temperature ($T = 4.2$ K), both states are populated with a ratio of about 2 : 1 for thermal equilibrium.

3.1.3 Free exciton: X

A free exciton X can be described as a weakly bound electron-hole pair. Even though the free exciton is not a localized state, the correlated motion of the electron and hole does follow the hydrogenic equation of motion. For the mass one now has to use the reduced electron-hole mass $m_r = (1/m_e^* + 1/m_h^*)^{-1} = 0.05\ m_e$, where $m_h^* = 0.2 m_e$ of the weighted average of the heavy and light hole effective masses in GaAs [1]. The binding energy of the $n = 1$ free exciton $E_X = 4.3$ meV and the corresponding Bohr radius is $r_X = 133$ Å. The optical transitions associated with excitation of free excitons require an energy equal to bandgap energy E_g minus the binding energy of the exciton E_X, corresponding to $\lambda_X \simeq 818$ nm in zero magnetic field.

3.1.4 X in a magnetic field

When a magnetic field is applied the wavefunction of the free exciton is perturbed and the binding energy decreases [1]. In weak fields, where Coulomb attraction between an electron and a hole is larger than the cyclotron orbit energy, the magnetic field is treated as a perturbation to the excitons wavefunction resulting in a diamagnetic shift for the exciton energy that scales as $\propto B^2$:

$$\Delta E_d = +\frac{e^2}{12 m_r} r_X^2 B^2 \tag{3.5}$$

For the values given above this yields an energy shift $\Delta E_d \sim 0.052$ meV/T^2.

In strong magnetic fields, the cyclotron energy is stronger than the electron-hole Coulomb interaction and both electrons and holes form Landau levels. Now

the Coulomb interaction can be treated as a perturbation. In this regime the dependence of the exciton energy on magnetic field becomes linear and corresponds to the difference in energy between the electron and hole Landau levels:

$$\Delta E_L = +\frac{\hbar e}{m_r} B \tag{3.6}$$

The expected energy shift with magnetic field follows $\Delta E_L \sim 2.3$ meV/T.

Even though this description of the diamagnetic shift of X using the reduced mass m_r provides a good indication of the system's behavior, understanding high-resolution spectroscopy of this system requires a more detailed description that takes into account the difference in mass for light holes and heavy holes, and the Zeeman splittings of all particles involved. A complete picture of the energy shifts of free excitons is therefore rather complicated, and beyond the scope of this thesis. It is, however, important to note that the energy of optical transitions associated with the creation or destruction of free excitons increases with magnetic field, since the cyclotron shifts are typically larger than the Zeeman splitting.

3.1.5 Neutral donor-bound exciton: D^0X

The neutral donor forms an attractive potential to which an exciton can be bound, thus creating the donor-bound exciton complex D^0X. This is a three-body complex (two electrons and one hole) around an ionized Si^+ donor core. The lowest energy levels of this system have the two electrons in a singlet state.

The energy of the optical transition associated with excitation of a D^0X complex is (besides the fine structure) equal to the energy for exciting a free exciton X minus the binding energy of the exciton to the neutral donor D^0. The binding energy for an exciton to the D^0 system (with both systems in their ground state)is for $B = 0$ T approximately 0.9 meV (corresponding to a difference in wavelength between such X and $D^0 - D^0X$ excitation of $\Delta\lambda = 55$ Å) [2–9].

3.1.6 Neutral donor-bound excitons D^0X in a magnetic field

Since the energy for exciting free excitons X increases with magnetic field, also the energy of the $D^0 - D^0X$ transitions increase according to similar diamagnetic-shift laws. The optical spectra of the donor-bound exciton also shows a fine structure due to Zeeman splitting of the electron and the hole's spin. For the transitions with lowest energy this concerns the Zeeman splitting of the D^0 electron spin, and the Zeeman and the orbital energy of the hole in the D^0X complex which has a spin $J = 3/2$ character (heavy hole) [1, 3]. The spin of electron in the D^0X complex can be disregarded since the two electrons are in a singlet state.

In order to characterize the diamagnetic shifts and the fine structure of the GaAs exciton complexes we have performed magneto-photoluminescence experiments (see also Chapter 5). Results of this study are shown in the gray scale plot of Fig. 3.1.

The fine structure of the neutral donor was described earlier. To describe the energy levels of the D^0X complex in magnetic field one has to account for an interplay between the Zeeman splitting of the hole spin and formation of cyclotron orbits. This requires a rather complicated theoretical treatment [1], which goes beyond the scope of this thesis. Instead, we will focus on an empirical study of the

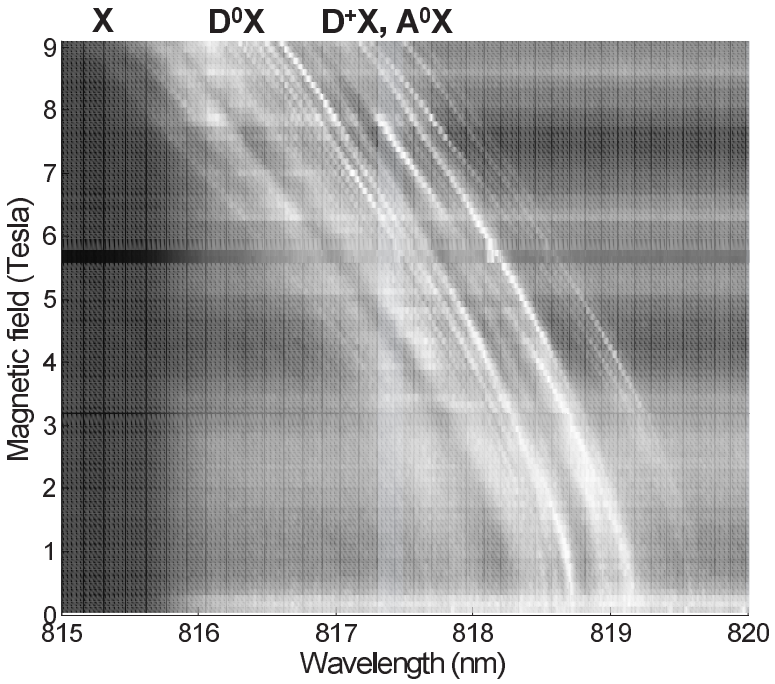

Figure 3.1: Grayscale plot with magneto-photoluminescence spectrums for a range of magnetic fields B, for a GaAs sample with Si doping at $n_{Si} = 3 \times 10^{13}$ cm^{-3}. Dark represents strong luminescence, light represent weak luminescence. The leftmost broad transition corresponds free-exciton luminescence (X). The narrow lines that start for $B = 0$ T at 818.7 nm and evolve into rich spectrum of transitions is the $D^0 - D^0X$ system. Other transitions that are observed (as labeled) are due to acceptor-bound excitons ($A^0 - A^0X$) and ionized donor-bound excitons ($D^+ - D^+X$).

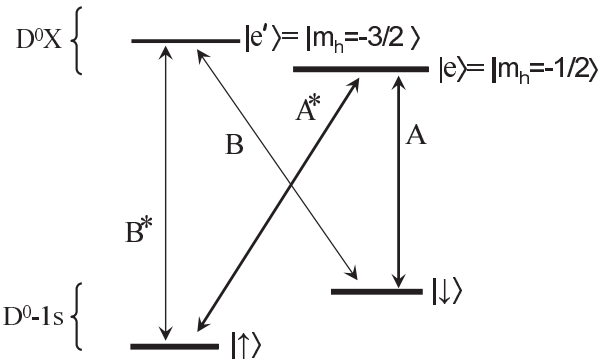

Figure 3.2: Schematic with energy levels and optical transitions associated with excitation of a donor-bound exciton D^0X in an external magnetic field. The ground state of the system (neutral donor D^0, with an electron in a hydrogen-like $1s$ orbital) Zeeman split and labeled as $|\uparrow\rangle$ and $|\downarrow\rangle$. The excited states are donor-bound excitons states (D^0X), with two electrons in a singlet state and a hole that can have various z-projections for its total angular momentum. The lowest D^0X level $|e\rangle$ this is $m_h = -1/2$ due the hole's spin and orbital state $L = 1$. For the second-lowest D^0X level $|e'\rangle$ this is expected to be a $m_h = -3/2$ and $L = 0$ hole's state [7] The two pairs of optical transitions $A-A^*$ and $B-B^*$ form so-called Λ-systems. Such pairs of transitions can be used for implementing EIT.

lowest energy levels of the D^0X complex. This provides adequate information for the investigations later in this thesis. Notably, the associated optical transitions show very strong polarization dependent selection rules [3].

The polarization dependent transmission spectroscopy, that will be described later in the thesis (Chapter 5) provides a very strong indication that the lowest D^0X level corresponds to a state with $m_h = -\frac{1}{2}$ for the z-projection of the hole spin. This also agrees recent reports by Fu *et al.* [7] (this also provides an example of the complex character of the D^0X complex, since one expects in fact $m_h = -\frac{3}{2}$ lowest hole level). A schematic picture of the two lowest D^0X levels together with the two D^0 Zeeman-split electron spin states is shown in Fig .3.2. Each pair of transitions that start from the two D^0 spin states to a particular D^0X level form a so-called Λ-system that can be applied in studies of EIT.

3.2 Polarization selection rules of the optical transitions in $D^0 - D^0X$ system

The strength of optical transition is determined by the magnitude of the dipole moment associated with this transitions, which in general form is written as:

$$\langle \vec{\mu} \rangle = \langle i|\hat{\mu}|f\rangle \tag{3.7}$$

where $|i\rangle$ and $|f\rangle$ are the initial and the final state of the optical transitions and $\hat{\mu} = e \cdot \vec{r}$ is a quantum mechanical dipole operator where e is the charge of electron. Owing to the presence of the $\vec{r}$ in the dipole's operator, the expectation value of the dipole moment is also expected to be a vector.

Knowing the dipole moment, the interaction Hamiltonian for light-matter interaction can be written as:

$$\hat{V}_{int} = -\vec{\mu} \cdot \vec{E} \tag{3.8}$$

where $\vec{E} = E_0 \cdot \vec{e}$ with E_0 being an amplitude of the electric field associated with the optical excitation and $\vec{e}$ is an unitary cartesian vector that describes a polarization of the optical field.

Using the expression for the optical field and the dipole operator the expectation value of the interaction Hamiltonian can be written as:

$$\langle i|\vec{V}_{int}|f\rangle = qE_0\langle i|\vec{r}\cdot\vec{e}|f\rangle = qE_0\langle i|(x\cdot\vec{e_x} + y\cdot\vec{e_y} + z\cdot\vec{e_z})|f\rangle \tag{3.9}$$

The non-zero value of the expectation value in the angled brackets will result in the optical transition that is dipole allowed.

It is often possible to determine whether the interaction Hamiltonian results in zero expectation value based on the principles of symmetry, which creates a basis for sets of polarization and other selection rules.

Lets consider the interaction of the optical field with a donor bound electron spin D^0 that can be excited to the donor-bound exciton complex D^0X. The initial and the final states for the optical transitions of the $D^0 - D^0X$ type can be factorized in the product of the envelope wavefunction and the Bloch wevefunction amplitude as $F(\vec{r}) \cdot \Psi(\vec{r})$. Since the amplitude of the dipole oscillations is comparable to the period of the lattice, while the spread of the envelope function is much larger then that [1] the expectation value in the equation 3.9 can be approximated as:

$$\langle i|\vec{V}_{int}|f\rangle = qE_0F_i(\vec{r})\cdot F_f(\vec{r})\,\langle\Psi_i(\vec{r})|(x\cdot\vec{e_x} + y\cdot\vec{e_y} + z\cdot\vec{e_z})|\Psi_f(\vec{r})\rangle \tag{3.10}$$

The expression $F_i(\vec{r}) \cdot F_f(\vec{r})$ is a scalar product of two functions in integral sense (product integral) and is non-zero only when both functions have the same parity, which demonstrates an example of the parity optical selection rules.

On the other hand, the product $\langle \Psi_i(\vec{r}) | (x \cdot \vec{e_x} + y \cdot \vec{e_y} + z \cdot \vec{e_z}) | \Psi_f(\vec{r}) \rangle$ is interesting from the spherical symmetry point of view. The angular part of the Bloch wavefunctions $\Psi_{i,f}(\vec{r})$ that describes the electron's or the hole's spin is the spherical harmonics of the type $Y_l^m(\theta,\phi)$, where l is the orbital momentum quantum number and m is the projection momentum quantum number. Exact expressions in terms of the angles ϕ and θ for the spherical harmonics can be found in most textbooks on quantum mechanics [10].

Electron spin, for example, which possess an angular momentum of $1/2$ is described by the $Y_{1/2}^{\pm 1/2}$ spherical harmonics. The spherical part of the heavy hole's spin, that has an angular momentum of $3/2$ and therefore four projections, will be a set of four functions $Y_{3/2}^{-3/2..+3/2}$.

The product of the type $\vec{r} \cdot \vec{e}$ can be written as a sum of the spherical harmonics by using the following set of transformations [10]:

$$\sqrt{\frac{3}{4\pi}} z = r \cdot Y_1^0(\theta,\phi) \tag{3.11}$$

$$\sqrt{\frac{3}{4\pi}} x = \frac{r}{\sqrt{2}} \cdot \left[Y_1^{-1}(\theta,\phi) - Y_1^{-1}(\theta,\phi) \right] \tag{3.12}$$

$$-i\sqrt{\frac{3}{4\pi}} y = \frac{r}{\sqrt{2}} \cdot \left[Y_1^{-1}(\theta,\phi) + Y_1^{-1}(\theta,\phi) \right] \tag{3.13}$$

Using the spherical representation of the wavefunctions and operators, the expectation value of the interaction Hamiltonian for the optical transitions of the type $D^0 - D^0X$ reduces to calculating a following integral product:

$$\langle \hat{V}_{int} \rangle \sim \langle Y_{1/2}^{\pm 1/2} | Y_1^{1,0,-1} | Y_{3/2}^{-3/2..+3/2} \rangle \tag{3.14}$$

A conservation of the angular momentum requires that $\Delta l = 0, \pm 1$ and $\Delta m = 0$. The first condition is always satisfied in GaAs owing to the fact that in the process of electron-hole pair generation the spin of electron is $1/2$, the maximum angular momentum of the hole's spin is $3/2$ and the angular momentum carried by the photon is $1 \cdot \hbar$. The second condition depends on the choice of the polarization of the optical field and on the actual projection of the electron's and hole's spin that are participating in the transition.

Lets consider a situation, where an external magnetic field is applied along the $\vec{z}$ direction, which sets a quantization axis for electron's and hole's spins. A light is

propagating along the direction that is collinear with the applied field. If polarization of the light is a right-circular then its polarization state is $\vec{e_x} + i \cdot \vec{e_y}$, which leads to the calculation of the expectation value that is $x + i \cdot y$. In terms of the spherical harmonics this expression is proportional to the Y_1^1 function and when using it in the expression 3.14, the only non-zero products will be obtained between the pair of states $Y_{1/2}^{-1/2}$ (electron spin $m_h = -1/2$) and $Y_{3/2}^{+1/2}$ (heavy hole's spin $m_h = +1/2$) and the pair $Y_{1/2}^{+1/2}$ (electron $m_h = +1/2$) and $Y_{3/2}^{+3/2}$ (heavy hole $m_h = +3/2$). The result of this exercise could have been easily predicted on a basis of the fact that right-circularly polarized photon is inducing an optical transitions with a change in projection of angular momentum by $+\hbar$. In a similar fashion one can show that the left-circularly polarized light induces an optical transition with a change of angular momentum of $-\hbar$. The left and the right circular light's polarization are often referred to as σ^+ and σ^- respectively.

It is interesting to note that in the geometry where the propagation direction of light is along the direction of magnetic field no transitions without change in projection of angular momentum are possible since light can not have polarization vector that is along the propagation direction. If, however, light propagates along the $\vec{x}$ or $\vec{y}$ - direction that is orthogonal to the magnetic field, it can be linearly polarized along the direction of the field - $\vec{z}$-direction. This polarization state leads to the integration of the z function, which is described by the Y_1^0 spherical harmonic. When using it in the expression (3.14) we obtain that only the transitions between $Y_{1/2}^{-1/2}$ and $Y_{3/2}^{-1/2}$ and between $Y_{1/2}^{+1/2}$ and $Y_{3/2}^{+1/2}$ are allowed. These transitions do occur without a change in the total projection of angular momentum and polarization of light that is used is often referred to as a π polarization.

It is quite evident that when light is linearly polarized and orthogonal to both magnetic field and propagation direction it will be seen by the spins system as a superposition of σ^+ and σ^- polarizations, which we will label as σ polarization later in this thesis.

Throughout this thesis we are using the orthogonal to magnetic field light propagation geometry which allows us to selectively address transitions from the D^0 spin $|\uparrow\rangle (m_e = +1/2)$ and D^0 spin $|\downarrow\rangle (m_e = -1/2)$ states to the common excited state D^0X that has $m_h = -1/2$ by using two orthogonal linear polarization of the excitation light.

We also utilize the ability to map polarization state of light on the polarization state of the electron's spin and we show in the Chapter 7 of this thesis that together with coherent optical driving any spin state on the Bloch sphere can be generated.

References

[1] M. Cardona and P. Y. Yu, *Fundamentals of Semiconductors* (Springer-Verlag, 2001).

[2] K.-M. C. Fu, S. M. Clark, C. Santori, C. R. Stanley, M. C. Holland, and Y. Yamamoto, *Ultrafast control of donor-bound electron spins with single detuned optical pulses*, Nature Physics **4**, 780 (2008), ISSN 1745-2473.

[3] V. A. Karasyuk, D. G. S. Beckett, M. K. Nissen, A. Villemaire, T. W. Steiner, and M. L. W. Thewalt, *Fourier-transform magnetophotoluminescence spectroscopy of donor-bound excitons in GaAs*, Physical Review B **49**, 16381 (1994), ISSN 0163-1829.

[4] E. Bogardus and H. Bebb, *Bound-Exciton, Free-Exciton, Band-Acceptor, Donor-Acceptor, and Auger Recombination in GaAs*, Physical Review **176**, 993 (1968), ISSN 0031-899X.

[5] D. Reynolds, C. Litton, T. Collins, S. Nam, and C. Wolfe, *Zeeman studies of photoluminescence of excited terminal states of a bound-exciton-donor complex in GaAs* (1975), URL `http://link.aps.org/doi/10.1103/PhysRevB.12.5723`.

[6] K.-M. Fu, C. Santori, C. Stanley, M. Holland, and Y. Yamamoto, *Coherent Population Trapping of Electron Spins in a High-Purity n-Type GaAs Semiconductor*, Physical Review Letters **95**, 187405 (2005), ISSN 0031-9007.

[7] K. Fu, *Optical manipulation of electron spins bound to neutral donors in GaAs*, PhD thesis, Stanford University (2007).

[8] K.-M. Fu, W. Yeo, S. Clark, C. Santori, C. Stanley, M. Holland, and Y. Yamamoto, *Millisecond spin-flip times of donor-bound electrons in GaAs*, Physical Review B **74**, 121304 (2006), ISSN 1098-0121.

[9] M. Sladkov, A. U. Chaubal, M. P. Bakker, A. R. Onur, D. Reuter, A. D. Wieck, and C. H. van der Wal, *Electromagnetically Induced Transparency with an Ensemble of Donor-Bound Electron Spins in a Semiconductor*, Phys. Rev. B **82**, 121308(R) (2010).

[10] C. Cohen-Tannoudji, *Quantum Mechanics* (Willey, 1977).

Chapter 4

Optical control of three-level systems: Theory

In this chapter I will present a general approach to the mathematical treatment of three-level systems, based on the density matrix formalism. I will focus on the calculation of the optical spectra in the steady state regime, when optical excitations are provided by continuous wave lasers (CW), and explain how it is used to explain the experiment on electromagnetically induced transparency (EIT). Based on the equation of motion of the density matrix I will also calculate the time evolution of the spin ensemble during and after the resonant excitation by a fast optical pulse.

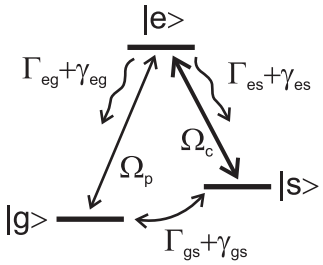

Figure 4.1: Model 3-level system. Two optical fields: probe and control are tuned to excite transitions from the ground $|g\rangle$ to the excited $|e\rangle$ and from the spin-flip $|s\rangle$ to the excited $|e\rangle$ state. Γ_{ij} and γ_{ij} are corresponding population relaxation and dephasing rates.

4.1 Introduction

The three-level system is a key object in the field of quantum electrodynamics. Typically the three-level system consists of a long living ground state $|g>$, long-living "spin-flip" state $|s>$ and an excited state $|e>$, see Fig. 4.1. The crucial property of the system is that quantum coherence between states $|g>$ and $|s>$ is preserved for a time that is long enough on a timescale needed for spin manipulation. In the case of the Λ-system, which will be considered throughout this thesis, optical transitions are only allowed from the ground to the excited state ($|g> - |e>$ transition) and from the spin-flip to the excited state ($|s> - |e>$ transition). Provided that the coherence time of the ground and the spin-flip state of such a system is long enough, any superpositions and coherent populations transfers from the ground to the spin-flip state are theoretically achievable via designed optical manipulation of this system.

To describe how optical fields interact with a model three-level system, we will turn our attention to the technique involving the density matrix formalism. We are interested in the response of the system to excitations provided by two optical fields, where one field (control field) will be treated exactly, while the other field (probe field) will be calculated only to the first order approximation. We will show how the spectral response of the three-level system changes according to the ratio between the strength of the optical excitation and the rate of the relaxation and decoherence processes in the system.

4.2 Density matrix and equation of motion

The concept of the density matrix is based on the idea that any quantum mechanical system can be described not in terms of its wave function, but rather by using an operator describing both the population of each eigenstate and the correlation between each pair of eigenstates, known as coherence. For the three-level system, the used density matrix operator will be a 3-by-3 matrix:

$$\hat{\rho} = \begin{pmatrix} \rho_{gg} & \rho_{gs} & \rho_{ge} \\ \rho_{sg} & \rho_{ss} & \rho_{se} \\ \rho_{eg} & \rho_{es} & \rho_{ee} \end{pmatrix}, \tag{4.1}$$

where the diagonal elements are the populations of the ground, spin-flip and excited states respectively, while off-diagonal elements are coherences.

The density matrix operator obeys the operators equation of motion with relaxation term:

$$\frac{d\rho}{dt} = -\frac{i}{\hbar}\left[\hat{H}_{total}, \hat{\rho}\right] + \hat{L}(\hat{\rho})_{relax}, \tag{4.2}$$

where the first term describes the dynamics of the density matrix operator driven by $\hat{H}_{total}$ - a complete Hamiltonian of the system, while the second term of this equation is a superoperator, which describes all the relaxation and decoherence processes.

The total Hamiltonian consists of the Hamiltonian of the bare three-level system $\hat{H}_0$ and the interaction Hamiltonian $\hat{H}_{int}$. The three-level system Hamiltonian is, as expected, just a 3-by-3 matrix with diagonal elements being the energy of the ground, spin-flip and excited state, while the off-diagonal elements are equal to zero.

The interaction Hamiltonian consists of the elements that describe the interaction of the optical fields with the system. We will treat the optical fields classically and define the control field ϵ_c and the probe field ϵ_p as the product of the time periodic functions and the complex amplitudes:

$$\begin{aligned} \epsilon_c(t) &= \frac{1}{2}E_c e^{-i\omega_c t} + c.c. \\ \epsilon_p(t) &= \frac{1}{2}E_p e^{-i\omega_p t} + c.c. \end{aligned} \tag{4.3}$$

Here E_c and E_p are the complex amplitudes of the control and probe fields and $c.c.$ stands for complex conjugate.

If we consider only dipole optical transitions in the system, the interaction Hamiltonian $\hat{V}$ is written as:

$$\hat{V} = -\hat{\mu}\vec{\epsilon}(t) = -\hat{\mu}\left[\vec{\epsilon}_c(t) + \vec{\epsilon}_p(t)\right], \tag{4.4}$$

where $\hat{\mu}$ is the matrix dipole operator of the three-level system. Assuming only optical transitions from the ground to the excited and from the spin-flip to the excited state are possible, we can write the dipole matrix operator as:

$$\hat{\mu} = \begin{pmatrix} 0 & 0 & \mu_{ge} \\ 0 & 0 & \mu_{se} \\ \mu_{eg} & \mu_{es} & 0 \end{pmatrix} \tag{4.5}$$

Combining all these operators together, the total Hamiltonian can be written as:

$$\hat{H}_{total} = \begin{pmatrix} \hbar\omega_g & 0 & V_{ge} \\ 0 & \hbar\omega_s & V_{se} \\ V_{eg} & V_{es} & \hbar\omega_e \end{pmatrix} \tag{4.6}$$

where V_{ij} are products of the optical fields with the corresponding dipole operators and $\hbar\omega_g, \hbar\omega_s, \hbar\omega_e$ are the energies of the ground, spin-flip and excited state respectively.

Now, after calculating all the necessary commutators and neglecting for a while the relaxation operator, we can write down the equation of motion for each component of the density matrix operator:

$$\begin{aligned}
\frac{d\rho_{gg}}{dt} &= -\frac{i}{\hbar}\left[V_{ge}\rho_{eg} - \rho_{ge}V_{eg}\right] \\
\frac{d\rho_{ss}}{dt} &= -\frac{i}{\hbar}\left[V_{se}\rho_{es} - \rho_{se}V_{es}\right] \\
\frac{d\rho_{eg}}{dt} &= -\frac{i}{\hbar}\left[V_{eg}\left(\rho_{gg} - \rho_{ee}\right) + \rho_{eg}\hbar\omega_{eg} + V_{es}\rho_{sg}\right] \\
\frac{d\rho_{es}}{dt} &= -\frac{i}{\hbar}\left[V_{es}\left(\rho_{ss} - \rho_{ee}\right) + \rho_{es}\hbar\omega_{es} + V_{eg}\rho_{gs}\right] \\
\frac{d\rho_{sg}}{dt} &= -\frac{i}{\hbar}\left[\rho_{sg}\hbar\omega_{sg} + V_{se}\rho_{eg} - \rho_{se}V_{eg}\right]
\end{aligned}$$

4.3 Rotating frame transformation and rotating wave approximation (RWA)

Since off-diagonal elements of the density matrix operator are fast time varying functions, it is more easy to search for the solution of the equation by applying a rotation frame transformation. This is done by writing each component of the density matrix as the product of a slow and a fast time varying functions:

$$\begin{aligned} \rho_{eg} &= \sigma_{eg} e^{-i\omega_p t} \\ \rho_{es} &= \sigma_{es} e^{-i\omega_c t} \\ \rho_{sg} &= \sigma_{sg} e^{-i(\omega_p - \omega_c)t} \end{aligned}$$

Here σ_{eg}, σ_{es}, σ_{sg} are slowly varying amplitudes and ω_p, ω_c are the frequencies of the probe and the control field respectively. Diagonal elements of the density matrix operator do not have any fast time varying part and therefore remain the same.

We will also write down explicit expressions for the components V_{ij} of the interaction Hamiltonian in terms of the product of the dipole matrix operator and the optical field:

$$\hat{V}(t)_{ij} = -\hat{\mu}_{ij}\left[\frac{1}{2}E_c e^{-i\omega_c t} + c.c. + \frac{1}{2}E_p e^{-i\omega_p t} + c.c.\right] \tag{4.7}$$

After substituting explicit form of the interaction Hamiltonian it is easy to see that many time dependencies are canceling each other, while those that are left can be neglected as soon as the following condition is satisfied:

$$\left|\omega_p - \omega_c\right| << \omega_p, \omega_c \tag{4.8}$$

This is the essence of the rotation wave approximation (RWA) - it neglects contributions from off-resonance terms. In addition to that we will introduce Rabi frequencies for the probe and control field, which represent the strength of the interaction between the optical fields and the three-level system:

$$\begin{aligned} \Omega_c &= \mu_{es} E_c / \hbar \\ \Omega_p &= \mu_{eg} E_p / \hbar \end{aligned}$$

Having done all this and after introducing the frequency detuning of the probe and control fields with corresponding optical transitions: $\Delta_c = \omega_c - \omega_{es}$ - the control laser single photon detuning, $\Delta_p = \omega_p - \omega_{eg}$ - the probe laser single photon

detuning and $\delta = \Delta_p - \Delta_c$ - the two photon detuning, we obtain the following set of equations:

$$\begin{aligned}
\frac{d\rho_{gg}}{dt} &= -\frac{1}{2}\Omega_p^*\sigma_{eg} + \frac{1}{2}\Omega_p\sigma_{eg}^* \\
\frac{d\rho_{ss}}{dt} &= -\frac{1}{2}\Omega_c^*\sigma_{es} + \frac{1}{2}\Omega_c\sigma_{es}^* \\
\frac{d\sigma_{eg}}{dt} &= -\Delta_p\sigma_{eg} - \frac{1}{2}\Omega_p\left(\rho_{gg} - \rho_{ee}\right) - \frac{1}{2}\Omega_c\sigma_{sg} \\
\frac{d\sigma_{es}}{dt} &= -\Delta_c\sigma_{es} - \frac{1}{2}\Omega_c\left(\rho_{ss} - \rho_{ee}\right) - \frac{1}{2}\Omega_p\sigma_{sg}^* \\
\frac{d\sigma_{sg}}{dt} &= -\delta\sigma_{sg} - \frac{1}{2}\Omega_c^*\sigma_{eg} + \frac{1}{2}\Omega_p\sigma_{es}^*
\end{aligned}$$

4.4 Lindblad relaxation operator

Now we will introduce the relaxation Hamiltonian $\hat{L}(\rho)$ where we will account for all possible relaxations and dephasing processes in the system:

$$\hat{L}\left(\hat{\rho}\right) = \left(\begin{array}{cccc}
-\Gamma_{gs}\rho_{gg} + \Gamma_{sg}\rho_{ss} + \Gamma_{eg}\rho_{ee} & & & \\
-\left(\frac{\Gamma_{gs}+\Gamma_{sg}}{2} + \gamma_s\right)\rho_{sg} & & & \\
-\left(\frac{\Gamma_{gs}+\Gamma_{eg}+\Gamma_{es}}{2} + \gamma_{ea,eb}\right)\rho_{eg} & & & \\
 & -\left(\frac{\Gamma_{gs}+\Gamma_{sg}}{2} + \gamma_s\right)\rho_{gs} & & \\
 & \Gamma_{gs}\rho_{gg} - \Gamma_{sg}\rho_{ss} + \Gamma_{es}\rho_{ee} & & \\
 & -\left(\frac{\Gamma_{gs}+\Gamma_{eg}+\Gamma_{es}}{2} + \gamma_{ea,eb}\right)\rho_{eg} & & \\
 & & -\left(\frac{\Gamma_{gs}+\Gamma_{eg}+\Gamma_{es}}{2} + \gamma_{ea,eb}\right)\rho_{ge} & \\
 & & -\left(\frac{\Gamma_{sg}+\Gamma_{eg}+\Gamma_{es}}{2} + \gamma_{ea,eb}\right)\rho_{se} & \\
 & & -\left(\Gamma_{eg} + \Gamma_{es}\right)\rho_{ee} &
\end{array}\right) \tag{4.9}$$

To see how this Hamiltonian describes relaxations it is instructive to see how it appears for different populations and coherences.

For populations it takes the following form:

$$\frac{d\rho_{gg}}{dt} = -\Gamma_{gs}\rho_{gg} + \Gamma_{sg}\rho_{ss} + \Gamma_{eg}\rho_{ee}, \tag{4.10}$$

which indicates that the population in the ground state can change (increase) due to the relaxation of the excited state $\Gamma_{eg}\rho_{ee}$ and due to competing relaxation-excitation processes between ground and spin flip state $-\Gamma_{gs}\rho_{gg}+\Gamma_{sg}\rho_{ss}$.

The same can be written for spin-flip state:

$$\frac{d\rho_{ss}}{dt}=\Gamma_{gs}\rho_{gg}-\Gamma_{sg}\rho_{ss}+\Gamma_{es}\rho_{ee} \tag{4.11}$$

Relaxation of the excited state population can be also derived from the first principle, but also from the property of the density matrix which implies that for any closed system the trace of the density matrix must be equal to unity.

For coherences:

$$\frac{d\sigma_{eg}}{dt}=-\left(\frac{\Gamma_{gs}+\Gamma_{eg}+\Gamma_{es}}{2}+\gamma_{ea,eb}\right)\rho_{eg} \tag{4.12}$$

Coherence ρ_{eg} is lost due to direct dephasing of the excited states $\gamma_{ea,eb}$ and due to population relaxations of ground and excited states. Same arguments hold for the rest of coherences.

The last step is to make the following substitutions: for populations we can write that $\rho_{ee}=W-\rho_{gg}-\rho_{ss}$, where $W=1$ in most of the cases, but keeping this in a general form we can use it later for describing dynamics of any open systems, where relaxations can happen outside the three-level system. We will introduce new complex frequency detuning that include the relaxations terms: $\tilde{\Delta}_c=\Delta_c+i\left(\frac{\Gamma_{sg}+\Gamma_{eg}+\Gamma_{es}}{2}+\gamma_{ea,eb}\right)$ - control laser single photon detuning, $\tilde{\Delta}_p=\Delta_p+i\left(\frac{\Gamma_{gs}+\Gamma_{eg}+\Gamma_{es}}{2}+\gamma_{ea,eb}\right)$ - probe laser single photon detuning, $\tilde{\delta}=\delta+i\left(\frac{\Gamma_{gs}+\Gamma_{sg}}{2}+\gamma_s\right)$ - two photon detuning.

The resulting set of algebraic equations reads as follows:

$$
\begin{aligned}
i\Gamma_{eg}W &= -\frac{1}{2}\Omega_p^*\sigma_{eg} + \frac{1}{2}\Omega_p\sigma_{eg}^* - i\left(\Gamma_{gs}+\Gamma_{eg}\right)\rho_{gg} - i\left(\Gamma_{eg}-\Gamma_{sg}\right)\rho_{ss} \\
i\Gamma_{es}W &= -\frac{1}{2}\Omega_c^*\sigma_{es} + \frac{1}{2}\Omega_c\sigma_{es}^* - i\left(\Gamma_{sg}+\Gamma_{es}\right)\rho_{ss} - i\left(\Gamma_{es}-\Gamma_{gs}\right)\rho_{gg} \\
-\frac{1}{2}\Omega_p W &= -\tilde{\Delta}_p\sigma_{eg} - \frac{1}{2}\Omega_p\left(2\rho_{gg}+\rho_{ss}\right) - \frac{1}{2}\Omega_c\sigma_{sg} \\
-\frac{1}{2}\Omega_c W &= -\tilde{\Delta}_c\sigma_{es} - \frac{1}{2}\Omega_c\left(2\rho_{ss}+\rho_{gg}\right) - \frac{1}{2}\Omega_p\sigma_{sg}^* \\
0 &= -\tilde{\delta}\sigma_{sg} - \frac{1}{2}\Omega_c^*\sigma_{eg} + \frac{1}{2}\Omega_p\sigma_{es}^* \\
-\frac{1}{2}\Omega_p^* W &= -\tilde{\Delta}_p^*\sigma_{eg}^* - \frac{1}{2}\Omega_p^*\left(2\rho_{gg}+\rho_{ss}\right) - \frac{1}{2}\Omega_c^*\sigma_{sg}^* \\
-\frac{1}{2}\Omega_c^* W &= -\tilde{\Delta}_c^*\sigma_{es}^* - \frac{1}{2}\Omega_c^*\left(2\rho_{ss}+\rho_{gg}\right) - \frac{1}{2}\Omega_p^*\sigma_{sg} \\
0 &= -\tilde{\delta}^*\sigma_{sg}^* - \frac{1}{2}\Omega_c\sigma_{eg}^* + \frac{1}{2}\Omega_p^*\sigma_{es}
\end{aligned}
\tag{4.13}
$$

4.5 Analytical solution in no-population transfer approximation

This set of equations can be significantly simplified if we assume that no population transfer happens in the system. This is for example the case in systems where initially all the population is trapped in the ground state and the probe field is much weaker then the control field. Mathematically it can be described by the following inequalities: $\Omega_p << \Omega_c$, $\rho_{gg} \simeq 1 = W$, $\rho_{ss} \simeq \rho_{ee} \simeq 0$. When we also neglect all the terms nonlinear in Ω_p we obtain the following solution for σ_{eg}:

$$
\sigma_{eg} = \frac{\frac{1}{2}\Omega_p}{\left(-\tilde{\Delta}_p + \frac{\left|\frac{1}{2}\Omega_c\right|^2}{\tilde{\delta}}\right)} \tag{4.14}
$$

If we will set $\Omega_c = 0$ we obtain the expected solution for the two-level system, where the absorbtion spectra follows a Lorentzian profile.

4.6 Full solution of the density matrix equation

The 8-by-8 matrix equation 4.13 can be solved analytically, but the result is quite bulky and therefore we will solve it numerically on the desired frequency domain.

Before we proceed to the result, it is instructive to explain how to calculate photoluminescence excitation and absorbtion spectra of the system using the density matrix.

Optical photoluminescence in the three-level system can occur from the excited state and therefore is proportional to the population ρ_{ee} of this state.

On the other hand, to obtain absorbtion spectra we have to focus on the off-diagonal elements of the density matrix. First, we have to apply the inverse rotating frame transformation:

$$\rho_{eg} = \sigma_{eg} e^{-i\omega_p t} \tag{4.15}$$

Then we calculate expectation value of the dipole matrix operator by using the following relation:

$$\left\langle \hat{\mu}(t) \right\rangle = tr\left[\hat{\rho}(t)\hat{\mu}(t)\right] \tag{4.16}$$

Explicitly it is written in the following form:

$$\left\langle \hat{\mu}(t) \right\rangle = tr\left(\hat{\rho}(t)\hat{\mu}(t)\right) = \rho_{eg}\mu_{ge} + \rho_{es}\mu_{se} + c.c. \tag{4.17}$$

This expression gives us the value of the expectation value of the electric dipole of a single oscillator. To obtain the full polarization $\vec{P}(\omega_p)$ of the media we have to multiply it by the concentration of the dipoles. By using the general expression of the polarizability of the media, we can calculate the electric susceptibility $\chi(\omega)$:

$$\vec{P}(\omega) = N\left\langle \hat{\mu}(t) \right\rangle = \varepsilon_0 \chi\left(\omega_p\right)\vec{E}\left(\omega_p\right) \tag{4.18}$$

$$\chi\left(\omega_p\right) = \frac{2N}{\varepsilon_0 \vec{E}\left(\omega_p\right)}\left\langle \hat{\mu}\left(\omega_p\right)\right\rangle = \frac{2N\mu_{ge}}{\varepsilon_0 \vec{E}\left(\omega_p\right)}\sigma_{eg}\left(\omega_p\right) = \frac{2N\left|\mu_{ge}\right|^2}{\varepsilon_0 \hbar \Omega_p}\sigma_{eg}\left(\omega_p\right) \tag{4.19}$$

Note that we got rid of time dependence since the coherence of the density matrix is following the same time evolution as the probe field. We also neglected the effect of the ρ_{es} coherence, since it follows from the RWA, or in other words, it is off-resonant with the probe field.

Now we can calculate the absorbtion coefficient as:

$$\alpha\left(\omega_p\right) = \frac{\omega_p}{c} Im\left[\chi\left(\omega_p\right)\right] \tag{4.20}$$

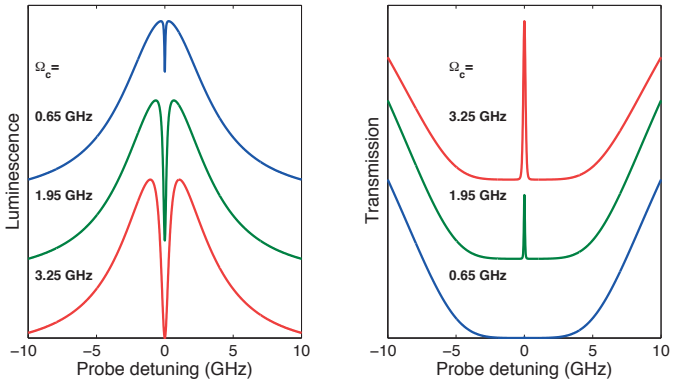

Figure 4.2: Calculated luminescence and transmission spectra of the three level system with interaction parameters close to those previously determined in experiments with donor bound excitons in GaAs [1].

4.7 Optical spectra of $n-GaAs$ in a strong optical driving regime

To demonstrate how to use the method described above we calculate the luminescence and the absorbtion spectra of the system of donor bound electron spins ensemble in lightly doped $GaAs$, for which we assume the parameters following [2].

The population relaxation rate from the spin-flip to the ground state $\Gamma_{sg} = (2.6\,\mu s)^{-1}$, and is mostly conducted by emitting a phonon. Therefore the inverse process is just the thermal excitation from the ground to the spin-flip state and its rate has to be weighed by the Boltzman factor $\Gamma_{gs} = \Gamma_{sg} e^{-\frac{E_{sg}}{kT}}$.

The radiative population relaxation from the excited to the spin-flip state $\Gamma_{es} = (1\ ns)^{-1}$, while radiative relaxation into the ground state $\Gamma_{eg} = 0.08\Gamma_{es}$. Because of the large energy separation we neglect thermal excitations to the excited state and set $\Gamma_{se} = \Gamma_{ge} = 0$.

The pure dephasing rate between the ground and the spin-flip state γ_s is difficult to guess, therefore we use a combined lower level dephasing rate $\gamma_{gs} = \frac{1}{2}\left(\Gamma_{gs} + \Gamma_{sg}\right) + \gamma_s = (1.7\ ns)^{-1}$ This is the value which has to be used during complex two-photon detuning.

Dephasing γ_e apparently depends strongly on the presence of the control field (probably due to a temperature effect). Therefore we define two dephasing values

$\gamma_{sa} = 4.6\ GHz$ (no field) and $\gamma_{sb} = 22\ GHz$ (with control field present). For Rabi frequency of the control field we will use $\Omega_c = 650\ MHz$. The strength of the probe field is $\Omega_p = 16\ MHz$.

Results of the spectra calculated using the density matrix equation for the case when control field is exactly on resonance is plotted on Fig. 4.2 and, as was expected, a dip in the luminescence appears and grows larger with increasing Ω_c. This effect is called coherent population trapping (CPT) and the dip in luminescence is attributed to the population being trapped in a coherent superposition of the ground and the spin-flip state, often called a dark state.

In the transmission spectra an increase in the transmission, when the probe and control fields are on resonance, is called electromagnetically induced transparency (EIT). While being a complementary effect to CPT it is usually described as a consequence of destructive interference of the transition amplitudes induced by the control and probe field on the excited state.

More detailed analysis of the properties of EIT spectra as function of the detuning and the strength of the driving field can be found elsewhere [3–5]

References

[1] K.-M. Fu, W. Yeo, S. Clark, C. Santori, C. Stanley, M. Holland, and Y. Yamamoto, *Millisecond spin-flip times of donor-bound electrons in GaAs*, Physical Review B **74**, 121304 (2006), ISSN 1098-0121.

[2] K. Fu, *Optical manipulation of electron spins bound to neutral donors in GaAs*, PhD thesis, Stanford University (2007).

[3] M. Fleischhauer, A. Imamoglu, and J. Marangos, *Electromagnetically induced transparency: Optics in coherent media*, Reviews of Modern Physics **77**, 633 (2005), ISSN 0034-6861.

[4] X. L. Liu, *Electromagnetically induced transparency with electron spins in a GaAs quantum well*, Master thesis, Rijksuniversiteit Groningen (2006).

[5] M. P. Bakker, *Electromagnetically induced transparency with electron spins bound to neutral Si donors in GaAs*, Master thesis, Rijksuniversiteit Groningen (2010).

Chapter 5

Polarization-preserving confocal microscope for optical experiments in a dilution refrigerator with high magnetic field

We present the design and operation of a fiber-based cryogenic confocal microscope. It is designed as a compact cold-finger that fits inside the bore of a superconducting magnet, and which is a modular unit that can be easily swapped between use in a dilution refrigerator and other cryostats. We aimed at application in quantum optical experiments with electron spins in semiconductors and the design has been optimized for driving with, and detection of optical fields with well-defined polarizations. This was implemented with optical access via a polarization maintaining fiber together with Voigt geometry at the cold finger, which circumvents Faraday rotations in the optical components in high magnetic fields. Our unit is versatile for use in experiments that measure photoluminescence, reflection, or transmission, as we demonstrate with a quantum optical experiment with an ensemble of donor-bound electrons in a thin GaAs film.

5.1 Introduction

Fundamental research on quantum coherence in solid state is currently strongly driven by the goal to implement quantum information tasks [1–3]. Electron and hole spins in semiconductors are here of special interest since these material systems give access to realizing compact devices where quantum correlations between coherence of spins and optical signal fields can be established. However, optical manipulation and detection of spins is a challenging task since experiments demand a combination of conflicting requirements such as cryogenic temperatures, high optical intensities, high magnetic fields, and precise control of the optical polarizations.

In recent years research in this direction nevertheless developed into a very active field that showed many impressive results, in particular with localized spins in quantum dots or spins bound to donor sites [4–12]. Most of these experiments were carried out at temperatures of a few Kelvin. Lower temperatures were till now typically not useful since spin states can be prepared via optical pumping, and the coherence of localized spins is in all III-V and most II-VI semiconductors limited by hyperfine coupling to fluctuating nuclear spins. We anticipate, however, that dephasing by nuclear spins can be removed with controlled dynamical nuclear polarization effects [10, 12] or with spin echo techniques [13]. If such techniques are fully exploited, optical experiments at milliKelvin temperatures become of interest, since freezing out the phonons at energies of the Zeeman splitting of electron or hole spins will be important for exploring the ultimate limit of controlling spin coherence in solid state. We report here the design and operation of a fiber-based confocal microscope in a dilution refrigerator that is suited for this research. This instrument also has relevance for related quantum optical studies with spin coherence of quantum Hall states [14, 15], or optical studies of the Kondo effect [16–18].

When designing optical experiments in a dilution refrigerator one has to deal with a number of restrictions. (*i*) The sample space is typically inside a series of heat shields that forbid free-space optical access to the sample. The sample volume can be reached with optical fibers, but this requires a method to couple light from the fiber to the sample. (*ii*) The limited sample volume requires compact solutions which can withstand cryogenic temperatures and high magnetic fields. (*iii*) Using high optical intensities is in conflict with the need to maintain low power dissipation. High intensity at low optical power can obviously be realized with tight focussing, but this requires a microscope with good performance in the sample volume. (*iv*) If the experiments require well-defined polarizations, one needs to deal with the fact that in high fields most optical components will cause a substantial Faraday rotation of the polarization.

To address all these constraints we build on an earlier design of a fiber-based confocal microscope for use at 4.2 Kelvin [19, 20]. Our key innovations are that we circumvent Faraday rotations by using a polarization maintaining fiber and by using a compact cryogenic microscope with all propagation through free-space elements in a direction that is orthogonal to the magnetic field. In addition, we make the approach suited for application at milliKelvin temperatures and we report how we deal with stronger constraints for the heat load from various functions, as for example the wiring to piezo motors that drive the microscope focussing.

We demonstrate application of the microscope on an ensemble of donor-bound electrons in a thin GaAs film. We performed optical spectroscopy of spin-selective transitions of the donor-bound electron states to donor-bound trion states, both via photoluminescence and in direct transmission experiments. We also directly demonstrate a quantum optical effect, known as electromagnetically induced transparency, with this material system.

5.2 Microscope design and operation

5.2.1 Modular compact microscope unit

We designed the confocal microscope as a compact cold-finger that fits inside the bore of a superconducting magnet, and which is a modular unit that can be easily swapped between use in a dilution refrigerator (Leiden Cryogenics DRS1000) and a helium bath cryostat. Both systems are equipped with a superconducting magnet (Cryogenics Ltd.), with a bore that yields a cylindrical sample space of 60 mm diameter (for the dilution refrigerator this concerns a 78 mm bore with a series of heat shields around the sample volume). In both cryostats the magnetic field is applied along the vertical direction (defined as z-direction).

5.2.2 Polarization maintaining fiber

For delivering light into the sample volume we use a single-mode polarization-maintaining PANDA-type fiber [21] (PMF) with $NA = 0.13$. Its mode-field diameter is 5 μm and the cut-off wavelength is 700 nm. Operation of the PMF is based on built-in stress that induces a linear birefringence (different index of refraction, n_V and n_H) for two TEM propagation modes with orthogonal linear polarizations. Linear light coupled into one of these two modes does not couple into the other mode during propagation. We apply this for delivering fields with polarization parallel (defined as V polarization) and orthogonal (defined as H polarization) to the magnetic field.

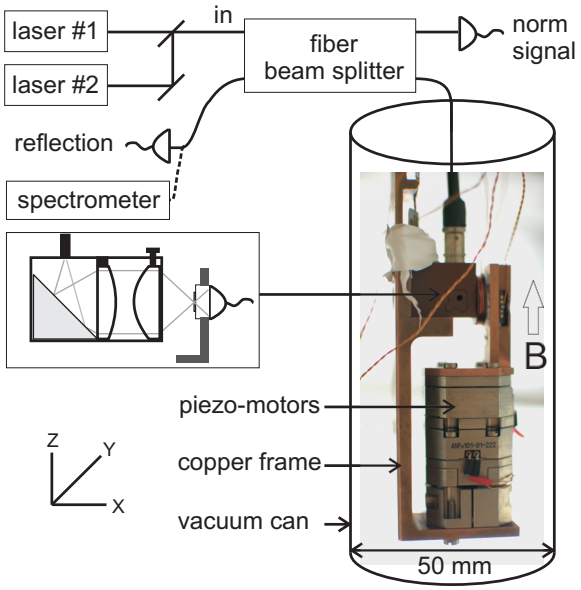

Figure 5.1: Schematics of the experimental setup. Excitation light of two tunable lasers is coupled into a polarization-preserving fiber-based beam splitter (port IN) and one of the outputs is connected to the fiber that runs to the microscope. This fiber delivers excitation light to the sample, which is mounted on an xyz-stack of piezo-motors. The sample position can be tuned to be in or out of the focal spot of the two-lens microscope. The microscope is mounted in a tube, which is vacuum pumped and immersed in a Helium bath (4.2 K) or used in a dilution refrigerator. A superconducting coil provides magnetic fields up to 9 T. A silicon *pin*-photodetector is positioned right behind the sample for detection of the optical transmission. Both the sample and the detector are mounted on a Γ-shaped sample holder. The second output of the beam splitter is coupled to a photodetector for monitoring the optical powers. Signals that come from reflection on the sample, as well as emission by the sample, retraces the optical path through the fiber. After passing the beam splitter is can be diverted to a regular photodetector, or to a spectrometer. Inset: microscope components mounted on the copper frame that forms the cold finger.

Using a PMF has the advantage that we can deliver well-defined polarizations that remain pure in the field range -9 T to +9 T. This removes the need for *in-situ* polarization analysis for calibrating and pre-compensating Faraday rotations and other effects that influence the polarizations [19]. In addition, the polarizations remain pure when the fiber is subject to stress from bending and thermal gradients, and the polarization purity is thereby also more resilient against mechanical vibrations.

To evaluate whether the PMF will indeed suppress all Faraday rotations in fields up to ±9 T we need to compare the stress induced birefringence to the Faraday effect. This can be quantified by comparing the associated beat length and rotation length, respectively. If linearly polarized light is coupled into the PMF but not along one of the TEM eigenmodes, its polarization will undergo periodic unitary transformation due to the difference between n_V and n_H. The period of transformation is the linear birefringence length L_{LB} (the smaller L_{LB}, the better the polarization maintaining properties of the fiber). For the fiber in use [21] $L_{LB} = 2.4$ mm. The Faraday effect occurs when an optical fiber is a subject to magnetic field along its optical axis. It then shows circular birefringence and its strength is characterized by the Verdet constant. This yields a circular birefringence rotation length $L_{CB} = 2\pi/(V \cdot B) \approx 4$ cm for a magnetic field $B = 9$ T and with the Verdet constant of the fiber [21] $V = 6$ rad T^{-1}m^{-1}. Our fiber thus has $L_{LB} < L_{CB}$ and we therefore expect that linear polarization of light coupled into one of the fiber TEM eigenmodes will not be affected by magnetic field. We do check that this is indeed the case by using polarization selective optical transitions of donor-bound electrons as a polarization probe (further discussed in Sec. 5.3).

The single-mode nature of the PMF is useful for experiments where two co-propagating fields should drive the same system. The beam overlap for these two fields will then be ideal in the sample volume.

5.2.3 Confocal microscope in Voigt geometry

To focus light from the fiber in the sample volume we use a compact home-built microscope objective, based on two aspheric lenses. The approach is similar to the system used by A. Högele [19] *et al.*, but we incorporated changes that avoid circular birefringence that occurs when light propagates through lens material in high fields. This can rotate linear polarizations by several degrees in 1 mm lens material in a 9 T magnetic field [22] (typical values for the Verdet constant of materials [23, 24] as BK7 and Corning glass are 1–10 rad T^{-1}m^{-1}). Before light is collimated and focused its propagation direction is diverted 90^o by means of a surface mirror (dielectric prism, Thorlabs MRA05-E02) after which its $\vec{k}$-vector is orthogonal to the direction of the magnetic field and this eliminates the magnetic field induced

rotation of the polarization.

Another advantage of this approach is that it gives access to optical experiments in Voigt geometry (light propagation direction orthogonal to the magnetic field direction). In this geometry, light with V polarization can drive atomic π-transitions (no change in angular momentum), and light with H polarization can drive atomic σ-transitions (a change in angular momentum of $\pm\hbar$). Thus, this yields that for the typical optical selection rules of electron spins in semiconductors, transitions that start from the electron spin-up or spin-down state can be addressed selectively with two orthogonal linear polarizations. Another advantage is that one of these two fields can be easily blocked by polarization filtering before the two co-propagating modes reach a detector (as required for several resonant-Raman control schemes [25]). Such a filter with high extinction ratio can be realized before any propagation through glass material as a metal nanowire-grid polarizer on a transparent substrate [26].

The first lens of the microscope objective collimates the light from the fiber. We use an aspheric lens (Thorlabs 350430) with focal length $f = 5.0$ mm, numerical aperture $NA = 0.15$ and clear aperture 1.5 mm. After collimating, light is focused by a second aspheric lens (Thorlabs 350140) with focal distance $f = 1.45$ mm, $NA = 0.55$ mm and clear aperture 1.6 mm. Since we do not have perfect NA matching between the fiber and the collimating lens, the numerical aperture of the full objective system will be less than that of the focusing lens, resulting in $NA_{obj} = 0.45$. Using this we can estimate the theoretical value for the spot diameter to be $D_{spot} = 1.42 \cdot \lambda$.

The prism mirror and the collimating lens are firmly glued into a DuPont Vespel-SP1 housing. This material was chosen (instead of copper for example) since its thermal expansion is smaller, and also lies closer to that of the lenses [1]. The focusing lens is fixed inside a separate Vespel-SP1 frame and then fitted into the housing of the objective. This allows for removing the focusing lens from the objective while aligning the fiber with respect to the collimating lens. In addition, the focussing lens has a certain positioning freedom (along the propagation direction, about 1 mm). This can be used to fit in a plastic thin-film $\lambda/4$ retardation plate, which can be used if one wishes to transform the linear polarizations into circular polarizations.

[1] As was pointed out by the referee, our information about the thermal expansion coefficients was not completely correct and the real numbers demonstrate that the thermal expansion coefficient of DuPont Vespel-SP1 is, according to the brochure of DuPont, is $45 \cdot 10^{-6}\mathrm{K}^{-1}$ while copper and BK7 have a thermal expansion coefficient of $16 \cdot 10^{-6}\mathrm{K}^{-1}$ and $7 \cdot 10^{-6}\mathrm{K}^{-1}$, respectively, i.e, copper should be better than SP1.

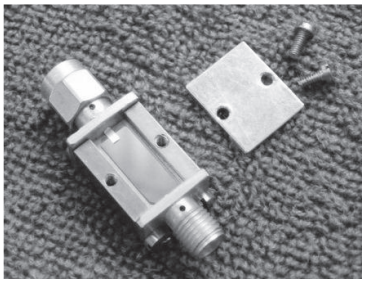

Figure 5.2: Photo of a home-built heat-sink for use in cryogenic coaxial lines, with SMA connectors and a gold-plated sapphire substrate in a copper housing unit.

5.2.4 Focussing mechanics and wiring to the piezo motors

For positioning the sample in the focus of the objective we use a three-axes xyz-translation stage on the cold finger in the form of slip-stick piezo-motors (Attocube, model ANP101). This gives a travel range of 5 mm in all three directions. Both the piezo stack and the objective are fixed on a home-built copper frame (Fig. 5.1).

Applying such piezo motors in a dilution refrigerator is not straightforward since the wires to the motors should have a resistance of 5 Ω at most. In the dilution refrigerator the length of the wires exceeds a few meters, such that wires with low resistivity must be used. This, however, creates an unacceptable heat load on the mixing chamber with most types of wiring. We circumvented this problem by using coaxial lines with low DC resistance values. This works very well since the need for the low resistance values is partly driven by the need for high bandwidth for getting triangular control pulses (~100 V) with a fast edge to the piezo-motors without much smoothing.

We implemented this by installing a set of 7 of multi-purpose coaxial lines to the mixing chamber (Micro-Coax, semi-rigid model UT 85-B-SS, 60 GHz bandwidth, stainless steel outer conductor, silver-plated BeCu inner conductor, ~0.5 Ωm^{-1} DC resistance). These have an excellent trade-off between low electrical resistance and low thermal conductance at low temperatures. The piezo-motors use 3 of these coaxial lines.

Realizing a low heat load on the mixing chamber still requires to heat-sink the inner conductor of the coaxial lines at several stages between room temperature and base temperature. We use home-built heat sinks at 4.2 K, the 1K-pot (~1.5 K), the still (~600 mK), the cold plate (~100 mK) and at the mixing chamber. The heat sinks are made with sapphire substrates in a copper housing unit (Fig. 5.2),

since sapphire combines high electrical resistance with good thermal conductivity at low temperatures. We gold-plated one of the surfaces of the sapphire. The non-plated sapphire surface is then glued onto a copper plane in the housing unit with thin stycast. Two SMA connectors are then mounted on this unit, and we solder the inner conductors on opposite sides of the gold plated sapphire surface. Our units show more than sufficient bandwidth (a few MHz) for the piezo-motor application, but this can be increased by engineering the sapphire plates as microwave strip lines. After installing these coaxial lines we did not observe an effect on the cooling power of the dilution refrigerator (base temperature well below 20 mK), and we achieved driving of the piezo-motors via these coaxial lines without any problems.

5.2.5 Optical detection and cooling down procedure

For optical detection in transmission experiments we use a photodiode (Hamamatsu, pin, 5106) on the Γ-shaped copper sample holder that is mounted on the piezo-motor stack (Fig. 5.1). The sample can be mounted in front of the photodiode. The detection of signals from reflection and photoluminescence experiments is discussed below.

The use of the photodiode on the cold finger shows in practice the risk that it breaks while cooling down the system. Most likely, this is because thermal shrinking causes a crack in the plastic laminate of the diode that also breaks the semiconductor chip underneath. To avoid this, we cool down with He contact gas at a pressure which does not exceed 10^{-2} mbar. This enforces the system to cool very slowly (in about 6 hours). With this approach, our photodiodes survive in 9 out of 10 cases.

5.2.6 Focal plane positioning and spot size

Since we do not have direct free optical access to the system, it is necessary to design a procedure for positioning and focussing that rely on using the transmitted and reflected signal only. For positioning in the plane orthogonal to the optical axis, we use the trivial approach with high-contrast markers on the sample that can be detected in the transmission signal. For positioning the sample plane in the focal point of the objective (along x-axis), we use the fact that the output of the fiber and the objective unit together constitute a confocal microscope. We use this in a procedure with a fiber-coupled diode laser (Thorlabs LPS-785-FC) operated below the lasing threshold (incoherent light for avoiding interferences in the back-reflected signal). The light is delivered into the sample volume via the optical fiber, with a fiber-based beam splitter (OZ optics) in its path (Fig. 5.1). This allows for

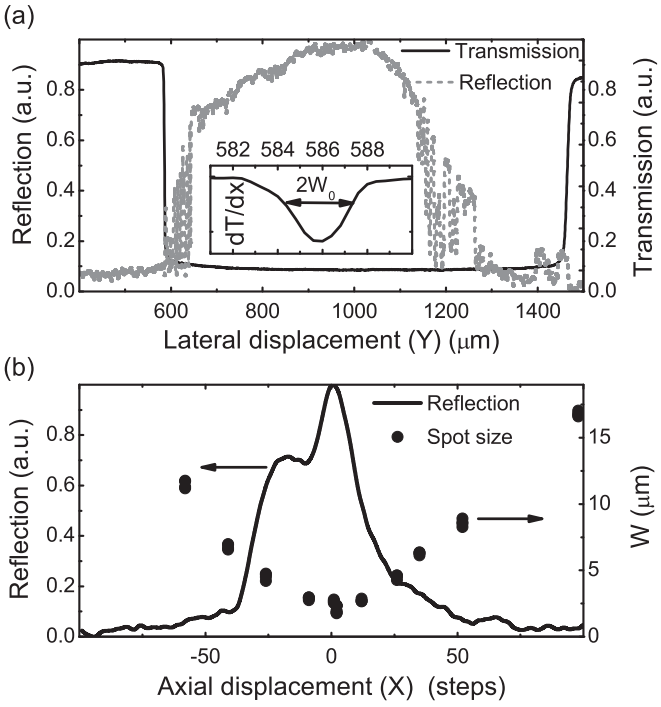

Figure 5.3: (a) Reflected and transmitted signal as a function of the lateral position (y-axis) of the sample. The spot size W of the beam on the sample surface (waist W_0 when in focus) is determined with the knife-edge technique (inset). (b) Reflected signal (solid line) and the spot size W (dots) as a function of the axial displacement (x-axis) of the sample.

measuring the reflected signal while the position of the sample surface is scanned along the x-axis through the focus of the objective.

A typical focal plane scan is shown in Fig. 5.3(b). As expected, the reflected signal reaches a maximum when the sample plane is positioned exactly in the focus of the objective and drops smoothly while going out of focus. In contrast to the previously reported microscopes [19] we observe not a single Lorentzian reflection profile but a superposition of two Lorentzians, which indicates a small misalignment within the confocal microscope. This is most likely due to a non-uniaxial arrangement of the lenses with respect to the optical axis of the fiber that results from a small misalignment of the prism mirror. We did not correct this for the

data presented here since we have the prism mirror firmly glued in the objective housing, and it did not compromise the experiments we present below.

To determine the spot size we use the knife-edge technique, where we fix the axial position (along the x-axis) of the microscope at different locations on the reflection curve (Fig. 5.3(b)) and perform a lateral scan (y-direction) across the sample. A typical scan, taken with the sample plane in focus, is shown in the Fig. 5.3(a). The solid black curve is the transmitted signal and the dashed gray curve is the reflected signal. As expected, a high signal level in reflection corresponds to low signal level in transmission since we use here an n-GaAs sample that is opaque for the used wavelength, on a transparent substrate. Light that is reflected from the sample surface is efficiently collected back into the fiber because of the confocal geometry. The reflection profile is also influenced by the morphology of the sample surface, which is not uniform due to fabrication imperfections. It is, however, always possible to find a spot on the sample with a clean reflection profile.

Since we know the size of the sample we can calculate the lateral (y-axis) step size of the piezo-motors (which depends on temperature and mechanical load). From the slope of the transmission signal when scanning across a sharp edge we can determine the spot size of the beam (inset of the Fig. 5.3(a)). We define the spot size on the surface of the sample as the radius W of a Gaussian beam (waist W_0 when in focus). The black dots in the Fig. 5.3(b) are results for W after fitting the knife-edge profile with a Gaussian function.

The measured beam waist was found to be $W_0 = 2.3$ μm, which is almost four times larger than our theoretical estimate for the diffraction limited spot size. This is related to the small misalignment, since the aspheric lenses are highly optimized for realizing a small focus exactly on the optical access, and with correcting the alignment this type of objective at low temperatures can yield a spot size that is well within a factor 2 from the diffraction limit [19]. The larger spot was compromising the efficiency of collecting light in our photoluminescence experiments, but it did not compromise our transmission experiments (further discussed below). In the transmission experiments we also work at least a small amount out of focus in order to eliminate interference effects that occur when working in focus. These then result from the Fabry-Perot cavity that is formed between the sample surface and the facet of the fiber output.

5.3 Characterization of performance

A characterization of the focussing protocol and the spot size was already included in the previous section. In this section we focus on the polarization purity and achieving a low heat load and good heat-sinking on the cold finger.

5.3.1 Polarization purity

In order to characterize the polarization preserving properties of the setup we used the optical transitions of donor-bound electrons (D^0 system) to a donor-bound trion state (the lowest level of the D^0X complex) in a strong magnetic field. Our sample was a thin GaAs epilayer with Si doping at very low concentration (further discussed below). The relevant level scheme with transitions labeled A and A^* is presented in Fig. 5.4(a). The states $|\uparrow\rangle$ and $|\downarrow\rangle$ are the spin-up and spin-down state of the electron in the D^0 system, which is localized at the donor site in a Hydrogen-like $1s$ orbital. These two states are Zeeman-split by the applied magnetic field. The optical transitions A and A^* are to the lowest energy level of the D^0X system (state $|e\rangle$, well separated from the next level $|e'\rangle$), which has two electrons in a singlet state and a spin-down hole with $m_h = -\frac{1}{2}$ localized at the donor site [13]. The optical selection rules of this system have been characterized very well [27] and show a strong polarization dependence. For the D^0 system, H-polarized light couples to the A^* transition (with a change in angular momentum of $\hbar$) but not to the A transition. In contrast, V-polarized light couples to the A transition (and not to A^*), since this is a transition without a change in angular momentum.

For performing this test we took scanning-probe transmission spectra with tunable CW Ti:sapphire lasers (Coherent MBR-110, linewidth below 1 MHz) around the D^0X resonances (Fig. 5.4(b,c)). These spectra are results of pump-assisted transmission spectroscopy. This approach is needed for avoiding bleaching of transitions due to optical pumping by the probe, and it is also useful for identifying whether spectral lines are from transitions that start from $|\uparrow\rangle$ or from $|\downarrow\rangle$. For further explanation it is best to focus on a typical result (Fig. 5.4(c)): Here, we fixed the pump laser on the frequency of the A^* transition with H polarization, while we scan the probe laser frequency with V polarization and study its transmission. We then observe that the absorption of the A transition is strongly enhanced by the pump (compare to absorption by A in Fig. 5.4(b)). These results appear with respect to a background signal with slower modulation of the transmission that is due to a Fabry-Perot effect in the sample (further discussed below). In these experiments we use a chopper in the probe beam and lock-in techniques for separating the detected signal from the pump and probe beam.

The strong polarization dependence of the absorption lines A and A^* in the transmission spectra in Fig. 5.4(b,c) demonstrates that the linear polarizations H and V are indeed well preserved in our setup. We performed such experiments with magnetic fields in the range from $B = 5$ to 9 T, and the effective polarization selectivity did not show a dependence on B. We analyzed that in our experiments the characterization of the polarization purity is in fact limited by the accuracy of the polarization preparation on the optical table, and the alignment of the H and

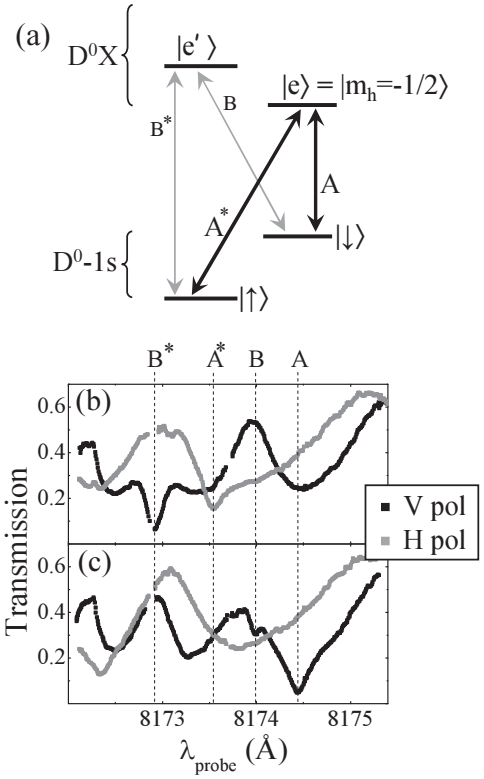

Figure 5.4: (a) Energy level diagram and optical transitions for the D^0-D^0X system in GaAs. (b) Pump-assisted spectroscopy with pumping V-polarized light at the A transition (at 8174.45 Å). This results in enhanced absorption for H-polarized light at the A^* transition (8173.55 Å). (c) Complementary to the observation of (b), pumping with H-polarized light at the A^* transitions results in enhanced absorption for V-polarized light at the A transition. Similar cross-pumping effects are observed for the nearby B and B^* transitions. Data taken at $B = 8$ T.

V mode of the PMF fiber output with respect to the direction of the magnetic field. Characterizing this with all instrumentation at room temperature showed that the error from coupling light purely into one of the eigenmodes of the PMF is at the level of 1 part in 100. In our experiment this was sufficiently low, evidenced by the fact that an attempt to pump transition A with H-polarized light did not induce any changes in the transmission spectrum from such pump-assisted spectroscopy.

Later in this thesis (Chapter 6 and 7) we use the pump assisted spectroscopy

technique for identifying the optical transitions of the Λ system and optical polarization selection rules associated with them.

For characterizing the polarizations we could not implement the approach of A. Högele *et al.* [19] with cryogenic polarizing beam splitters near the sample volume. Our sample space is too small, and it would also be difficult to deal with Faraday rotations in the beam splitter cube itself.

5.3.2 Heat load and heat-sinking of optical power

With our unit installed in the dilution refrigerator, we could cool down to milliKelvin temperatures without any problems, and running the optical experiments with typical conditions did not show excessive heating. In particular, in the next section we discuss experiments in which we drive the A transition with optical Rabi frequencies Ω_c up to $2\pi \cdot 2$ GHz. We performed this with a spot size as large as 200 μm^2, where this driving corresponds to an optical heat load of 20 μW. This is well below the cooling power of our dilution refrigerator at 100 mK.

Obviously, the semiconductor material in the focus of the optical fields can be at a much higher temperature than the mixing chamber material. We indeed found that it is crucial to thoroughly heat-sink our n-GaAs epilayers. The only experiments where we could avoid this heating used n-GaAs epilayers that were directly attached to a sapphire substrate with binding by van der Waals forces, and a good thermal contact between the sapphire and the cold finger. These samples were prepared by first using an epitaxial lift-off technique [28] for removing the GaAs epilayers from the original GaAs wafer. This was followed by transferring the epilayer to a wedged sapphire substrate.

While we thus successfully operated this unit at sub-Kelvin temperatures, the experimental data did not show features that differed from the 4.2 K data. For the experiments on D^0 system that we present below, this could be expected. The optical transitions at 4.2 K show an inhomogeneous linewidth of 6 GHz, which is not expected to narrow at lower temperatures. Also, the electron spin dephasing time for the D^0 system is limited by hyperfine coupling to fluctuating nuclear spins, and this mechanism is temperature independent in the range 10 mK to 4.2 K. Our attempts to suppress these fluctuations via dynamical nuclear polarization (DNP) only showed a very small improvement of the dephasing time till now, since the optically induced DNP effects appeared to be very weak in our experiments [29]. For the discussion of applications of our system we therefore focus on data taken at 4.2 K.

5.4 Application: Spectroscopy and EIT with n-GaAs

In order to demonstrate the versatility of our setup we performed an optical study of the coherent properties of an ensemble of D^0 systems in GaAs. This system was already introduced in Sec. 5.3.1. We present here data from epitaxially grown 10 μm films of GaAs with Si doping at $n_{Si} = 3 \times 10^{13}$ cm^{-3}. At such low concentrations the wavefunction of the neighboring donors do not overlap, which yields an ensemble of non-interacting D^0 systems.

To study the coherent properties of such ensembles we first find the spectral position of the relevant optical transitions [30] with photoluminescence and transmission spectroscopy. We then resolve the fine spectra of the Zeeman-split levels [27] with the pump-assisted transmission spectroscopy. After identifying the D^0-D^0X system in this manner, we could demonstrate electromagnetically induced transparency [31] (EIT) with this medium, which is a quantum optical effect that uses the D^0 spin coherence.

5.4.1 Photoluminescence

We performed photoluminescence experiments to identify the spectral region where emission by the donor-bound excitons occurs. We brought excitation light (wavelength λ = 8050 Å) to the sample with a fiber-based beam splitter in the optical path (Fig. 5.1). The reflection channel of the beam splitter is coupled to a PI Acton spectrometer, equipped with a nitrogen cooled CCD camera. The light at the excitation wavelength was suppressed by passing the reflected signal through a bandpass filter (λ_c = 8200 Å, $\Delta\lambda$ = 100 Å). The sample surface was positioned in the focus of the confocal microscope in order to maximize efficiency of the luminescence collection.

A typical photoluminescence spectrum taken at B = 5 T is shown in Fig. 5.5. The spectrum is dominated by three structured peaks, which result from emission by free excitons (X), excitons bound to neutral donor sites (D^0X), and excitons bound to ionized donor sites in the sample's depletion layer near the surface (D^+X). The fine structure due to the Zeeman splitting of the electron and hole spins of the (D^0X) and (D^+X) bound excitons is observed, but does not provide sufficient information for identifying all the transitions due to the highly unequal oscillator strengths [4].

5.4.2 Transmission spectroscopy

While photoluminescence is useful for initial characterization of a material and for finding the main spectral features, a more detailed characterization of the D^0 sys-

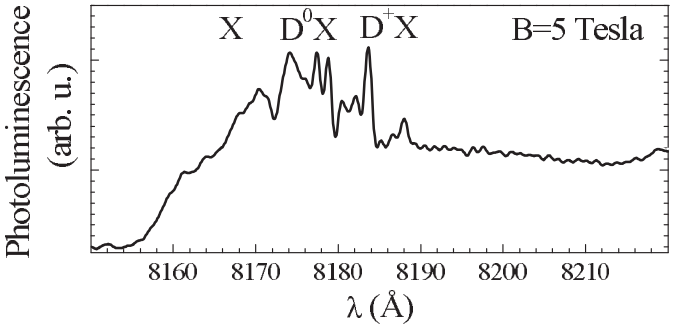

Figure 5.5: Photoluminescence spectrum of low-doped n-GaAs, showing luminescence by free excitons (X), excitons bound to neutral donor sites (D^0X), and excitons bound to ionized donor sites in the sample's depletion layer (D^+X). Data taken at $B = 5$ T, the resolution of the spectrometer is ~ 0.2 Å.

tems requires transmission spectroscopy with tunable CW lasers. A few results of this approach were already presented in Fig. 5.4 and discussed in Sec. 5.3.1. Before performing such pump-assisted transmission spectroscopy on the D^0 systems, we first take scans with a single laser over a much larger wavelength region for finding the D^0 lines. Figure 5.6(a,b) show such transmission spectra taken with H and V-polarized probe light. These results show a strong free-exciton absorption band (labeled X), and weaker D^0X resonances. The oscillating background that is superimposed on the transmission spectra is due to a Fabry-Perot effect in the 10 μm GaAs film, and its chirped wavelength dependence is due to the wavelength-dependent refractive index associated with the strong free exciton absorption. After locating the D^0 lines, we zoom in on this region for identifying the A and A^* transitions with the pump-assisted spectroscopy, as presented in Fig. 5.4(b,c).

5.4.3 Electromagnetically induced transparency with donor-bound electrons

We identified the A and A^* transitions because it was our goal to investigate whether these could be used for implementing electromagnetically induced transparency (EIT) with electron spin coherence in a semiconductor. EIT is the phenomenon that an absorbing optical transition becomes transparent because destructive quantum interference with another driven optical transition prohibits populating the optically excited state [31]. This phenomenon lies at the heart of various quantum-

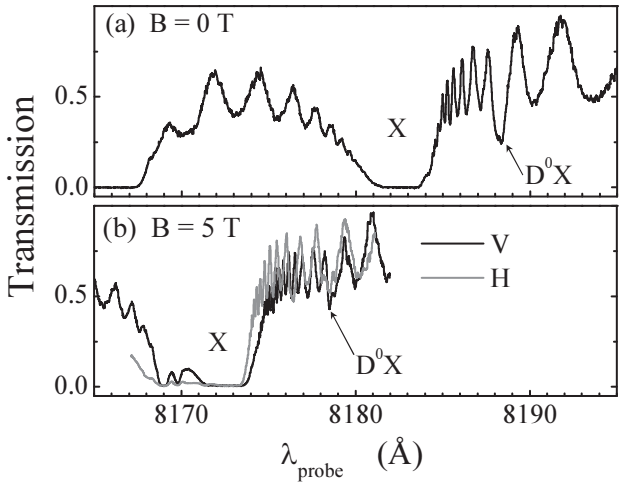

Figure 5.6: Scanning-probe transmission spectra taken at B = 0 T (a) and B = 5 T (b). Traces were recorded with linear H or V polarization for the probe light (giving identical results at 0 T). For performing these experiments the microscope was defocussed to a spot diameter of about 16 μm. The strong absorption due to free excitons (X) and much weaker features due to donor-bound excitons (D^0X) are labeled. The data at 5 T shows a diamagnetic shift of about 10 Å with respect to the data at 0 T.

optical control schemes that have been designed for preparing nonlocal entanglement between spins, quantum communication, and applying strong optical nonlinearities [25, 31].

EIT can occur with three-level systems as formed by the states $|\uparrow\rangle$, $|\downarrow\rangle$ and $|e\rangle$ (Fig. 5.4(a)), for which it is then essential that the two low-energy spin states can have a long-lived quantum coherence and that one can selectively address the two optical transitions. An ensemble of these systems can become transparent for a probe field that drives one of the transitions (in our case A^*) when this meets the condition for a two-photon Raman resonance with an applied control field (in our case driving of transition A). Under these conditions the systems are trapped in a dark state which is in the ideal case $(\Omega_c|\uparrow\rangle - \Omega_p|\downarrow\rangle)/\sqrt{|\Omega_c|^2+|\Omega_p|^2}$, where Ω_c and Ω_p are the Rabi transition frequencies of the control and probe field [31, 32]. Photoluminescence studies on GaAs already showed that optical control can prepare D^0 systems in this dark state [4].

We could demonstrate EIT, and typical results are presented in Fig. 5.7. For these results we fixed the control laser on resonance with the A transition (V polarization), while the probe laser is scanned across the A^* transition (H polariza-

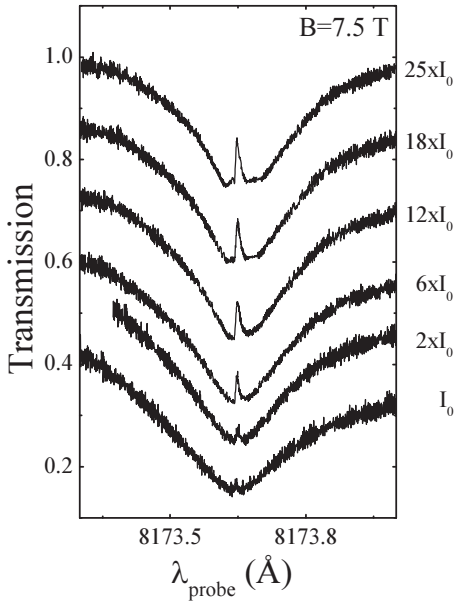

Figure 5.7: Electromagnetically induced transparency within the A^* absorption dip, induced by a strong control field that addresses the A transition. Spectra are taken for different intensities I of the control field, with $I_0 = 0.4$ Wcm^{-2}. Traces are offset vertically for clarity.

tion) and we measure its transmission. When the control and probe field meet the condition for two-photon Raman resonance (the difference in photon energy exactly matches the D^0 spin splitting), a narrow peak with enhanced transmission appears inside the broader A^* absorption dip. This is the fingerprint of EIT. In Fig. 5.7 we present traces for various intensities of the control field. We observe a wider and higher EIT peak for stronger driving with the control field, in agreement with theory for EIT.

EIT relies on quantum coherence between the electron spin states, and in systems with a very long electron spin dephasing time T_2^* EIT can fully suppress absorption. The EIT peak then reaches up to ideal transmission. The EIT peaks in Fig. 5.7 are clearly lower, even in the trace for the strongest control field. From fitting these EIT traces to the established theory [31] we derive that the T_2^* value for our system is about 2 ns, and this compromises the EIT peak height. This T_2^* value is consistent with earlier work [4, 13] that showed that electron spin dephasing results from hyperfine coupling between each electron spin and $\sim 10^5$ fluctu-

ating nuclear spins (the D^0 systems have a ~ 10 nm Bohr radius). Our EIT studies also showed weak signatures of dynamical nuclear polarization (DNP) which confirmed the role of nuclear spin fluctuations. We anticipate that T_2^* can be enhanced with controlled DNP effects that suppress the nuclear spin fluctuations. A longer account of this EIT study can be found in Ref. [29] and in Chapter 6.

5.5 Summary

We presented the realization of a fiber-based confocal microscope that can be used in a dilution refrigerator (base temperature well below 20 mK) with high magnetic field. Faraday rotations in optical materials were circumvented by using a polarization maintaining fiber and by having the light propagation in the sample volume in a direction orthogonal to the applied magnetic field. This also gives access to performing experiments in Voigt geometry, which has several advantages. With experiments on an ensemble of donor-bound electrons in GaAs we confirmed the ability to focus optical control fields with a small spot on any desired point of a sample. We also confirmed that pure linear polarizations can be delivered to the sample, and that this instrument can perform optical experiments at milliKelvin temperatures without excessive heating.

5.6 Acknowledgements

We thank B. Wolfs, A. Slachter, M. Schenkel, J. Sloot and A. Onur for contributions, and J. De Hosson and D. Vainchtein for lending of a spectrometer. Financial support by the Dutch NWO and FOM, and the German programs DFG-SPP 1285, BMBF nanoQUIT and Research school of Ruhr-Universität Bochum is acknowledged.

References

[1] D. D. Awschalom, D. Loss, and N. Samarth, *Semiconductor Spintronics and Quantum Computation* (Springer Verlag, Berlin, 2002).

[2] P. Zoller, T. Beth, D. Binosi, R. Blatt1, H. Briegel, D. Bruss, T. Calarco, J. Cirac, D. Deutsch, E. J., et al., Eur. Phys. J. D **36** (2005).

[3] K. Southwell, *Special issue on quantum coherence*, Nature **453**, 1003 (2008).

[4] K.-M. Fu, C. Santori, C. Stanley, M. Holland, and Y. Yamamoto, *Coherent Population Trapping of Electron Spins in a High-Purity n-Type GaAs Semiconductor*, Physical Review Letters **95**, 187405 (2005), ISSN 0031-9007.

[5] M. Atatüre, J. Dreiser, A. Badolato, and A. Imamoglu, *Observation of Faraday rotation from a single confined spin*, Nature Physics **3**, 101 (2007), ISSN 1745-2473.

[6] K.-M. C. Fu, S. M. Clark, C. Santori, C. R. Stanley, M. C. Holland, and Y. Yamamoto, *Ultrafast control of donor-bound electron spins with single detuned optical pulses*, Nature Physics **4**, 780 (2008), ISSN 1745-2473.

[7] D. Press, T. D. Ladd, B. Zhang, and Y. Yamamoto, *Complete quantum control of a single quantum dot spin using ultrafast optical pulses.*, Nature **456**, 218 (2008), ISSN 1476-4687.

[8] J. Berezovsky, M. H. Mikkelsen, N. G. Stoltz, L. A. Coldren, and D. D. Awschalom, *Picosecond coherent optical manipulation of a single electron spin in a quantum dot.*, Science (New York, N.Y.) **320**, 349 (2008), ISSN 1095-9203.

[9] A. Greilich, S. E. Economou, S. Spatzek, D. R. Yakovlev, D. Reuter, A. D. Wieck, T. L. Reinecke, and M. Bayer, *Ultrafast optical rotations of electron spins in quantum dots*, Nature Physics **5**, 262 (2009), ISSN 1745-2473.

[10] X. Xu, W. Yao, B. Sun, D. G. Steel, D. Gammon, A. S. Bracker, and L. J. Sham, *Optically controlled locking of the nuclear field via coherent dark-state spectroscopy.*, Nature **459**, 1105 (2009), ISSN 1476-4687.

[11] D. Brunner, B. D. Gerardot, P. A. Dalgarno, G. Wüst, K. Karrai, N. G. Stoltz, P. M. Petroff, and R. J. Warburton, *A coherent single-hole spin in a semiconductor.*, Science (New York, N.Y.) **325**, 70 (2009), ISSN 1095-9203.

[12] C. Latta, A. Hogele, Y. Zhao, A. N. Vamivakas, P. Maletinsky, M. Kroner, J. Dreiser, I. Carusotto, A. Badolato, D. Schuh, et al., *Confluence of resonant laser excitation and bidirectional quantum-dot nuclear-spin polarization*, Nature Physics **5**, 758 (2009), ISSN 1745-2473.

[13] S. Clark, K.-M. Fu, Q. Zhang, T. Ladd, C. Stanley, and Y. Yamamoto, *Ultrafast Optical Spin Echo for Electron Spins in Semiconductors*, Physical Review Letters **102**, 247601 (2009), ISSN 0031-9007.

[14] C. H. van der Wal and M. Sladkov, *Towards quantum optics and entanglement with electron spin ensembles in semiconductors*, Solid State Sciences **11**, 935 (2009), ISSN 12932558.

[15] A. Imamoglu, *Electromagnetically induced transparency with two dimensional electron spins*, Optics Communications **179**, 179 (2000), ISSN 00304018.

[16] H. Türeci, M. Hanl, M. Claassen, A. Weichselbaum, T. Hecht, B. Braunecker, A. Govorov, L. Glazman, J. von Delft, and A. Imamoglu, arXiv: 0907.3854 (2009).

[17] N. A. J. M. Kleemans, J. van Bree, A. O. Govorov, J. G. Keizer, G. J. Hamhuis, R. Notzel, A. U. Silov, and P. M. Koenraad, *Many-body exciton states in self-assembled quantum dots coupled to a Fermi sea*, Nature Physics **6**, 534 (2010).

[18] C. Latta and et al., to be published (2010).

[19] A. Högele, S. Seidl, M. Kroner, K. Karrai, C. Schulhauser, O. Sqalli, J. Scrimgeour, and R. J. Warburton, *Fiber-based confocal microscope for cryogenic spectroscopy.*, The Review of scientific instruments **79**, 023709 (2008), ISSN 0034-6748.

[20] P. J. Rizo, A. Pugzlys, J. Liu, D. Reuter, A. D. Wieck, C. H. van der Wal, and P. H. M. van Loosdrecht, *Compact cryogenic Kerr microscope for time-resolved studies of electron spin transport in microstructures.*, The Review of scientific instruments **79**, 123904 (2008), ISSN 1089-7623.

[21] Purchased and data sheet from Schäfter und Kirchhoff (Germany), *(http://www.sukhamburg.de)*.

[22] E. Munin, J. Roversi, and A. Villaverde, *Faraday effect and energy gap in optical materials*, Journal of Physics D: Applied Physics **25**, 1635 (1992).

[23] V. K. Valev, J. Wouters, and T. Verbiest, *Precise measurements of Faraday rotation using ac magnetic fields*, American Journal of Physics **76**, 626 (2008), ISSN 00029505.

[24] C. C. Robinson, *The Faraday Rotation of Diamagnetic Glasses from 0334 μ to 19 μ*, Applied Optics **3**, 1163 (1964), ISSN 0003-6935.

[25] L. M. Duan, M. D. Lukin, J. I. Cirac, and P. Zoller, *Long-distance quantum communication with atomic ensembles and linear optics.*, Nature **414**, 413 (2001), ISSN 0028-0836.

[26] J. J. Wang, L. Chen, X. Liu, P. Sciortino, F. Liu, F. Walters, and X. Deng, *30-nm-wide aluminum nanowire grid for ultrahigh contrast and transmittance polarizers made by UV-nanoimprint lithography*, Applied Physics Letters **89**, 141105 (2006), ISSN 00036951.

[27] V. A. Karasyuk, D. G. S. Beckett, M. K. Nissen, A. Villemaire, T. W. Steiner, and M. L. W. Thewalt, *Fourier-transform magnetophotoluminescence spectroscopy of donor-bound excitons in GaAs*, Physical Review B **49**, 16381 (1994), ISSN 0163-1829.

[28] E. Yablonovitch, T. Gmitter, J. Harbison, and R. Bhat, *Extreme selectivity in the lift-off of epitaxial GaAs films*, Applied Physics Letters **51**, 2222 (1987).

[29] M. Sladkov, A. U. Chaubal, M. P. Bakker, A. R. Onur, D. Reuter, A. D. Wieck, and C. H. van der Wal, *Electromagnetically Induced Transparency with an Ensemble of Donor-Bound Electron Spins in a Semiconductor*, Phys. Rev. B **82**, 121308(R) (2010).

[30] E. Bogardus and H. Bebb, *Bound-Exciton, Free-Exciton, Band-Acceptor, Donor-Acceptor, and Auger Recombination in GaAs*, Physical Review **176**, 993 (1968), ISSN 0031-899X.

[31] M. Fleischhauer, A. Imamoglu, and J. Marangos, *Electromagnetically induced transparency: Optics in coherent media*, Reviews of Modern Physics **77**, 633 (2005), ISSN 0034-6861.

[32] T. Wang, R. Rajapakse, and S. Yelin, *Electromagnetically induced transparency and slow light with n-doped GaAs*, Optics Communications **272**, 154 (2007), ISSN 00304018.

Chapter 6

Electromagnetically induced transparency in low-doped n-GaAs

We present measurements of electromagnetically induced transparency with an ensemble of donor-bound electrons in low-doped n-GaAs. We used optical transitions from the Zeeman-split electron spin states to a bound trion state in samples with optical densities of 0.3 and 1.0. The electron spin dephasing time $T_2^* \approx 2$ ns *was limited by hyperfine coupling to fluctuating nuclear spins. We also observe signatures of dynamical nuclear polarization, but find these effects to be much weaker than in experiments that use electron spin resonance and related experiments with quantum dots.* [1]

[1] The content of this chapter have been published in Physical Review B 82, 121308(R), 2010

6.1 Introduction

A localized electronic spin in a semiconductor is a promising candidate for implementing quantum information tasks in solid state. Optical manipulation of single-electron and single-hole systems has been realized with quantum dots [1–5] and by using donor atoms that are not ionized at low temperature (D^0 systems) [6–8]. These results illustrate the potential of quantum-optical control schemes that come within reach when adapting techniques from the field of atomic physics. An advantage of the D^0 systems over dots is that these can be operated as an ensemble with very little inhomogeneity for the optical transition energies. Such ensembles at high optical density are key for robust quantum-optical control schemes that have been designed for preparing nonlocal entanglement between spins, quantum communication, and applying strong optical nonlinearities [9, 10]. A critical step toward implementing these schemes is the realization of electromagnetically induced transparency (EIT). We present here measurements of EIT with an ensemble of donor-bound electron spins in low-doped n-GaAs, in samples with optical densities of 0.3 and 1.0 [11]. We build on an earlier indirect observation of coherent population trapping with this system [6]. Extending this to a direct realization of EIT with an optically dense medium is essential for getting access to strong field-matter interactions without using optical cavities, and for the application and study of transmitted signal fields [9, 10].

We implemented EIT in its most typical form where a spin-up and a spin-down state ($|\uparrow\rangle$ and $|\downarrow\rangle$ of the electron in the D^0 system) have an optical transition to the same excited state $|e\rangle$ (Fig. 6.1(e)). We Zeeman-split the states $|\uparrow\rangle$ and $|\downarrow\rangle$ with an applied magnetic field. For the state $|e\rangle$ we used the lowest energy level of a donor-bound trion system (D^0X, with two electrons in a singlet state and a spin-down hole with $m_h = -\frac{1}{2}$ [8] localized at the donor site). EIT is then the phenomenon that absorbtion by one of the optical transitions is suppressed because destructive quantum interference with the other transition prohibits populating the state $|e\rangle$. The D^0 systems are then trapped in a dark state that is in the ideal case a coherent superposition of the states $|\uparrow\rangle$ and $|\downarrow\rangle$ only [6, 11]. This state is proportional to $\Omega_c|\uparrow\rangle - \Omega_p|\downarrow\rangle$, with Ω_c and Ω_p the Rabi frequencies of the control and probe field that drive the two transitions [10].

We present results of implementing EIT in GaAs, and we studied the interactions between the solid-state environment and driving EIT. In particular, the D^0 systems have a single electron in a hydrogen-like $1s$ wavefunction with a Bohr radius of ~ 10 nm, and each electron spin has hyperfine coupling to $\sim 10^5$ fluctuating nuclear spins. We studied how this limits the electron spin dephasing time and how driving EIT can result in dynamical nuclear polarization (DNP). In addition,

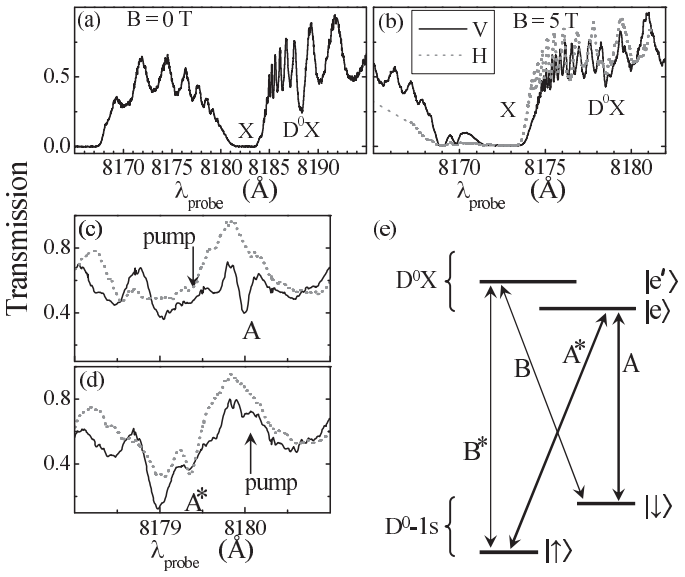

Figure 6.1: (a) Transmission spectroscopy at $B = 0$ T. (b) Transmission at $B = 5.0$ T for H and V polarization. (c) Pump-assisted spectroscopy with H-polarized pumping at the A^* transition shows enhanced absorption for the A transition for the scan with a V-polarized probe (solid line), but not with an H-polarized probe (dashed trace). (d) Complementary to (c), V-polarized pumping at A shows enhanced absorption for the A^* transition with an H-polarized probe. (e) Energy levels and optical transitions of the D^0-D^0X system.

we find that it is crucial to suppress heating effects from the nearby free exciton resonance, and demonstrate that with direct heat sinking of GaAs layers EIT can be driven with $\Omega_c/2\pi$ up to 2 GHz, while keeping the spin dephasing time $T_2^* \approx 2$ ns near the level that results from the nuclear spin fluctuations.

6.2 Samples preparation and measurements technique

We used epitaxially grown GaAs films of 10 μm thickness with Si doping at $n_{\mathrm{Si}} = 3 \times 10^{13}$ and 1×10^{14} cm^{-3}. At these concentrations the wavefunctions of neighboring donor sites do not overlap, which yields an ensemble of non-interacting D^0 systems. The films were transferred to a wedged sapphire substrate with an epitaxial lift-off process [12], and fixed there by Van der Waals forces which assures

high heat sinking. The sapphire substrate was mounted on the copper cold finger of a bath cryostat (4.2 K) in the center of a superconducting magnet with fields B up to 8 T in the plane of the sample (z-direction). Laser light was brought to the films at normal incidence (Voigt geometry) via a polarization-maintaining single-mode fiber. The two linear polarizations supported by the fiber are set parallel (V polarization) and orthogonal (H polarization) to the applied magnetic field. The V polarization can drive π transitions (no change of z-angular momentum) and the H polarization can drive transitions with a change in z-angular momentum of $\pm\hbar$.

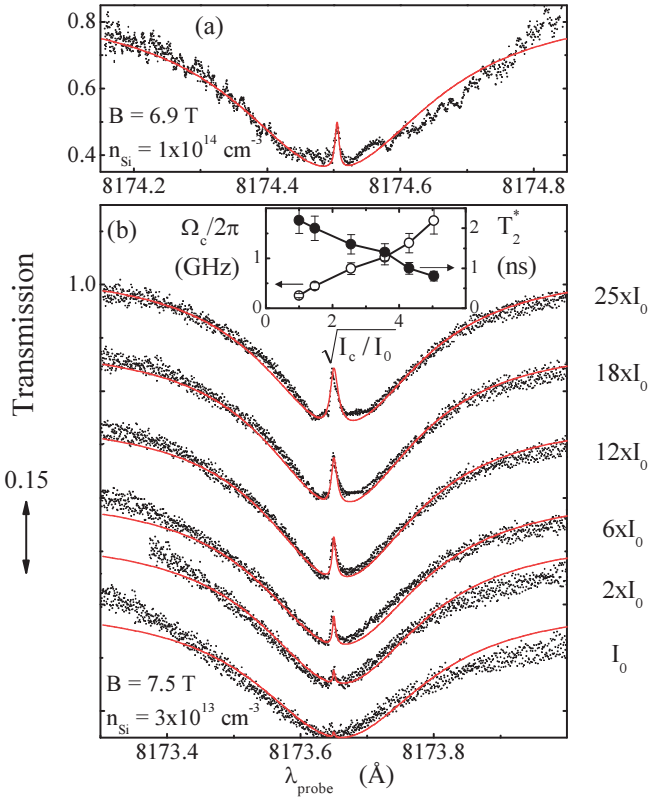

Figure 6.2: (a) EIT spectrum from sample with Si doping at 1×10^{14} cm^{-3}. Dots - experiment. Line - numerical fit. (b) EIT spectra from sample with Si doping at 3×10^{13} cm^{-3}, for probe-field intensity 0.04 Wcm^{-2} and a range of control-field intensities I_c with $I_0 = 0.4$ Wcm^{-2}. The inset shows the fitting results for Rabi frequency Ω_c and spin dephasing time T_2^*.

Two CW Ti:sapphire lasers (Coherent MBR-110, linewidth below 1 MHz) provided tunable probe and control fields. Focussing in the sample volume was achieved with a piezo-motor controlled confocal microscope. During transmission experiments we defocussed the microscope to a spot of ~16 μm diameter to avoid interference effects from the cavity that is formed between the sample surface and the facet of the fiber. The probe field was amplitude modulated at 6 kHz and we used lock-in techniques for detecting light that is transmitted through the sample with a photodiode directly behind the sample. The signal due to unmodulated control field is rejected by AC coupling of the measurement electronics.

6.3 Transmission spectroscopy

We first report transmission experiments that identify the spectral position of the D^0X related resonances. Only the probe laser was used. Figure 6.1(a) shows a spectrum taken at $B = 0$ T (identical result for H and V polarization), and Fig. 6.1(b) shows a result for $B = 5.0$ T with a separate trace for H and V polarization. The strong absorbtion labeled X is due to excitation of free excitons. Resonant absorption by donor-bound excitons (D^0X) occurs at 8187.5 Å for $B = 0$ T and at 8179.5 Å for $B = 5.0$ T. The shift of the resonances with magnetic field is the diamagnetic shift. The spacing of 5 Å between the X and D^0X resonances is in good agreement with previously reported binding energies [13, 14]. The oscillating background superimposed on the resonances is due to a Fabry-Perot effect in the GaAs film, and its chirped wavelength dependence around X is due to the wavelength dependent refractive index that is associated with the strong free exciton absorption.

6.4 Pump assisted transmission spectroscopy

For identifying the A and A^* transitions of Fig. 6.1(e) within the fine structure of D^0X spectra at high fields we performed scanning-probe laser spectroscopy while the control laser is applied for optical pumping of a particular D^0X transition (this also eliminates bleaching by the probe). Figure 6.1(c) shows spectra obtained with pumping at A^* (8179.3 Å) with H polarization. This leads to enhanced absorbtion at the A resonance (8180.0 Å) for the probe scan with V polarization. The complementary experiment with pumping V-polarized light into this A transition leads to enhanced absorption of H-polarized light at transition A^* (Fig. 6.1(d)). We could also perform such cross-pumping experiments using the B and B^* transitions to the level $|e'\rangle$ (the first excited state of the series of energy levels of the D^0X complex, see Fig. 6.1(e)). We thus confirmed that the pair of transitions labeled as A

and A^* address a so-called closed three-level Λ-system, and that this is the pair with lowest energies within the D^0X resonances. This interpretation is also consistent with the polarization dependence of these transitions [6, 14]. In the field range 5 to 8 T, the A and A^* transitions are spectrally well separated from the transitions B, B^*, and transitions to higher excited states of the D^0X complex. The observed D^0 Zeeman splitting corresponds to an electron g factor $|g| = 0.42$, and also agrees with previous reports [6, 14].

6.5 Demonstration of EIT

We now turn to the observation of EIT (Fig. 6.2). For these results we fixed the control laser central on the A transition (V polarization), while the probe laser is scanned across the A^* transition (H polarization). When the control and probe field meet the condition for two-photon Raman resonance (the difference in photon energy exactly matches the D^0 spin splitting), a narrow peak with enhanced transmission appears inside the broader A^* absorption dip, which is the fingerprint of EIT. In Fig. 6.2(a) this occurs inside an A^* absorption with optical density 1.0, while for the sample with $n_{\mathrm{Si}} = 3 \times 10^{13}$ cm^{-3} this is 0.3 (Fig. 6.2(b)). We further focus on this latter sample since higher resolution of the EIT spectra makes it more suited for our further studies.

The lines in Fig. 6.2 and 6.3 are results of fitting EIT spectra with the established theory [10]. This involves calculating the steady-state solution of a density-matrix equation for the three-level system, and accounts for coherent driving by the lasers and relaxation and dephasing rates between the levels. The free parameters are the inhomogeneous broadening γ_{A^*} (typically 6 GHz) for the optical transition A^*, the spin dephasing time T_2^* and the control-field induced Rabi frequency Ω_c (and $\Omega_p << \Omega_c$). The rest of the parameters are the same as in Ref. [6], and we found Ω_c always consistent with an independent estimate from the optical intensity and electric dipole moment. We note that the shape of the optical resonances generally appear to be quite asymmetric. This is caused by the presence of the Fabry-Perot interference in the sample. Since the effective period of the Fabry-Perot interference pattern is significantly larger than the line-width of the optical transition of interest we approximate the contribution of the Fabry-Perot background by a linear function of wavelength. Subtraction of this background contribution is performed for every curve prior to applying the fitting procedure. We obtain good fits and the main features in our results are consistent with EIT, as we discuss next.

Figure 6.2(b) shows EIT spectra taken at different intensities I_c of the control field, where a stronger control field yields a higher and broader EIT peak. As expected for EIT, we observe that Ω_c from fits scales linearly with $\sqrt{I_c}$ (Fig. 6.2(b),

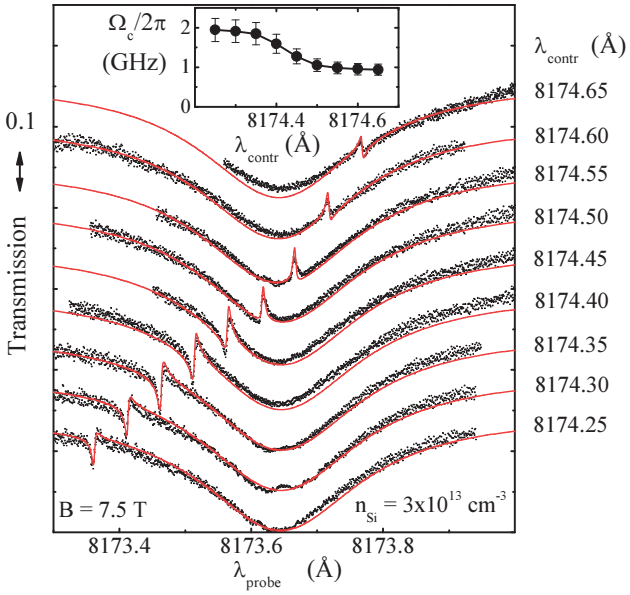

Figure 6.3: Dependence of EIT spectra on control-field detuning. The position of the EIT peak follows precisely the control-field detuning from transition *A*. Dots - experiment with control (probe) intensity 6 (0.04) Wcm^{-2}. Lines - fits with $T_2^* = 2$ ns and Ω_c as presented in the inset.

inset). The Ω_c values reach $2\pi \cdot 2$ GHz, and we could only obtain clear EIT spectra with such high Ω_c in samples with complete adhesion onto the sapphire substrate. Our results from samples with incomplete adhesion (and work with epi-layers that are not removed from the original GaAs substrate [6–8]) suffer from heating, which is observed as a broadening of the free exciton line into the region of the D^0X resonances. The values of T_2^* that we find in our experiments are discussed below.

Figure 6.3 shows how the EIT peak position depends on detuning of the control field from the *A* transition. As expected, the EIT peak follows the detuning of the control field. However, the EIT peak in the blue-detuned traces is clearly more prominent than in the red-detuned cases. We attribute this to a change in the effective Rabi frequency Ω_c that results from the weak Fabry-Perot interference within the GaAs film, and we can indeed fit the results with fixed $T_2^* = 2$ ns and varying Ω_c (Fig. 6.3, inset). We can exclude that the difference in the quality of EIT spectra is coming from optical coupling to a level outside our Λ-system, since all other transitions are well separated spectrally and in polarization dependence

(*e.g.* the B and B^* transitions, see Fig. 6.1(e)).

6.6 Spin coherence time T_2^* and signatures of Dynamic Nuclear Polarization

An important topic that needs to be addressed next with this realization of EIT concerns the influence of the hyperfine coupling between each electron spin and $\sim 10^5$ nuclear spins. A polarization of the nuclear spins acts on the electron spin as an effective magnetic field B_{nuc}. The average polarization affects the Zeeman splitting, and this can be directly observed in EIT spectra as a red (blue) shift of the EIT peak for a reduced (enhanced) Zeeman splitting. The nuclear spin fluctuations around the average dominate via this mechanism the inhomogeneous electron spin coherence time T_2^*. This is a key parameter for the shape of the EIT peak (longer T_2^* gives a sharper peak), and the magnitude of these fluctuations can therefore be derived from the EIT spectra as well. At our fields and temperature nuclear spins are in equilibrium close to full random orientation. The expected value for T_2^* for this case is ~ 2 ns [6, 15], and is in agreement with the values that we observe.

The hyperfine coupling can also result in dynamical nuclear polarization (DNP), which is the transfer of angular momentum from the electron to the nuclear spins when the electron spin is driven out of equilibrium. Earlier experiments on our type of D^0 system with microwave-driven electron spin resonance (ESR) [15] and optical experiments on quantum dots showed strong DNP [3, 5]. In both cases the effects were so strong that it gave an unstable resonance condition for tuning at ESR and EIT (the systems trigger a DNP cycle that drives them out of resonance). DNP can also result in a suppression of the nuclear spin fluctuations, which yields a longer T_2^* [2, 3, 5, 16]. Our experiment, however, only shows weak DNP. We never observed a significant change in the Zeeman energy (as derived from subtracting the probe and control photon energies at the EIT peak) from the EIT driving itself. We only observed in several data sets a moderate EIT peak narrowing over the course of a few hours of data taking (at fixed settings of the EIT parameters). In order to confirm the role of nuclear spins we carried out various attempts to induce stronger DNP effects.

An example of the strongest DNP effects that we could induce is presented in Fig. 6.4. Here we first applied strong driving of the A^* transition for 30 min with an intensity equivalent to a Rabi frequency of $2\pi \cdot 10$ GHz. This pumps the system fully into $|\downarrow\rangle$. After pumping we take fast 'snapshots' of the EIT peak (50 sec A^* scans, $\Omega_p/2\pi = 25$ MHz and control at A with $\Omega_c/2\pi = 1$ GHz). Between scans

we kept the system in the dark for 10 min. Figure 6.4 shows 6 subsequent snapshots. Right after pumping we observe a blue-shifted and sharpened EIT peak (T_2^* = 3 ns). This enhancement of T_2^* probably results from suppressed nuclear spin fluctuations, which generally occurs when the polarization gets squeezed between a polarizing and depolarizing mechanism with rates that are both enhanced due to the DNP [3, 5, 16]. The peak shift agrees in sign with Ref. [15] but corresponds to B_{nuc} = 21 mT only (the ESR studies [15] and the work on dots easily induced 200 mT - 1 T). Subsequent spectra show a clear broadening of the EIT peak, which also shifts back to the red. After about 1 hour, T_2^* (Fig. 6.4, inset) and the peak position stabilize at the values that were observed before pumping. This agrees with the relaxation time for DNP with D^0 systems [15]. Upon exploring how DNP occurs for various EIT and pump conditions we found the effects to be too weak for systematic control and drawing further conclusions, and full understanding goes beyond the scope of the present work. The work with dots showed that the mechanism that dominates the DNP rate can be complex and needs to account for driving-field assisted processes [3, 5]. We can nevertheless conclude that our spin dephasing time is indeed limited by coupling to nuclear spins.

6.7 Conclusions

In conclusion, we presented direct evidence that a D^0 ensemble in GaAs can be operated as a medium for EIT. The electron spin dephasing time limits the quality of the EIT, and is in the range $T_2^* \approx 2$ ns that results from hyperfine coupling to fluctuating nuclear spins. The EIT spectra form a sensitive probe for detecting how DNP changes the fluctuations and the average of nuclear spin polarization. However, direct optical driving of D^0 transitions yields much weaker DNP effects than in electron spin resonance experiments with D^0 systems and related EIT experiments on quantum dots, and a complete physical picture of DNP effects in our system is not available. Still, initial signatures of controlled DNP effects show that the electron spin-dephasing time can be prolonged. Our experimental approach is suited for exploring this further in conjunction with experiments that aim to implement various applications of EIT [9, 10].

References

[1] D. Press, T. D. Ladd, B. Zhang, and Y. Yamamoto, *Complete quantum control of a single quantum dot spin using ultrafast optical pulses.*, Nature **456**, 218 (2008), ISSN 1476-4687.

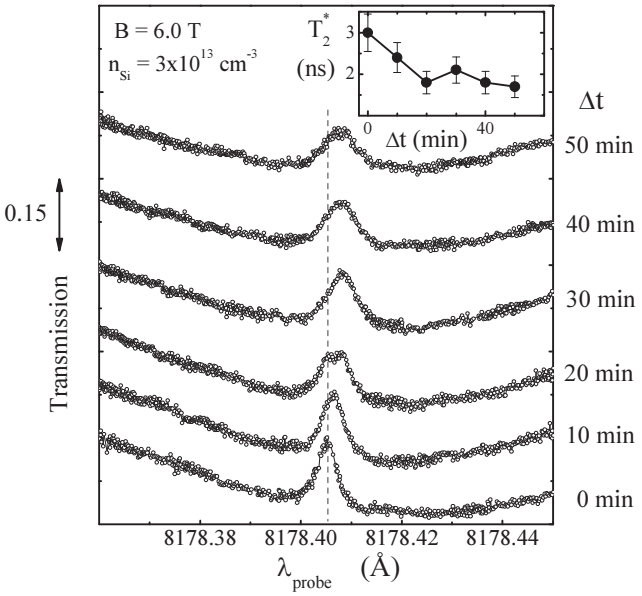

Figure 6.4: Evolution of the EIT peak after 30 min pumping of the A^* transition. Fast EIT 'snapshots' were taken at 10 min intervals during which the sample was kept in the dark. The dashed line is a guide for showing the shift in peak position. The inset presents fitting results that show the change in T_2^*.

[2] A. Greilich, S. E. Economou, S. Spatzek, D. R. Yakovlev, D. Reuter, A. D. Wieck, T. L. Reinecke, and M. Bayer, *Ultrafast optical rotations of electron spins in quantum dots*, Nature Physics **5**, 262 (2009), ISSN 1745-2473.

[3] X. Xu, W. Yao, B. Sun, D. G. Steel, D. Gammon, A. S. Bracker, and L. J. Sham, *Optically controlled locking of the nuclear field via coherent dark-state spectroscopy.*, Nature **459**, 1105 (2009), ISSN 1476-4687.

[4] D. Brunner, B. D. Gerardot, P. A. Dalgarno, G. Wüst, K. Karrai, N. G. Stoltz, P. M. Petroff, and R. J. Warburton, *A coherent single-hole spin in a semiconductor.*, Science (New York, N.Y.) **325**, 70 (2009), ISSN 1095-9203.

[5] C. Latta, A. Hogele, Y. Zhao, A. N. Vamivakas, P. Maletinsky, M. Kroner, J. Dreiser, I. Carusotto, A. Badolato, D. Schuh, et al., *Confluence of resonant laser excitation and bidirectional quantum-dot nuclear-spin polarization*, Nature Physics **5**, 758 (2009), ISSN 1745-2473.

[6] K.-M. Fu, C. Santori, C. Stanley, M. Holland, and Y. Yamamoto, *Coherent Population Trapping of Electron Spins in a High-Purity n-Type GaAs Semiconductor*, Physical Review Letters **95**, 187405 (2005), ISSN 0031-9007.

[7] K.-M. C. Fu, S. M. Clark, C. Santori, C. R. Stanley, M. C. Holland, and Y. Yamamoto, *Ultrafast control of donor-bound electron spins with single detuned optical pulses*, Nature Physics **4**, 780 (2008), ISSN 1745-2473.

[8] S. Clark, K.-M. Fu, Q. Zhang, T. Ladd, C. Stanley, and Y. Yamamoto, *Ultrafast Optical Spin Echo for Electron Spins in Semiconductors*, Physical Review Letters **102**, 247601 (2009), ISSN 0031-9007.

[9] L. M. Duan, M. D. Lukin, J. I. Cirac, and P. Zoller, *Long-distance quantum communication with atomic ensembles and linear optics.*, Nature **414**, 413 (2001), ISSN 0028-0836.

[10] M. Fleischhauer, A. Imamoglu, and J. Marangos, *Electromagnetically induced transparency: Optics in coherent media*, Reviews of Modern Physics **77**, 633 (2005), ISSN 0034-6861.

[11] T. Wang, R. Rajapakse, and S. Yelin, *Electromagnetically induced transparency and slow light with n-doped GaAs*, Optics Communications **272**, 154 (2007), ISSN 00304018.

[12] E. Yablonovitch, T. Gmitter, J. Harbison, and R. Bhat, *Extreme selectivity in the lift-off of epitaxial GaAs films*, Applied Physics Letters **51**, 2222 (1987).

[13] E. Bogardus and H. Bebb, *Bound-Exciton, Free-Exciton, Band-Acceptor, Donor-Acceptor, and Auger Recombination in GaAs*, Physical Review **176**, 993 (1968), ISSN 0031-899X.

[14] V. A. Karasyuk, D. G. S. Beckett, M. K. Nissen, A. Villemaire, T. W. Steiner, and M. L. W. Thewalt, *Fourier-transform magnetophotoluminescence spectroscopy of donor-bound excitons in GaAs*, Physical Review B **49**, 16381 (1994), ISSN 0163-1829.

[15] T. Kennedy, J. Whitaker, A. Shabaev, A. Bracker, and D. Gammon, *Detection of magnetic resonance of donor-bound electrons in GaAs by Kerr rotation*, Physical Review B **74**, 161201 (2006).

[16] I. T. Vink, K. C. Nowack, F. H. L. Koppens, J. Danon, Y. V. Nazarov, and L. M. K. Vandersypen, *Locking electron spins into magnetic resonance by electronâĂŞnuclear feedback*, Nature Physics **5**, 764 (2009), ISSN 1745-2473.

Chapter 7

Ultrafast preparation and detection of coherent dark states in low-doped n-GaAs

We report an optical pump-probe study of spin coherence of donor-bound electrons in GaAs. We find that single pump pulses prepare the spins in a coherent dark state via an ultra-fast stimulated Raman process. Two orthogonal polarization components in the pump pulses each address one leg of the Raman system. The phase and amplitude difference between these components govern which spin state is prepared, and we can prepare any superposition of spin states. This preparation occurs 1000 times faster than the system's spontaneous emission and decoherence times. The fast preparation and detection of these coherent states allows for a direct time-resolved study of the coherent dynamics and dephasing of the electron spin in this system, which is difficult to study with other optical methods.

7.1 Introduction

In order to implement quantum algorithms for computing, one has to follow the same approach as for developing a classical computer in several ways. The state upon which the quantum operation has to be performed first has to be initialized, then manipulated, and eventually read. All these three ingredients are crucial for creating an operational quantum computer, and were tackled together or separately in different physical systems with different levels of success [1]. Existing research on creating registers for quantum information includes systems where a bit of information is stored on a degree of freedom of a single particle, like the polarization state of an optical photon [2], the quantum state of a trapped atom [3], the electron spin state in a semiconductor quantum dot [4, 5], the nuclear spin state of an individual paramagnetic dopant in silicon [6], and the spin state of an NV center in diamond [7]. Other types of qubits include those that store quantum information on the state of an ensemble of particles with many degrees of freedom, as in NMR based quantum computers [8–10] and quantum computing with macroscopic states of superconducting currents in Josephson junction circuits [11].

Work on spin ensembles in n-GaAs includes successful experiments on ultrafast spin rotations by means of detuned optical pulses [12–14]. In those experiments the initial state of the spin ensemble was prepared in a pure state (ground state of the spin system) by means of optical pumping [5, 15] and then rotated using a dynamic ac-Stark shift that is caused by a detuned optical pulse [16, 17]. The spin rotation does happen on a time scale that is set by the optical Rabi frequency that is associated with the optical pulse, which can easily reach more than 100 GHz. What is limiting the overall performance in time is the preparation step, which requires a few cycles of the system's spontaneous emission time for the optical transitions. This is $T_{rad} = 1$ ns for donor-bound excitions in GaAs [18]. Much faster preparation is crucial in situations where qubits need to be re-prepared during a computation, as for example in quantum error-correction schemes.

In this Chapter we present an experiment where, by means of ultrafast optical pulses that are tuned in resonance with optical transitions, we can prepare an arbitrary coherent spin state in a donor-bound electron ensemble. The preparation occurs via a stimulated Raman process, on a time scale which is set by the optical Rabi frequency and which is about 1000 times faster than the system's radiative lifetime. In contrast to the use of detuned optical pulses for spin rotation via the ac-Stark effect, where only virtual optical transitions are excited that do not result in actual population of the optically excited state, in our scheme the resonant pulses drive strong Rabi transitions that cause actual population of the excited states. In this Chapter we study this ultra-fast preparation mechanism, and

investigate whether it can be useful in quantum information processing.

In order to study the preparation and subsequent coherent dynamics of the spin ensembles we employ the Time-Resolved Kerr Rotation (TRKR) technique [19–22]. This is widely used in studies of spin dynamics of electrons in the conduction band of semiconductors. In these studies, electron spin coherence is created with an optical pump pulse tuned at or just above the band gap, and this process injects spin-oriented photo-electrons in the conduction band. Detection in this scheme relies on the rotation of the linear polarization of a probe pulse upon reflection. This rotation is caused by the dependence of the absorbtion coefficient and the refractive index on the state of the electron spins, due to the polarization selection rules that apply for these electron-hole excitations [23]. For our experiment, we used pump pulses that are resonant with the $D^0 - D^0X$ transitions, which do not inject photo-electrons in the conduction band. We will investigate in this Chapter how the TRKR signal depends on the polarizations for pump and probe in the case of the $D^0 - D^0X$ transitions. This analysis has a close link to EIT-like physics that occurs during the presence of the optical pulses, and we find that we can prepare the ensemble in a coherent dark state that is purely determined by the polarization state of the pump pulse. We also make a first step towards explaining how the probe pulse is probing the spin coherence of these donor-bound electrons.

7.2 Spectral properties of D^0 electron spin system

The electron that is bound at a neutral donor site is described by a hydrogen-like envelope wavefunction, and the ground state has the s-type spherical symmetry. This D^0 electron has a first excited state with a p-type symmetry, and optical transitions of the $D^0 - D^0X$ type associated with this p-level of the D^0 electron are 2 nm (3.7 meV) red shifted with respect to the transitions from the $D^0 - 1s$ orbital. When a magnetic field is applied, the ground state of the D^0 is Zeeman split into $|g\rangle = |\uparrow\rangle$, characterized by the angular momentum projection quantum number $m_e = +1/2$, and $|s\rangle = |\downarrow\rangle$ with $m_e = -1/2$ for this quantum number.

In order to address the electron spin states optically we use optical transitions from the D^0 state to the donor-bound exciton state D^0X. This D^0X state consists of two electrons forming a singlet and a heavy hole, and is denoted as $|\downarrow\uparrow, m_h\rangle$. The spins of a pair of electrons in a singlet state do not contribute to angular momentum. The heavy hole has a total angular momentum of $J_h = 3/2$, and the angular momentum projection quantum number can take a value in the range $m_h = -3/2 ... + 3/2$. We again assume that a magnetic field is applied. In order to then describe the energy levels of the donor-bound exciton system (the D^0X levels

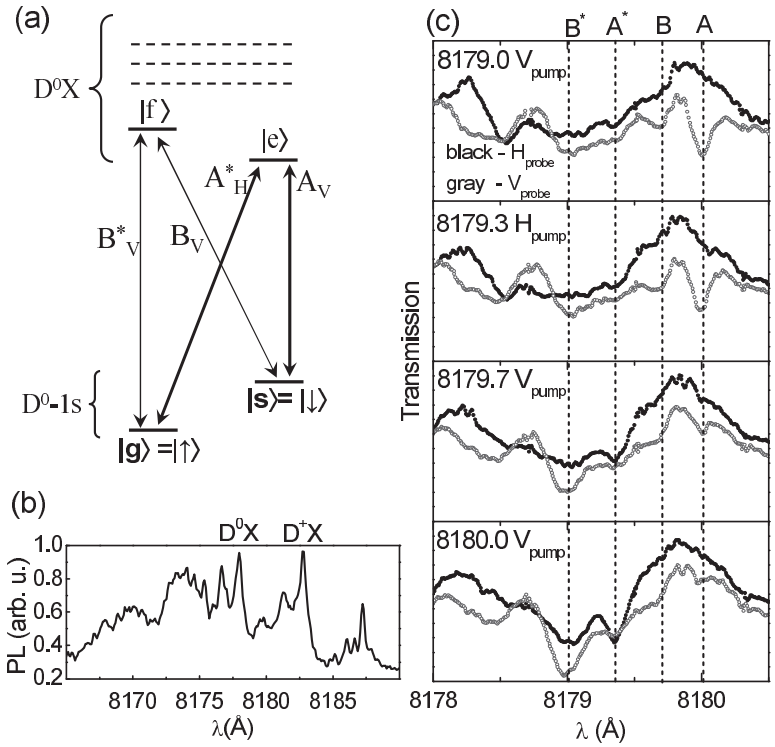

Figure 7.1: (a) The many-level system and optical transitions for the $D^0 - D^0X$ excitations in GaAs. The letter V indicates that a transition is sensitive to the vertical polarization, while the letter H indicates sensitivity to the horizontal polarization. (b) Photoluminescence collected from the n-GaAs sample in a magnetic field of $B = 7$ T. (c) Pump-assisted transmission spectroscopy of the $D^0 - D^0X$ system. The pump wavelength and polarization appear as labels in the top-left of panels. Gray (black) traces are results obtained with H (V) polarization for the probe.

in Fig. 7.1(a)), the orbital excited states of the envelope wavefunction also have to be taken in account [24]. This, in turn, leads to a very complicated level structure for the D^0X complex and there is at this stage no consensus in the community on labeling the states with angular momentum quantum numbers. From systematic magneto-luminescence studies it was concluded that the lowest level of the D^0X complex corresponds to $m_h = -3/2$, while the first excited state has $m_h = -1/2$ with the orbital quantum number $L = 1$ [24]. Other studies, however, are not uni-

vocal with these findings and are using alongside similar labeling [18] the labeling where the lowest level of the D^0X complex has $m_h = -1/2$, as in our findings (Chapter 6 and Ref. [25]), while the first excited state is reported to be $m_h = -3/2$ [26].

In general, the knowledge of the quantum numbers allows to determine polarization selection rules in optical spectra (Chapter 3). Considering, however, the ambiguity of the angular momentum quantum numbers we performed a pump-assisted optical spectroscopy experiment to determine the optical selection rules. For this experiment we used two CW wavelength-tunable lasers that have perpendicular incidence on the sample surface. The magnetic field is applied in the plane of the sample and the polarization of both lasers is chosen to be linear. When the laser light is V polarized, namely its polarization is parallel to the applied magnetic field, it induces π-type optical transitions without a change in the angular momentum quantum number, $\Delta m = 0$. When the laser light is H polarized (orthogonal to the magnetic field) it induces σ-type optical transitions with a change in angular momentum quantum number $\Delta m = \pm 1$ (Chapter 3). This is the same experiment as was described in the Chapter 6 previously.

First, we find the spectral position of the $D^0 - D^0X$ transitions by performing a photoluminescence experiment. We excited the sample above the band gap with $\lambda_{exc} = 805$ nm light and detect photoluminescence using an Acton 750 spectrometer equipped with a nitrogen cooled CCD camera. The distinct bands of the free (X), neutral donor-bound (D^0X), and charged donor-bound (D^+X) excitons are observed, as shown in Fig. 7.1(b).

For the pump-assisted transmission spectroscopy one of the CW lasers (either H or V polarized) is set to optically pump into one of the D^0X transitions, while the other CW laser scans across the region of the donor-bound exciton absorption. We collect transmission spectra in both H and V polarization, while pumping in the first four D^0X transitions (Fig. 7.1(c)). From this pump-assisted spectroscopy study we can conclude that the first four transitions arise from the level scheme depicted in Fig. 7.1(a). When pumping with V-polarized light into the transition A, which is at 8180.00 Å, we see an enhancement in absorbtion for the transition A^* at 8179.30 Å for H-polarized probe light. This pair of transitions constitutes a so-called Λ-system, which we label as $A - A^*$. In the same manner we can identify a Λ-system with the pair of transitions labeled as $B - B^*$. The fact that all four of these transitions are can be spectrally resolved, and are sensitive to either V- or H-polarization, allows for implementing control of the D^0 electron spin: The $A - A^*$ system couples the electron spin states $|\uparrow\rangle$ and $|\downarrow\rangle$ to the common excited state $|e\rangle$, while the $B - B^*$ system couples the same electron spin states to the common excited state $|f\rangle$.

Since we experimentally identified the polarization selection rules we can pro-

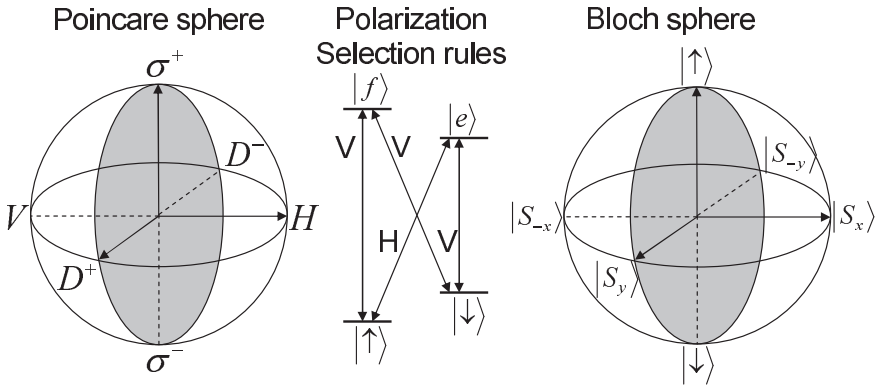

Figure 7.2: Poincare sphere for describing the light polarization state vector, and the Bloch sphere for describing the electron-spin state vector. The level scheme summarizes the polarization selection rules that determine the mapping between polarization states and spin states.

ceed with our study without having certainty about the proper labeling of angular momentum quantum numbers to the D^0X levels. For the sake of book-keeping, and based on our results, we can determine that the state $|e\rangle$ corresponds has $m_h = -1/2$. The the state $|f\rangle$ couples to both electron spin states via V-polarized transitions, and this sets a fundamental difficulty for determining its angular momentum quantum number since V-polarized light is expected to drive optical transitions with $\Delta m = 0$ (see also Chapter 3).

7.3 The coherent dark state for an electron spin in the optically driven Λ-system

In order to describe how optical orientation of the D^0 electron spin occurs while driving the $D^0 - D^0X$ transitions we have to consider the pair of transitions $A - A^*$ (or $B - B^*$) that constitute a Λ-system. We first consider two optical fields with polarizations that are chosen such that each fields is coupling to one of the optical transitions in the Λ-system. The optical Rabi frequencies of the two fields are denoted as Ω_1 and Ω_2 when both fields are on resonance with their transitions. Further, the $D^0 - D^0X$ system is characterized by a fast radiative lifetime and relatively long dephasing time for the spin in the ground state. Such a system has a

coherent dark state, which is:

$$|\Psi_{Dark}\rangle = \frac{1}{\sqrt{|\Omega_1|^2 + |\Omega_2|^2}} (\Omega_1 |\downarrow\rangle + \Omega_2 |\uparrow\rangle) \tag{7.1}$$

When the system is in this state, destructive quantum interference between the two optical transitions prohibits population of the optically excited state, as was demonstrated in the EIT experiment in Chapter 6 [25]. The system's tendency to evolve into this dark state was also observed as coherent population trapping, in spectroscopic measurements of photoluminescence from $D^0 - D^0X$ systems [18]. However, these experiment studied the steady-state response from driving with CW lasers, and do not give direct insight into the dynamics that brings the systems into this dark state, but this can be derived from the modeling that was presented in Chapter 4: If the spins are initially in a completely arbitrary but fully incoherent state, the $D^0 - D^0X$ systems will, in general, initially show some optical excitation after switching on the fields that drive the two transitions. Due to the damping of this dynamics from spontaneous emission, the system gradually evolves into the dark state, over a time scale that is a few times the spontaneous emission time (several nanoseconds). This seems to indicate that preparing an initially mixed spin state in the the dark state can not be carried with a picosecond pulse. We further comment on this after first discussing how the phase and amplitude of the two laser fields determine the actual spin orientation that corresponds to the dark state.

As can be seen from the Equation 7.1 the dark state depends solely on the phase and the amplitude of the optical Rabi frequencies of the two optical driving fields. It is easy to note that the dark state for $\Omega_1 = \Omega_2$ corresponds to maximum electron spin coherence, since it can be depicted on the electron spin Bloch sphere as a vector in the equatorial plane (Fig. 7.2). If both Ω_1 and Ω_2 are real numbers, which is equivalent to the having no phase difference between the two optical fields, the orientation of the dark state is collinear with the direction of the optical field propagation (x-direction), and results in a preparation of the spin state along the x-direction. This state is the superposition $|S_x\rangle = \frac{1}{\sqrt{2}}(|\uparrow\rangle + |\downarrow\rangle)$. In order to satisfy the condition that $\Omega_1 = \Omega_2$ on the $A - A^*$ system one optical field must have V polarization, while the other must have H polarization. Control over the amplitudes of the Rabi frequencies is done via changing the intensity of the fields. In a similar fashion one can generate a dark state that will correspond to the S_y spin state, which is the superposition $|S_y\rangle = \frac{1}{\sqrt{2}}(|\uparrow\rangle + i|\downarrow\rangle)$ superposition and therefore requires a $\pi/2$ phase shift between Ω_1 and Ω_2.

This phase shift can be controlled very well when the optical fields are derived from a single laser pulse, that is spectrally broad due to its short duration. This can

be applied when the spectral width of the pulse is larger than the Zeeman splitting of the electron spin, and when the central frequency of the pulse is such that the absolute value of the associated detunings for both transitions of the Λ-system are equal. A phase difference of 0 between Ω_1 and Ω_2 is then achieved when the laser light is linearly polarized along the direction $\frac{1}{\sqrt{2}}(H+V)$. A phase difference of $\pi/2$ between Ω_1 and Ω_2 is achieved when the laser light is $\sigma+$ polarized, since this can be presented as a superposition of the two linear polarizations as $\sigma+ = \frac{1}{\sqrt{2}}(H+iV)$.

These relations between polarization and spin orientation of the dark state can be pictured using a vector that represents the polarization on the Poincare sphere, and a similar vector for the spin state on the Bloch sphere (Fig. 7.2). This shows that by choosing the appropriate phase difference and relative amplitudes for the H and V components in a short laser pulse, the coherent dark state can correspond to any spin state of the D^0 system. The next Section discusses how this coherent dark state plays a role in the system's dynamics in response to a picosecond laser pulse.

7.4 Theory of the fast dark state preparation using picosecond optical pulses

When the $D^0 - D^0X$ system is subject to excitation by a picosecond optical pulse, the presence of the optical field during the pulse favors evolution into the dark state. We will concentrate here on the scenario where we assume a completely mixed spin state for the initial D^0 spin state, because this matches best with the experimental finding that are reported in the following Section. In this case, there is little rotational dynamics for the spin during the picosecond pulse, which would typically result in the situation that the spin orientation at the end of the pulse shows a strong dependence on the pulse area, and that is not observed (the spin part of such dynamics that occurs in parallel with coherent optical transitions is in fact precession of the spin about the axis that is defined by the dark state, such that any damping also results in evolution towards the dark state). With this assumption, a picosecond pulse can indeed show robust driving into the dark state. However, owing to the short duration of the pulse $T_{pulse} = 0.1 - 10$ ps as compared to the radiative relaxation times in the system $T_{rad} = 1$ ns, the population of the coherent dark state will still be a function of the strength of the optical field and duration of the pulse, which, as will be shown, reflects the coherent dynamics of the $D^0 - D^0X$ in a strong optical field.

In order to describe the dynamics of the $D^0 - D^0X$ system we have chosen to

solve the equation of motion for a density matrix defined on a 4-level system as in Fig .7.3: $|g\rangle$, $|s\rangle$ - electron spin states and $|e\rangle$, $|f\rangle$ - the ground and the first excited state of the D^0X complex, respectively. The 4-level system under consideration consist of the two Λ-systems labeled previously as $A-A^*$ and $B-B^*$ in Fig. 7.3. We have chosen to extend the number of levels in the present model, as compared to the 3-level model we have used for the EIT experiment (Chapter 6), because in the EIT experiment the use of CW lasers assures decoupling of the optical fields from the transitions that are outside the 3-level Λ-system. When picosecond optical pulses are used the linewidth of the laser is about $\Delta\lambda = 1$ nm, which results in coupling to several excited states of the D^0X complex. However, we restrict our analysis to a model that incorporates only 4 levels (2 for D^0 and 2 for D^0X), since this gives access to investigating the essential deviations from the dynamics of the 3-level system in a tractable manner, without too many parameters. The experimental results show in fact behavior that to a large extend matches with 3-level dynamics, with only a few small deviations. This indicates that the lowest levels of the D^0X complex are most important for the system's dynamics during a resonant optical pulse. In addition, we have indications that inter-level relaxation within the D^0X complex is very fast (further discussed below), including fast relaxation from the state $|f\rangle$ to the state $|e\rangle$, and this allows for considering the state $|f\rangle$ as one that describes effectively all the above lying states of the D^0X complex.

The equation of motion for the density matrix is:

$$\frac{d\hat{\rho}}{dt} = -\frac{i}{\hbar}\left[\hat{H}_{total}, \hat{\rho}\right] + \hat{L}\left(\hat{\rho}\right) \tag{7.2}$$

where and $\hat{H}_{total}$ is the Hamiltonian and $\hat{L}\left(\hat{\rho}\right)$ the Lindblad relaxation operator. The Hamiltonian describes the bare matter system and the driving by coherent laser fields, and will be described in the rotating frame under the rotating wave approximation (which is strictly speaking not valid in the situation that is considered, but still a good approximation because each transition most strongly responds to a fully resonant contribution in the pulse spectrum). The Hamiltonian then reads:

$$\hat{H} = \hbar \begin{pmatrix} 0 & 0 & -\Omega_1^* & -\Omega_3^* \\ 0 & \delta & -\Omega_2^* & -\Omega_4^* \\ -\Omega_1 & -\Omega_2 & \Delta_1 & 0 \\ -\Omega_3 & -\Omega_4 & 0 & \delta_{EF} \end{pmatrix} \tag{7.3}$$

where Δ_1 is the detuning of the optical field from the $g-e$ transition, δ is the two-photon detuning from the electron-Zeeman splitting and δ_{EF} is the two-photon detuning from the ground and excited state splitting of the D^0X states. Ω_1, Ω_2, Ω_3 and Ω_4 are the optical Rabi frequencies induced by the field of the optical pulse

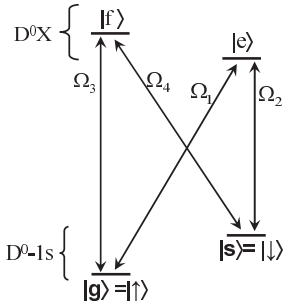

Figure 7.3: The 4-level system that is used for theoretical model

on the transitions $g-e$, $s-e$, $g-f$ and $s-f$ respectively. The optical pulse has temporal width ΔT and is assumed to be Fourier limited with a Gaussian profile characterized by the spectral width ΔE such that $\Delta E >> E_{gs} \gtrapprox E_{ef}$, where E_{gs} is the electron-spin Zeeman splitting, and E_{ef} the energy splitting between the two D^0X levels.

The relaxation operator is:

$$\hat{L}(\hat{\rho}) = \left(\begin{array}{l} -\Gamma_{gs}\rho_{gg} + \Gamma_{sg}\rho_{ss} + \Gamma_{eg}\rho_{ee} + \Gamma_{fg}\rho_{ff} \\ -\left(\left(\Gamma_{gs}+\Gamma_{sg}\right)/2+\gamma_s\right)\rho_{sg} \\ -\left(\left(\Gamma_{gs}+\Gamma_{eg}+\Gamma_{es}+\Gamma_{fe}\right)/2+\gamma_e\right)\rho_{eg} \\ -\left(\left(\Gamma_{gs}+\Gamma_{eg}+\Gamma_{es}+\Gamma_{fe}\right)/2+\gamma_f\right)\rho_{fg} \end{array} \right.$$

$$\left(\begin{array}{l} -\left(\left(\Gamma_{gs}+\Gamma_{sg}\right)/2+\gamma_s\right)\rho_{gs} \\ \Gamma_{gs}\rho_{gg} - \Gamma_{sg}\rho_{ss} + \Gamma_{es}\rho_{ee} + \Gamma_{fs}\rho_{ff} \\ -\left(\left(\Gamma_{sg}+\Gamma_{eg}+\Gamma_{es}+\Gamma_{fe}\right)/2+\gamma_e\right)\rho_{es} \\ -\left(\left(\Gamma_{gs}+\Gamma_{es}+\Gamma_{fs}+\Gamma_{fe}+\Gamma_{fg}\right)/2+\gamma_f\right)\rho_{fs} \end{array} \right.$$

$$\left(\begin{array}{l} -\left(\left(\Gamma_{gs}+\Gamma_{eg}+\Gamma_{es}\right)/2+\gamma_e\right)\rho_{ge} \\ -\left(\left(\Gamma_{sg}+\Gamma_{eg}+\Gamma_{es}\right)/2+\gamma_e\right)\rho_{se} \\ -\left(\Gamma_{eg}+\Gamma_{es}+\Gamma_{ef}\right)\rho_{ee} + \Gamma_{fe}\rho_{ff} \\ -\left(\left(\Gamma_{fe}+\Gamma_{ef}+\Gamma_{fs}+\Gamma_{fg}\right)/2+\gamma_X\right)\rho_{fe} \end{array} \right.$$

$$\left(\begin{array}{l} -\left(\left(\Gamma_{gs}+\Gamma_{eg}+\Gamma_{es}+\Gamma_{fe}\right)/2+\gamma_f\right)\rho_{gf} \\ -\left(\left(\Gamma_{gs}+\Gamma_{es}+\Gamma_{fs}+\Gamma_{fe}+\Gamma_{fg}\right)/2+\gamma_f\right)\rho_{sf} \\ -\left(\left(\Gamma_{fe}+\Gamma_{ef}+\Gamma_{fs}+\Gamma_{fg}\right)/2+\gamma_X+\right)\rho_{ef} \\ -\left(\Gamma_{fg}+\Gamma_{fs}+\Gamma_{fe}\right)\rho_{ff} + \Gamma_{ef}\rho_{ee} \end{array} \right) \quad (7.4)$$

where $\Gamma_{sg} = \left(2.6\ \mu s\right)^{-1}$ is the longitudinal spin relaxation rate, $\Gamma_{gs} = \Gamma_{sg} e^{E_{gs}/kT}$, $\Gamma_{eg} = \Gamma_{fg} = \Gamma_{es} = \Gamma_{fs} = (1\ \text{ns})^{-1}$ are the radiative relaxation rates from the D^0X levels to the D^0 spin levels, $\gamma_{gs} = (0.3\ \text{ns})^{-1}$ is the electron spin dephasing rate, which is shorter than for the EIT experiment from the Chapter 6 as a consequence of using a spectrally broad optical pulse, as will be shown at the end of this Chapter, $\gamma_{eg} = \gamma_{es} = \gamma_{fg} = \gamma_{fs} = 6$ GHz represent inhomogeneous optical broadening and $\gamma_{fe} = (1\ \text{ps})^{-1}$ is the hole spin dephasing time.

An important parameter in our model is $\Gamma_{fe} = (1\ \text{ps})^{-1}$, the rate for relaxation within the D^0X complex. We have to choose it to be very large, because, as will be shown in the experiment, with respect to the pump the system behaves like a 3-level system ($A - A^*$ part only). In order to describe response of the probe, however, all 4 levels need to be taken into account. We note that the assumption of the very fast relaxation is inconsistent with optical spectroscopy that was performed on this system since it would result in a transition linewidth as large as 1 THz, while in reality it was never observed to exceed the value of 35 GHz in the high-resolution spectroscopy experiments with CW lasers (see Chapter 6). This inconsistency disappears if one assumes that this high value $\Gamma_{fe} = (1\ \text{ps})^{-1}$ only is the relevant value during an intense picosecond optical pulse. We have, however, at this stage no knowledge to support such an assumption. This point therefore needs to be investigated in more detail in future experiments, as well as in work that improves the initial modeling that we present here.

We consider the $D^0 - D^0X$ transitions at $B = 7$ T, this gives the following wavelengths for the optical transitions: $\lambda_A = 8177.0$ Å, $\lambda_{A^*} = 8176.0$ Å, $\lambda_{B^*} = 8176.3$ Å, $\lambda_B = 8175.3$ Å.

For the numerical simulation we assume the absolute values of optical Rabi frequencies to be equal for all transitions if allowed by the polarization selection rules. The Rabi pulse follows the time profile described by a Gaussian function with temporal width $\Delta T = 5$ ps FWHM, and centered around time $t = 0$. The equation of motion for the density matrix of the 4-level system is solved numerically with the electron spin initially in a completely incoherent and depolarized state, which corresponds to $S_x = S_y = S_z = 0$.

Fig. 7.4 shows the transverse spin values S_x and S_y in units of $\hbar$ in the rotating frame as a function of time for optical excitation with three different polarizations: $D+ = \frac{1}{\sqrt{2}}(H+V)$, $\sigma+ = \frac{1}{\sqrt{2}}(H+iV)$ and V. We note that the theoretical maximum for the $S_{x,y}$ component of electron spin was chosen to be $\hbar$.

The $D+$ polarization results in the generation of a large amplitude for the spin S_x component, which was indeed expected from the analysis of the optical dark state in the previous Section. No spin amplitude S_y is generated since it requires a $\pi/2$ phase shift between the Rabi frequencies Ω_1 and Ω_2.

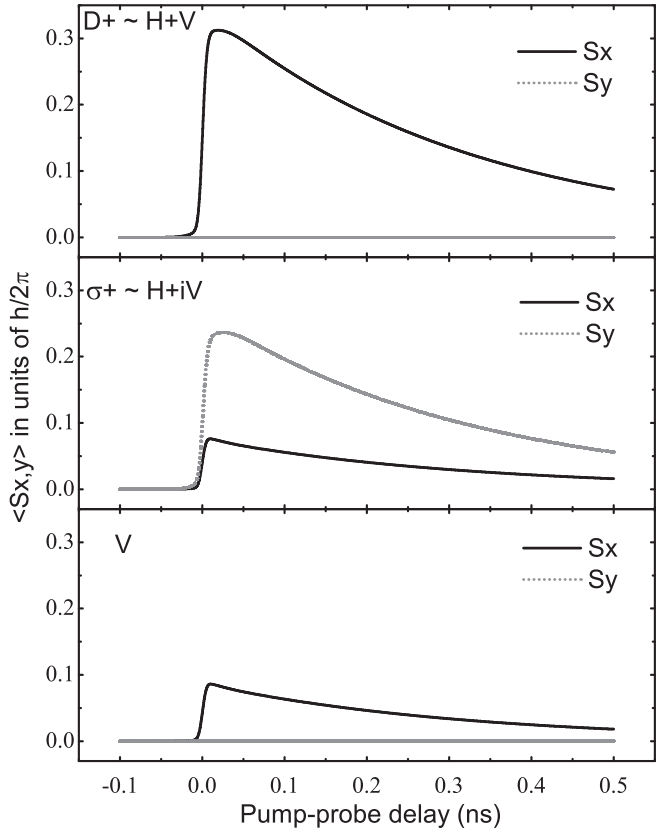

Figure 7.4: Time dependence of the transverse components S_x and S_y of the electron spin in the rotating frame after excitation with the optical pulse, for different polarizations.

In the case of $\sigma+$ polarization, based on the analysis of the optical dark state, the generation of the S_y spin dark state is expected. The simulation results indeed indicate that the S_y component is dominant. The presence of a smaller S_x result from the fact that our 4-level model consists of two Λ-systems, $A-A^*$ and $B-B^*$. Since the polarization selection rules associated with the optical transitions that constitute these two Λ-systems are different, the optical dark state that is gener-

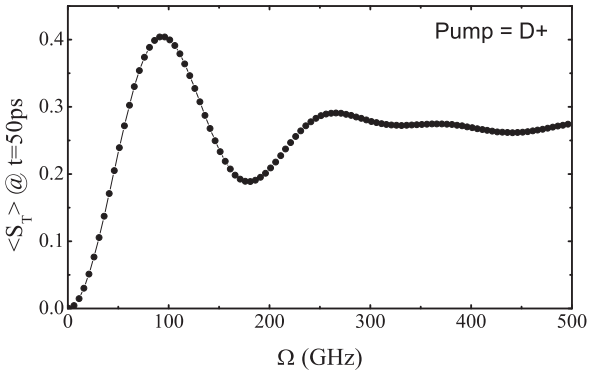

Figure 7.5: Simulation result for the amplitude of the TRKR signal at 50 ps pump-probe delay, as a function of pump pulse power (parameterized by Ω for the value of $\Omega_1 - \Omega_4$).

ated by both systems will also be different. Such, when the A-system favors the S_y spin state upon excitation with $\sigma+$ polarization, the B-system will yield a S_x spin state owing to the fact that both the B and the B^* transition couple to V polarization. The reason that the simulation results show a smaller amplitude for the S_x than the S_y component is due to the fast relaxation within the D^0X complex $\Gamma_{fe} = 1$ ps. The role of this relaxation is to "leak" the optical transition to the $A-A^*$ system which favors the pure S_y state preparation. For even larger $\Gamma_{fe} = (100\text{ fs})^{-1}$ the S_y component will virtually vanish.

Calculations for a purely V-polarized pump result in a small S_x component due to the dark state generation in the $B-B^*$ system. This component also vanishes when the Γ_{fe} relaxation rate is increased by a factor of 10.

The simulation results demonstrate that with strong optical pulses any coherent spin state can be prepared on a time scale that is much shorter than the radiative lifetime. This is a consequence of the coherent dynamics within the 4-level system. When the system is subject to excitation by an intense optical pulse, this induces optical Rabi oscillations in the 4-level system. When the area of the pulse satisfies the condition that $\int \Omega(t)dt = \pi$ (for each transition, *i.e.* $\Omega_1 - \Omega_4$) it will transfer some fraction of the spins from the completely incoherent state, via the states of donor-bound excitons, to the coherent dark state. Since it is relatively easy to induce optical Rabi frequencies that are larger then $1/T_{pulse}$, the ultra-fast population transfer to the spin dark state is possible. The simulated dependence of the transverse spin component on the Rabi frequency induced by a $D+$ polarized pump pulse is shown in Fig. 7.5. In order to achieve a maximum amplitude of the

prepared spin state either the duration or the intensity (which is experimentally is more easy to do) of the optical pulse has to be chosen such that the 4-level system undergoes exactly $(2n+1)/2$ periods of the optical Rabi oscillations.

It is important to note, that in contrast to the traditional optical pumping schemes [12, 15] that prepare spin in a pure spin up or down state, our technique allows for preparation of only a fraction of the electron spins. Inspection of the density matrix from the simulations shows that the ultra-fast preparation of the optically dark state gives a density matrix that is a linear combination of the pure coherent dark state, and a completely incoherent state with substantial population on all levels of the system. The fact that the spin ensembles can not be prepared fully in a dark state, on a timescale that is shorter then the radiative lifetime, is not necessarily a problem, since for many quantum algorithms it is not an amplitude of the coherence, but rather a fidelity with which this coherence can be prepared is important, as is well-established in the field of NMR quantum computing [10, 27].

7.5 Experiment on coherent dark state preparation with single picosecond optical pulses

In order to experimentally investigate the ultra-fast preparation of the coherent dark state in the electron spin ensembles we used the TRKR technique, which is a widely used method to study the dynamics of electron spin ensembles in the conduction band of semiconductors. In a TRKR experiment the system is excited with a polarized optical pulse, which, owing to the polarization selection rules, polarizes the electron spins system [23]. A linearly polarized probe, that comes with delay Δt after the pump arrival, is probing the remaining spin polarization via rotation of its polarization upon reflection. When the experiment is done in a magnetic field and the pump laser polarization is chosen to initially polarize electron spins with a component in the direction orthogonal to the external magnetic field, the spins will undergo a precessing motion and the response of the probe as a function of delay between pump and probe Δt will acquire an oscillatory character. While precessing, the initially polarized electron spin ensemble will be subject to energy relaxation that is characterized by the spin relaxation time T_1 and spin dephasing that is characterized by the spin dephasing time T_2^*. The "*" indicates here that it is a dephasing of the spin ensemble rather than the decoherence of an individual electron spin which loses its coherence over a time T_2.

The TRKR technique is widely used for exploring the dynamics of electron spins in the conduction band of bulk GaAs and two dimensional electron gas (2DEG) systems in GaAs/AlGaAs heterostructures [19, 21, 22]. In those experiments a cir-

cularly polarized light with a photon energy above the gap is used to polarize the electron spins in the conduction band [23]. Owing to the polarization selection rules fr bulk GaAs and 2DEG electrons, spins are being polarized along the light propagation direction, which is therefore often chosen to be orthogonal to the applied magnetic field (the so-called Voigt geometry).

It is important to note that the spin polarization due to above-gap optical excitation is a single photon process with optical generation of a free electron-hole pair. This, in turn, sets a challenge on applying a TRKR technique for studying the dynamics of the electron spins of D^0 systems, since the single photon process gives in this case excitation of the donor-bound exciton complex D^0X. Notably, this state carries no electron-spin angular momentum since the electrons form a singlet.

In order to polarize the donor-bound electron spin one has to rely on a two-photon stimulated Raman process which is the exact process that was described previously in this Chapter. Under strong excitation from a polarized optical pulse the ensemble of D^0 electron spins is polarized according to the ultra-fast dynamics of the coherent dark state preparation.

We performed our experiment using conventional [19, 22] mono-color time-resolved Kerr-rotation measurements in an optical cryostat at 4.2 K with magnetic fields (magnitude B) up to 7 T. We used a tunable Ti:sapphire laser with ~150 fs pulses at 80 MHz repetition rate. The spectrum of pulses was narrowed with a help of tunable liquid crystal Fabry-Perot filters, resulting in pulses with a spectral width $\Delta\lambda = 1$ nm and duration of approximately $T_{pulse} = 5$ ps. The central wavelength of the pulses was chosen to be close to resonance with the $D0 - D^0X$ transitions, which is $\lambda_c = 817.5$ nm at $B = 7$ T. Samples were excited at normal incidence. In initial measurements we employed a lock-in detection scheme with intensity modulation for the train of pump pulses (with an optical chopper at a few kHz), at constant pump polarization. For later measurements we used a lock-in scheme with polarization modulation for the pump, with a photoelastic modulator at 50 kHz. This yields better signal-to-noise, and we first confirmed that we could still unambiguously derive the dependence on pump polarization. We were able to modulate the polarization either between $\sigma+/\sigma-$, $D+/D-$, or H/V, in order to cover all important polarization states on the Poincare polarization sphere. This creates spin orientation for the donor-bound electrons ensemble due to the coherent-dark-state formation. The evolution of the spin ensemble is recorded by measuring the Kerr rotation of a reflected probe pulse with a polarization bridge, at the frequency of the pump modulation. Measuring this as a function of pump-probe delay Δt yields the TRKR traces. The polarization of the probe could also be chosen arbitrarily. We used spot diameters of about 100 μm, and data was taken at different pump-photon densities in order to cover a broad range of values for the

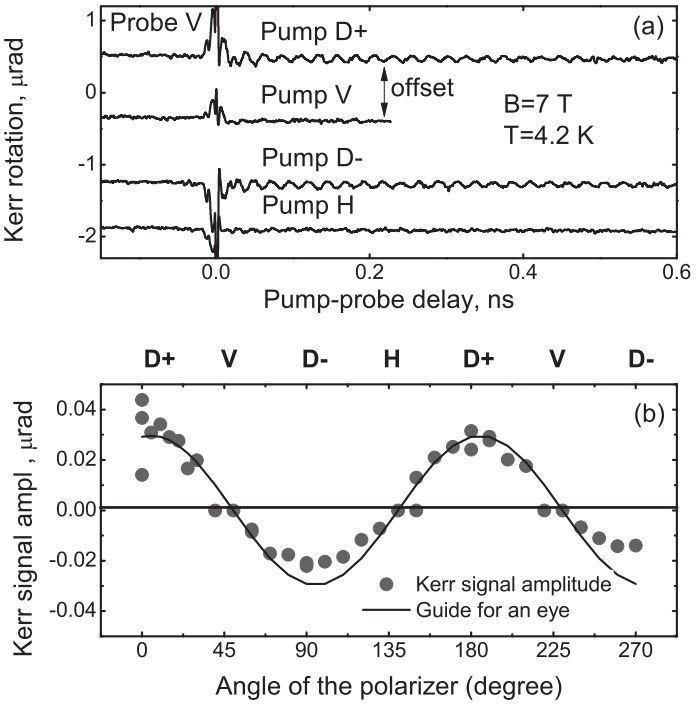

Figure 7.6: (a) TRKR signal for different polarizations of the pump pulse. The probe is V polarized. Traces are offset for clarity. (b) Amplitude of the TRKR signal as a function of the orientation of the linear polarization of the pump with respect to the applied magnetic field, expressed in degree units for the angle of the polarizer.

optical Rabi frequencies. Unless states otherwise, we present data that is taken in a field of $B = 7$ T and at a temperature of 4.2 K.

Experimental results taken on a sample with Si donors at a concentration of $n_{Si} = 3 \times 10^{13}$ cm^{-3} are shown in Fig. 7.6. Panel (a) shows the TRKR response of a V polarized probe for different linear polarizations for the pump. When the pump is $D+/D-$ polarized, it results in a non-zero oscillating Kerr amplitude, while for the H/V polarized pump no Kerr oscillations are observed. Panel (b) of Fig. 7.6 shows the full dependence of the amplitude of Kerr oscillations (evaluated around $\Delta t =$ 50 ps) as a function of the orientation of the linear polarization of the pump with respect tot the magnetic field. The observed results are in a good agreement with

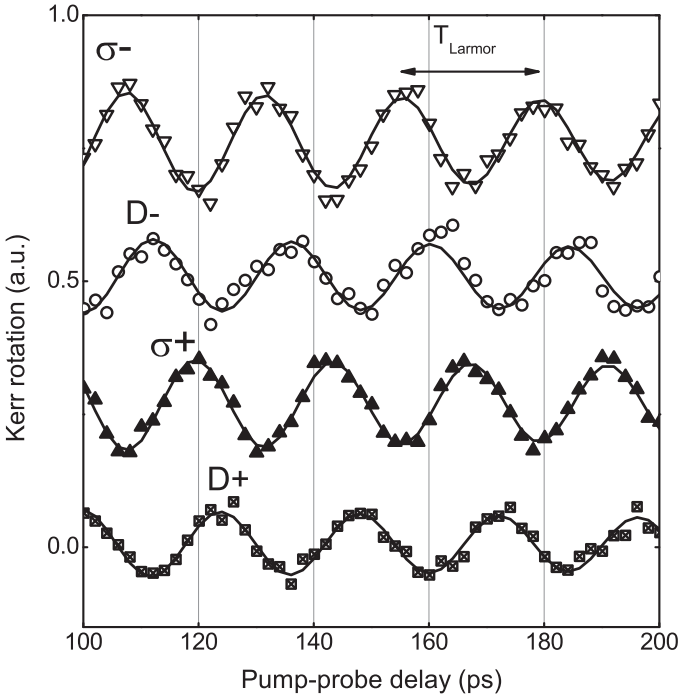

Figure 7.7: TRKR response of the D^0 spin ensemble, for different polarizations of the pump pulse. The $\pi/2$ phase difference between TRKR oscillations from pumping with $D+$ and $\sigma+$ polarization indicates the initial preparation of spin S_x and the spin S_y states, respectively. The probe was V polarized.

our theoretical description of the formation of a coherent dark state via a 2-photon stimulated Raman process, and its dependence on the polarization selection rules. For creating spin coherence in the D^0 system, the system demands both an H- and V-polarized component in the pump pulse, in order to address both electron spin states simultaneously. The fact that no spin coherence was created when pumping with V polarized light confirms our assumption that the $B-B^*$ Λ-system, which in general can lead to stimulated Raman processes with a V-polarized component of the pump only, is shunted by the fast relaxation rate Γ_{fe}.

Next we proceed with demonstrating that by controlling polarization state of the pump we can create any arbitrary spin state for the D^0 system. In the presentation we limit ourself to the generation of 4 spin states in the equatorial plane of

the Bloch sphere, which are the states of the the maximum coherence. These are the $\pm S_x$ and the $\pm S_y$ spin states, and these are the dark states for pumping with the $D+/D-$ and $\sigma+/\sigma-$ polarizations, respectively. The TRKR traces from these measurement are shown in Fig. 7.7. The phase of the oscillating TRKR traces taken at a fixed pump-probe delay ($\Delta t = 100$ ps, for example) directly reflects the initial phase of the TRKR response, and therefore the actual orientation of the coherent dark state that was prepared by the pump pulse.

The results of the experiment of Fig. 7.7 are in a good agreement with our theory for the ultrafast preparation of coherent dark states. The four optical polarizations in use, when presented on the Poincare sphere, have a phase difference $\pi/2$ between neighboring polarization vectors. The TRKR oscillation signals that correspond to these four cases demonstrate the same phase shift of $\pi/2$ for the sequence $\sigma-$, $D-$, $\sigma+$ and $D+$. This directly follow from the polarization selection rules. The $D+ = \frac{1}{\sqrt{2}}(H+V)$ polarization results in the $|S_x\rangle = \frac{1}{\sqrt{2}}(|\uparrow\rangle + |\downarrow\rangle)$ coherent dark state, the $\sigma+ = \frac{1}{\sqrt{2}}(H+iV)$ polarization on the other hand will yield the $|S_y\rangle = \frac{1}{\sqrt{2}}(|\uparrow\rangle + i|\downarrow\rangle)$ state, etc. When presented on the Bloch sphere, the phase difference between the spin states S_x and S_y is also $\pi/2$. With this experiment we therefore have demonstrated a direct mapping of the polarization state vector of the Poincare sphere onto the spin state vector of the Bloch sphere.

We also checked that the amplitude of TRKR traces is consistent with varying the relative intensity of the H and V components in the pulse, which varies the ratio $|\Omega_1|/|\Omega_2|$ for the dark state (data not shown). This gives access to preparing spin states that are tilted upward or downward from the equatorial plane of the Bloch sphere, and confirms our technique can prepare any spin state.

This technique is an interesting alternative to preparing spin states via conventional optical pumping. Firstly, it allows for direct preparation of an arbitrary state. Optical pumping can only prepare the pure spin-up or spin-down state, and needs a subsequent step with coherent spin manipulation for preparing an arbitrary state. In addition, our technique is about 1000 times faster. Conventional optical pumping requires a time that corresponds to a few cycles of the radiative lifetime $T_{rad} = 1$ ns, while our stimulated Raman technique can be realized with an optical pulse of $T_{pulse} \lessapprox 5$ ps, provided that the optical Rabi frequency during the pulse is high (giving at least a pulse area of the order π).

We can estimate the optical Rabi frequencies using the electrical dipole value that we estimated from the EIT observation in Chapter 6 ($\Omega/2\pi = 2$ GHz for $P = 10$ W/cm^2). In this pulsed experiment the maximum available pump power was $P = 10$ mW, with a spot size $D_{spot} \approx 100$ μm, and 80 MHz repetition rate of pulses with $T_{pulse} \approx 5$ ps duration. This corresponds to an optical intensity of about $I \approx 3 \cdot 10^5$ W/cm^2, resulting in the integrated Rabi frequency $\Omega/2\pi = 350$ GHz, and

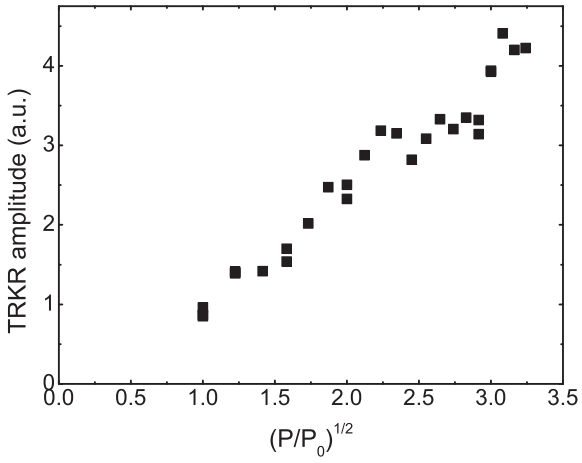

Figure 7.8: Experimentally measured amplitude of the TRKR oscillations as a function of the pump pulse power (P_0 = 1 mW). Measurements were done with a $\sigma+$ polarized pump and a V-polarized probe.

a pulse area of about π. It is, however, important to note that this estimate is quite rough, since the estimates for the spot size and the optical power loss on the windows of the cryostat have not been processed with good accuracy yet.

As was mentioned earlier, the ultra-fast preparation of the coherent dark state is possible because of the optical Rabi oscillations that take place in the system when a strong optical pulse is present. This should, according to the results of the calculation in Fig. 7.5, lead to a Kerr signal amplitude that is a strong function of the excitation pulse power. Figure 7.8 shows the amplitude of the TRKR signal measured as a function of the pump intensity for $\sigma+$ pump polarization. It demonstrates a steady monotonous increase in the Kerr signal amplitude. The fact that no oscillating-like behavior is observed does not allow us to estimate how close we are to the full π Rabi pulse. Attempts to see more then π Rabi pulses were limited by the available laser power.

7.6 Probing the coherent optical dark state

So far we have shown that by choosing the right polarization for the optical pump pulse, any coherent dark state for the D^0 spin ensemble can be prepared. This

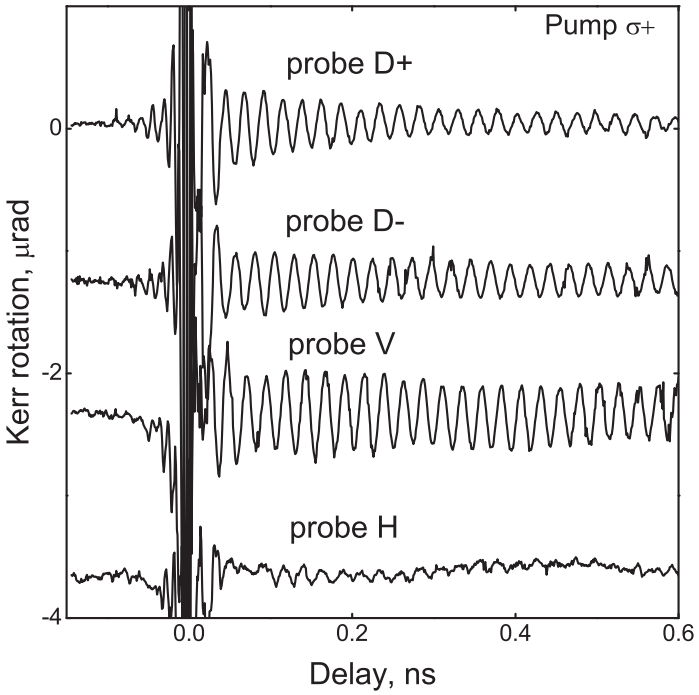

Figure 7.9: Dependence of the TRKR signal on the polarization of the probe. The pump pulse is chosen to be $\sigma+$ polarized.

happens only when the optical pulse can drive a Raman-like two-photon transition between the two electron spin levels. In the TRKR experiment that we presented till here, we have probed the dynamics of this dark state by measuring how the rotation of an initially V-polarized probe rotates upon reflection. For complete understanding of the interaction between D^0 systems and ultra-fast optical pulses it is of interest to also investigate the dependence on the initial polarization of the probe pulse.

For studying this, we have performed TRKR experiments where the pump pulse was chosen to be $\sigma+$ polarized, while polarization of the probe was chosen to be $D+$, $D-$, V or H. Results of this experiment are shown in Fig. 7.9. The most interesting observation is the fact that, in contrast to the other three polarizations, the H polarized probe leads to a Kerr signal that is much weaker than for the other

probe polarizations. Considering that the H polarization is the only polarization that couples only to one optical transition in the 4-four level system of Fig. 7.2, we conclude that the process of probing the spin dynamics is also a two-photon process.

A two-photon interaction between the probe pulse and the D^0 systems is indeed necessary if one wants to observe an oscillating Kerr signal that contains information about the spin state that precesses in external magnetic field. If one has a probe polarization that is sensitive to only one of the optical transitions, it would lead to probing either the population of the $|\uparrow\rangle$ or $|\downarrow\rangle$ state. This concerns eigenstates of the $\hat{S}_z$ operator, and these do not precess. It is the terms of the density matrix of the type $|\uparrow\rangle\langle\downarrow|$ that are time dependent, and probing this time dependence requires simultaneous probing of $|\uparrow\rangle$ and $|\downarrow\rangle$ states in order to capture the time dependence in a physically observable parameter, as for example the Kerr rotation of the probe polarization.

The other interesting observation from the experimental results in Fig. 7.9 is a relatively high Kerr amplitude for the V-polarized probe. The V probe polarization can indeed provide a necessary two-photon process via the optical transitions in the $B-B^*$ Λ-system in Fig. 7.1. In contrast to pumping, where the pure V polarization gives no D^0 spin coherence due to the shunting of the $B-B^*$ by the fast relaxation Γ_{fe}, probing with V polarization gives a clear Kerr signal. The reason is that rotation of the probe polarization can still occur, because the actual absorption and effective index of refraction is sensitive to the one-photon absorbtion processes for each leg of the Λ system, and these are still sensitive to a quantum interference between the two transitions.

7.7 Time resolved study of the coherence of electron spin bound to the neutral donor

We conclude this Chapter by presenting an experimental study which aimed at investigating how the spin dephasing time of D^0 spin ensembles depends on the power of the optical excitation. This experimental work was mainly driven by two factors. First, in the experiments with detuned optical pulses [12] that aimed at achieving deterministic spin rotation, the rotation angle was limited to $\pi/3$. It was assumed that larger rotation angles were not possible due to optical-pulse induced dephasing for the optical transitions at high powers. A second reason to perform the experiment is the fact that, up to our knowledge, there was no dedicated TRKR study yet of the dynamics of donor-bound electron spins. The lack of experimental work on the dynamics of the donor bound electrons is not due to the limited

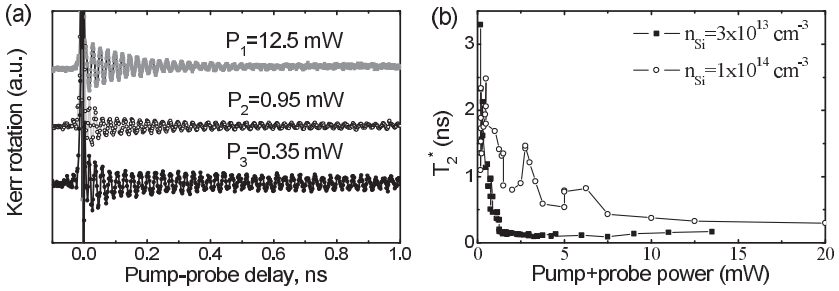

Figure 7.10: (a) TRKR signals for different pump powers P, taken on a sample with Si doping at $n_{Si} = 3 \times 10^{-13}$ cm^{-3}, and $\sigma+$ and V for the pump and probe polarization, respectively. (b) Spin dephasing time T_2^* versus pump power for samples with different concentration of donors.

interest in this system, but rather due to the fact, that the conventional Kerr rotation technique (with above the gap excitation) was mainly used for studies of electrons in the conduction band of semiconductors, where generation of electron spin coherence is a one-photon process [19]. Another technique, that uses polarization-resolved photo-luminescence in combination with the Hanle effect [28] cannot address the donor-bound electrons since the part of the signal that comes from the radiative relaxation of D^0X systems is not polarized because the electron spins in the D^0X system form a singlet.

We have performed the TRKR experiment on two samples with different concentration of dopants $n_{Si} = 3 \times 10^{13}$ cm^{-3} and $n_{Si} = 1 \times 10^{14}$ cm^{-3}. Experiments were performed using different excitations powers. Results are presented in Fig. 7.10. Panel (a) shows typical TRKR traces taken at three different pump power levels. It is interesting to note that the spin signal after excitation with the lowest pump level persists longer than for the cases with stronger pumping. In panel (b) we present the result of a systematic study of the dependence of the spin sephasing time T_2^* on the excitation power for the two samples. The T_2^* time for each power condition was found from making a mono-exponential fit on the Kerr signal [21, 22]. The behavior of the spin dephasing times T_2^* versus pump power shows a trend where T_2^* initially decreases exponentially with increasing of the optical power. At the high power levels the dephasing time stays nearly flat at the value $T_2^* \approx 0.2$ ns. The point where the change in the trend occurs is at the power level where the number of absorbed pump photons equals the number of D^0 donor sites.

The observed results are in good agreement with a model that predicts that the spin coherence time is limited by the correlation time of the local effective magnetic field felt by the electron spin. The D^0 system has an unpaired electron spin, and it will sense the non-zero hyperfine interaction at the donor site and therefore an Overhauser magnetic field. Slowly changing fluctuations of this Overhauser field cause an inhomogeneity for the Zeeman splitting of the D^0 systems, and this should result in a value $T_2^* \approx 2$ ns. This is the T_2^* value that is observed at the lowest pump powers. At higher pump powers, there are also a relatively high number of free excitons X in the system, up to a time that corresponds to the free-exciton recombination time (~300 ps [21]). These free excitons have at 4.2 K a capture and release dynamics with being bound at a D^0 site, temporarily forming a D^0X system. For the D^0X system, the two electrons form a singlet, resulting in no Overhauser field. Thus the capture and release of the free excitons creates an additional fluctuating magnetic field that is felt by the electron, and it can also cause a full electron spin-flip for the D^0 system in case the electron is exchanged.

The dynamics of the capture and release of the free excitons depends on the number of free excitons in the system. In the low pump-power regime the number of free excitations in the system does not strongly exceed the number of donors. This gives a low rate for capture-release events, and a high number of D^0 systems for which the spin dynamics is not disturbed by free excitons. In the case of higher optical pump powers, the number of optical excitations exceeds the number of donors and many free excitons are generated alongside the spin orientation of D^0 systems. Subsequent capture-release dynamics disturbs the D^0 spin dynamics. The effect of this on the spin dephasing time is captured by the following correlation [28]:

$$T_2^* \sim \langle \vec{S}_i(0)\, \vec{S}_i(t) \rangle \sim e^{-t/T_{cap}} \tag{7.5}$$

which, considering the free exciton capture rate must be in the sub-ns range which is supported by the strong luminescence from the donor bound excitons, results in a T_2^* value that is much shorter than the nuclear-field-limited value of $T_2^* \approx 2$ ns.

7.8 Conclusions

We have presented an experimental technique that allows optical generation of an arbitrary coherent state for D^0 spin ensembles on a timescale that is much shorter than the radiative lifetime. We have developed a theoretical model which relies on describing the $D^0 - D^0X$ system as a 4-level system, and which thereby consists of two optical Λ-systems. Within the framework of this model we were able to show that the mechanism of the ultra-fast coherent dark state preparation relies

on a two-photon stimulated Raman process. Despite being able to explain most of the results, we had to introduce an ultra-fast timescale for the relaxation between levels within the D^0X complex, in order to account for a difference in the system's response with respect to preparing and probing states with ultrafast optical pulses with well-defined polarizations. The reported theoretical model and experiments also do not address the question how the coherent dark states evolves when a second pump pulse is applied shortly after a first pump pulse (faster than T_2^*). such that pumping occurs on a system with an initial degree of coherence. More experimental and theoretical investigations in this direction will provide important test for better understanding of the physics that is reported in this Chapter.

Using the developed technique we were also able to make a systematic time-resolved study of the spin dynamics of an ensemble of oriented D^0 spins. Our findings demonstrate that by resonantly exciting the $D^0 - D^0X$ transitions with single optical pulses, a detectable and well-defined electron spin coherence can be generated, and its dynamics can be traced in time. We have also found that the spin coherence time is strongly dependent on the number of photons in the pump pulse, and in general decreases with increasing power.

References

[1] T. D. Ladd, F. Jelezko, R. Laflamme, Y. Nakamura, C. Monroe, and J. L. O'Brien, *Quantum computers.*, Nature **464**, 45 (2010), ISSN 1476-4687.

[2] E. Knill, R. Laflamme, and G. J. Milburn, *A scheme for efficient quantum computation with linear optics.*, Nature **409**, 46 (2001), ISSN 0028-0836.

[3] R. Blatt and D. Wineland, *Entangled states of trapped atomic ions.*, Nature **453**, 1008 (2008), ISSN 1476-4687.

[4] R. Hanson, J. R. Petta, S. Tarucha, and L. M. K. Vandersypen, *Spins in few-electron quantum dots*, Reviews of Modern Physics **79**, 1217 (2007), ISSN 0034-6861.

[5] D. Press, T. D. Ladd, B. Zhang, and Y. Yamamoto, *Complete quantum control of a single quantum dot spin using ultrafast optical pulses.*, Nature **456**, 218 (2008), ISSN 1476-4687.

[6] B. E. Kane, *Silicon-Based Nuclear Spin Quantum Computer*, Nature **393**, 133 (1997).

[7] M. V. G. Dutt, L. Childress, L. Jiang, E. Togan, J. Maze, F. Jelezko, A. S. Zibrov, P. R. Hemmer, and M. D. Lukin, *Quantum register based on individual electronic and nuclear spin qubits in diamond.*, Science (New York, N.Y.) **316**, 1312 (2007), ISSN 1095-9203.

[8] L. M. Vandersypen, M. Steffen, G. Breyta, C. S. Yannoni, M. H. Sherwood, and I. L. Chuang, *Experimental realization of Shor's quantum factoring algorithm using nuclear magnetic resonance.*, Nature **414**, 883 (2001), ISSN 0028-0836.

[9] S. Braunstein, C. Caves, R. Jozsa, N. Linden, S. Popescu, and R. Schack, *Separability of Very Noisy Mixed States and Implications for NMR Quantum Computing*, Physical Review Letters **83**, 1054 (1999), ISSN 0031-9007.

[10] D. G. Cory, A. F. Fahmy, and T. F. Havel, *Ensemble quantum computing by NMR spectroscopy.*, Proceedings of the National Academy of Sciences of the United States of America **94**, 1634 (1997), ISSN 0027-8424.

[11] J. H. Plantenberg, P. C. de Groot, C. J. P. M. Harmans, and J. E. Mooij, *Demonstration of controlled-NOT quantum gates on a pair of superconducting quantum bits.*, Nature **447**, 836 (2007), ISSN 1476-4687.

[12] K.-M. C. Fu, S. M. Clark, C. Santori, C. R. Stanley, M. C. Holland, and Y. Yamamoto, *Ultrafast control of donor-bound electron spins with single detuned optical pulses*, Nature Physics **4**, 780 (2008), ISSN 1745-2473.

[13] S. Clark, K.-M. Fu, T. Ladd, and Y. Yamamoto, *Quantum Computers Based on Electron Spins Controlled by Ultrafast Off-Resonant Single Optical Pulses*, Physical Review Letters **99**, 040501 (2007), ISSN 0031-9007.

[14] S. Clark, K.-M. Fu, Q. Zhang, T. Ladd, C. Stanley, and Y. Yamamoto, *Ultrafast Optical Spin Echo for Electron Spins in Semiconductors*, Physical Review Letters **102**, 247601 (2009), ISSN 0031-9007.

[15] X. Xu, Y. Wu, B. Sun, Q. Huang, J. Cheng, D. G. Steel, A. S. Bracker, D. Gammon, C. Emary, and L. J. Sham, *Fast Spin State Initialization in a Singly Charged InAs-GaAs Quantum Dot by Optical Cooling*, Physical Review Letters **99**, 97401 (2007), ISSN 0031-9007.

[16] M. Atatüre, J. Dreiser, A. Badolato, and A. Imamoglu, *Observation of Faraday rotation from a single confined spin*, Nature Physics **3**, 101 (2007), ISSN 1745-2473.

[17] J. Berezovsky, M. H. Mikkelsen, N. G. Stoltz, L. A. Coldren, and D. D. Awschalom, *Picosecond coherent optical manipulation of a single electron spin in a quantum dot.*, Science (New York, N.Y.) **320**, 349 (2008), ISSN 1095-9203.

[18] K.-M. Fu, C. Santori, C. Stanley, M. Holland, and Y. Yamamoto, *Coherent Population Trapping of Electron Spins in a High-Purity n-Type GaAs Semiconductor*, Physical Review Letters **95**, 187405 (2005), ISSN 0031-9007.

[19] J. Kikkawa and D. Awschalom, *Resonant Spin Amplification in n-Type GaAs*, Physical Review Letters **80**, 4313 (1998), ISSN 0031-9007.

[20] P. J. Rizo, A. Pugzlys, J. Liu, D. Reuter, A. D. Wieck, C. H. van der Wal, and P. H. M. van Loosdrecht, *Compact cryogenic Kerr microscope for time-resolved studies of electron spin transport in microstructures.*, The Review of scientific instruments **79**, 123904 (2008), ISSN 1089-7623.

[21] P. J. Rizo, A. Pugzlys, A. Slachter, S. Z. Denega, D. Reuter, A. D. Wieck, P. H. M. van Loosdrecht, and C. H. van der Wal, *Optical probing of spin dynamics of two-dimensional and bulk electrons in a GaAs/AlGaAs heterojunction system*, Accepted for publication in New J. Phys, arXiv:0910.1714 (2009).

[22] S. Z. Denega, T. Last, J. Liu, A. Slachter, P. J. Rizo, P. H. M. van Loosdrecht, B. J. van Wees, D. Reuter, A. D. Wieck, and C. H. van der Wal, *Suppressed spin dephasing for two-dimensional and bulk electrons in GaAs wires due to engineered cancellation of spin-orbit interaction terms*, Physical Review B **81**, 153302 (2010), ISSN 1098-0121.

[23] F. Meier and B. P. Zakharchenya, *Optical Orientation* (North Holland Physics Publishing, 1984).

[24] V. A. Karasyuk, D. G. S. Beckett, M. K. Nissen, A. Villemaire, T. W. Steiner, and M. L. W. Thewalt, *Fourier-transform magnetophotoluminescence spectroscopy of donor-bound excitons in GaAs*, Physical Review B **49**, 16381 (1994), ISSN 0163-1829.

[25] M. Sladkov, A. U. Chaubal, M. P. Bakker, A. R. Onur, D. Reuter, A. D. Wieck, and C. H. van der Wal, *Electromagnetically Induced Transparency with an Ensemble of Donor-Bound Electron Spins in a Semiconductor*, Phys. Rev. B **82**, 121308(R) (2010).

[26] K.-M. Fu, W. Yeo, S. Clark, C. Santori, C. Stanley, M. Holland, and Y. Yamamoto, *Millisecond spin-flip times of donor-bound electrons in GaAs*, Physical Review B **74**, 121304 (2006), ISSN 1098-0121.

[27] N. A. Gershenfeld and I. L. Chuang, *Bulk Spin-Resonance Quantum Computation*, Science **275**, 350 (1997), ISSN 00368075.

[28] R. Dzhioev, K. Kavokin, V. Korenev, M. Lazarev, B. Meltser, M. Stepanova, B. Zakharchenya, D. Gammon, and D. Katzer, *Low-temperature spin relaxation in n-type GaAs*, Physical Review B **66**, 245204 (2002), ISSN 0163-1829.

Summary

Donor-bound electron spins in GaAs are an interesting material system for experimental studies that investigate how quantum information can be stored on the quantum state of a collective spin excitation in an ensemble of spins. Such electron spin ensembles combine reasonably long spin coherence times with well-defined optical transitions, and can therefore be used as a medium for quantum optical studies and work that explores optical quantum-memory functions.

In this thesis we show that this idea is feasible, with experimental work that addresses the donor-bound electron spins with quantum optical techniques. These results provide a basis for future experiments that aim at the preparation and study of nonlocal quantum entanglement between collective spin excitations in two different ensembles, which can be achieved with quantum optical techniques.

In the reported experiments we used the fact that electron spin ensembles can be optically addressed with perpendicular-to-plane propagation of optical control and signal fields. The materials we were using were prepared by standard epitaxial growth techniques for GaAs/$Al_xGa_{1-x}As$ heterostructures. We analyzed that an optimal system is formed in n-GaAs where the level of Si doping is about 10^{14} cm^{-3}. One the one hand, this gives access to a medium with optical density as high as $OD = 1$. This is an important benchmark since the implementation of several quantum memory applications require OD values of 1 and higher. On the other hand, it still assures that each donor-bound electron behaves as an isolated system, without significant interaction with neighboring donor sites.

We can address electron spin degrees of freedom inside ensembles of three-level quantum systems with optical transitions that correspond to the excitation of donor-bound excitons (D^0X systems). These transitions start from the two Zeeman-split spin states of donor-bound electrons (D^0 systems). Selective control over these two transitions is possible with polarization selection rules that naturally occur in this system. In addition, these transitions have very narrow lines and this allows for using spectral selectivity as well.

In order to perform our optical experiments, we have designed and realized a fiber-based confocal microscope that can be used in cryostats with high magnetic field. It is a modular design that can be swapped between use in a helium bath cryostat (4.2 K) and a dilution refrigerator (base temperature well below 20 mK). Faraday rotations in optical materials were circumvented by using a polarization maintaining fiber and by having the light propagating in the sample volume in a direction orthogonal to the applied magnetic field. This also gives access to performing experiments in Voigt geometry, which has several advantages. With experiments on an ensemble of donor-bound electrons in GaAs we confirmed the ability to focus optical control fields with a small spot on any desired point of a sample. We also confirmed that pure linear polarizations can be delivered to the sample, and that this instrument can perform optical experiments at milliKelvin temperatures without excessive heating.

We performed spectroscopy measurements to confirm the optical selection rules and demonstrated the phenomenon Electromagnetically Induced Transparency (EIT). This provides evidence that this medium is suited for the quantum optical techniques that are needed for quantum memory functions and controlled preparation of nonlocal entanglement with ensembles of electron spins. We found that the electron spin dephasing time limits the quality of the EIT. It has the value $T_2^* \approx 2$ ns that results from hyperfine coupling to fluctuating nuclear spins. At the same time, we found that this hyperfine coupling provides a means for controlling the nuclear spin environment via Dynamical Nuclear Polarization (DNP). The EIT spectra form a sensitive probe for detecting how DNP changes the fluctuations and the average of nuclear spin polarization. However, direct optical driving of D^0 transitions yields much weaker DNP effects than that in electron spin resonance experiments with D^0 systems and related optical experiments on quantum dots, and a complete physical picture of DNP effects in our system is not available. Still, initial signatures of controlled DNP effects show that the electron spin-dephasing time can be prolonged. Our experimental approach is suited for exploring this further in conjunction with experiments that aim to implement various applications of EIT

The last chapter of this thesis presents an experiment that studies ultrafast optical preparation of arbitrary coherent dark states of donor-bound spin ensembles, on a timescale that is much shorter than the radiative lifetime of the system. We developed a theoretical model which relies on describing the D^0 systems as 4-level systems (two D^0 levels and two D^0X levels). Within the framework of this model we were able to show that the mechanism of the ultrafast preparation of the coherent dark states relies on a two-photon resonant Raman process. Despite being able to explain most of the results, we had to introduce an ultrafast relaxation time for intra-level relaxation in the D^0X complex, in order to account for the difference

in the system's susceptibility to the polarized probe and polarized pump. The existing model and experiments also do not address the question how the coherent dark states evolve when the system initially already had some degree of coherence. More experimental and theoretical investigations need to be done in this direction.

Using this ability to generate the coherent dark states in electron spin ensembles, we were able to make a first systematic study of the spin dynamics in an ensemble of electron spins bound to neutral donors in GaAs, with a time-resolved pump-probe Kerr experiment. Our findings demonstrate that by resonantly exciting the $D^0 - D^0X$ transitions with a single optical pulse, a detectable and well defined electron spin coherence can be generated and its dynamics can be traced in time. We have found that the spin coherence time is strongly dependent on the number of photons in the excitation pulse and in general decreases with increasing power.

The work described in this thesis is a first step towards a variety of quantum optical experiments that can be performed with electron spin ensembles. The observation of EIT allows to pursue an experiment that aims at achieving entanglement between the quantum states of an optical pulse and the state of an electron spin ensemble. Another highly interesting direction aims at extending the spin dephasing time via optical control of the nuclear environment of electron spins. The results in this thesis directly provide all the experimental techniques that are needed for such studies. Extending the spin dephasing time beyond the nuclear-spin-limited $T_2^* = 2$ ns value is of great interest, since it gives access to a much wider scope of experiments that explore quantum optical applications of low-doped n-GaAs.

Samenvatting

Donor-gebonden elektron-spins in GaAs is een interessant systeem voor het experimenteel bestuderen hoe quantum informatie kan worden opgeslagen in een quantum toestand bestaande uit de collectieve excitatie van een verzameling spins. Dergelijke verzamelingen elektron-spins combineren een redelijk lange coherentie tijd met goed gedefinieerde optische transities, en kunnen daardoor worden gebruikt als een medium voor het bestuderen van optische transities in quantum systemen en het onderzoeken van optisch quantum-geheugen.

In deze dissertatie laten we zien dat dit idee haalbaar is door middel van experimenteel werk dat de donor-gebonden elektron-spins aanslaat met behulp van quantum-optische technieken. Deze resultaten leveren een basis voor toekomstige experimenten welke gericht zijn op de preparatie en het bestuderen van niet-lokale quantum-entanglement tussen collectieve spin-excitaties van twee verschillende verzamelingen, wat gerealiseerd kan worden met quantum-optische technieken.

In de beschreven experimenten hebben we gebruikt dat elektron-spin verzamelingen optische geadresseerd kunnen worden met loodrecht-op-het-vlak propagerende optische controle en signaalvelden. De gebruikte materialen zijn gemaakt met behulp van standaard epitaxiale groeitechnieken (MBE) voor GaAs/$Al_xGa_{1-x}As$ heterostructuren. We analyseerden dat een optimaal systeem bestaat uit n-GaAs waarin de dichtheid van Si-donoren ongeveer 10^{14} cm^{-3} is. Dit resulteert in een medium met een optische dichtheid van $OD = 1$. Enerzijds is dit een belangrijke benchmark aangezien de implementatie van verscheidene quantum-geheugen applicaties OD waarden vereisen groter dan 1. Anderzijds zorgt dit er ook voor dat elk donor-gebonden electron zich gedraagt als een gesoleerd systeem, zonder significante interactie met zijn naastliggende donors.

We kunnen elektron-spin toestanden aanslaan binnen verzamelingen bestaande uit drie quantum-toestanden met optische transities die corresponderen tot het

exciteren van donor-gebonden excitons (D^0X systemen). Deze transities ontspringen uit twee Zeeman-gespleten spin toestanden van donor-gebonden electronen ($D0$ systemen). Selectieve controle over deze twee transities is mogelijk door middel van de polarisatie selectie-regels welke van nature aanwezig zijn in dit systeem. Deze transities zijn ook zeer nauw wat ons de noodzakelijk spectrale gevoeligheid verschaft.

Om onze optische experimenten uit te voeren hebben we een confocale microscoop met fibers ontworpen en gerealiseerd welke gebruikt kan worden in cryostaten waarin sterke magneetvelden aanwezig zijn. We hebben een modulair ontwerp gemaakt dat gebruikt kan worden in zowel een Helium-bad cryostaat (4.2 K) als een zgn. dilution-refrigerator (met een basistemperatuur kleiner dan 20 mK). Faraday rotaties in optische materialen zijn voorkomen door het gebruiken van een polarisatie-behoudende fiber en door het licht orthogonaal aan het magneetveld door het sample volume te sturen. Hierdoor kunnen wij ook experimenten in de Voigt-geometrie uitvoeren, wat verscheidene voordelen heeft. Door experimenten te doen op een verzameling donor-gebonden electronen in GaAs hebben we laten zien dat het mogelijk is een kleine spot op elk gewenst punt van het sample kunnen richten door het focussen van een optisch controle-veld. We hebben ook vastgesteld dat we licht met een pure lineaire polarisatie kunnen schijnen op een sample, en dat ons instrument optische experimenten kan uitvoeren op milliKelvin temperatuur zonder al te veel opwarming.

We hebben spectroscopische metingen uitgevoerd om de optische-selectie aan te tonen en hebben Electromagnetische genduceerde transparantie (EIT) gedemonstreerd. Dit laat zien dat dit medium geschikt is voor quantum-optische technieken welke nodig zijn voor quantum-geheugen functies en het prepareren van een niet-lokale entanglement met verzamelingen elektron-spins. We zagen dat de kwaliteit van de Electromagnetische genduceerde transparantie gelimiteerd is door de electron-spin dephasing-tijd. De electron-spin dephasing-tijd is $T_2^* \approx 2$ ns welke gelimiteerd is door hyperfijn-koppeling aan fluctuerende kern-spins. Tegelijkertijd levert deze hyperfijn-koppeling een manier om de kern-spin omgeving te controleren door middel van Dynamische Kern polarisatie (DNP). De EIT spectra zijn een gevoelige probe om te zien hoe DNP de fluctuaties in en het gemiddelde van de kern-spin polarisatie. Niettemin levert het optisch aanslaan van de $D0$ transitie veel zwakkere DNP effecten op dan in elektron-spin resonantie experimenten bestaande uit $D0$ systemen en gerelateerde optische experimenten aan quantum dots, en een volledig fysisch plaatje van de DNP effecten in ons systeem.

Het laatste hoofdstuk uit deze dissertatie beschrijft een experiment welke de optische preparatie met ultrakorte pulsen van een arbitraire coherente donkere-toestand van donor-gebonden elektronen onderzoekt, op een tijdschaal welke veel korter is dan de radiatieve levensduur van het systeem. We hebben een theo-

retisch model ontwikkelt welke de $D0$ systeem beschrijft als een 4-toestand systeem (twee $D0$ toestanden en twee $D0X$ toestanden). In dit model tonen we het mechanisme achter de preparatie van coherente donkere toestanden aan, welke bestaat uit een twee-foton resonant Raman proces. Ondanks dat dit model de resultaten verklaart, hebben we een ultrakorte relaxatietijd moeten introduceren voor intra-toestand relaxatie in het D^0X complex om het verschil in gevoeligheid van het systeem voor de gepolariseerde probe en pomp te verklaren. Het bestaande model en de experimenten adresseren niet de vraag hoe de coherente donkere-toestanden zich evolueren wanneer het systeem al een bepaalde hoeveelheid coherentie bezat. Meer experimentele en theoretisch onderzoek is nodig om deze vraag te beantwoorden.

Met behulp van deze mogelijkheid tot het creren van donkere-toestanden konden we een initile systematische studie doen naar de spin dynamica aan een verzameling elektron-spins gebonden aan neutrale donoren in GaAs door het gebruiken van een tijdsopgeloste pomp-probe Kerr experiment. Door het resonant exciteren van de $D0 - D^0X$ transities met een enkele optische puls was het mogelijk een gedefinieerde elektron-spin coherentie te genereren en de dynamica hiervan in de tijd te volgen. We zagen dat de spin coherentie tijd sterk afhankelijk is van de hoeveelheid fotonen in de excitatie puls en over het algemeen afneemt bij sterkere pulsen.

Het werk beschreven in deze dissertatie is een eerste stap naar verscheidene quantum-optische experimenten aan elektron-spin verzamelingen. De observatie van EIT stelt mensen in de gelegenheid om verdere experimenten uit te voeren welke zich richten op behalen van entanglement tussen de quantumtoestand van een optische puls en de toestand van het elektron-spin verzameling. Een hoogst interessante andere richting bestaat uit het vergroten van de spin-dephasing tijd door middel van optische controle van de kern-omgeving van de electronen-spins. De resultaten in deze dissertatie leveren de experimentele technieken welke benodigd zijn voor deze studies. Het groter maken van spin-dephasing tijd dan de kern-spin gelimiteerde $T_2^* = 2$ ns waarde is van groot belang, aangezien het direct toegang geeft tot veel groter scala aan experimenten dat de quantum-optische toepassingen onderzoekt van laaggedoteerde n-GaAs.

Acknowlegdements

Upon finishing this thesis, I would like to thank my promotor Prof. Caspar H. van der Wal for extensive guidance to help me to complete this work. I also would like to thank Prof. Bart van Wees and Prof. Tamalika Banejee for useful advices and comments on a daily basis throughout my PhD.

This work also would not be possible without the daily helps from Bernard Wolfs, Siemon Bakker and Johan Holstein. Bernard, I owe you the world for being ready for my helium and soldering and pumping needs even during the dutch public holidays. Siemon, you are the only person who knows all about the possessions of the group. Make sure that you stay with the new generations as well, otherwise they will never find all that exotic chemicals at the bottom of the orange cabinet (2-d floor, next to the entrance to the big measurements room. Keys are in the cabinet next door) or other surprises. Johan, you brought qualitative difference to the way we work in the clean room. The deal you've pulled out with a cryogenic pump for the "temescal" is priceless.

I would like to express my gratitude to my colleagues from the dil-fridge lab - Alok and Morten. You have not only made this thesis possible, but also given me the joy of working in a team, making my last year of PhD to be a pure joy.

Last but not least, really, I would like to thank all FND group members, Frank, Thomas, Alina, Paul, Arramel, Subir, Gaurav, Marcos, Sander, Joost, Fasil, Magda, Goraya and that guy Andreas I've never met, as well as all those poor students who had to work with me: Jorrit, Sander, Niels and others.

Anna, thanks for running around with arranging the defence date and being finally the secretary whom the entire group falls in love with.

As odd as it can happen after four years, there is no real need to thank on these pages to Erik, Pedro (from now on my lead will be only growing), Alex, Bram (how is it going with your writing?) and Csaba since we found ourselves working in the same company and I can thank them everyday. But anyway, thanks to you guys and let our borrels in Eindhoven to be as joyful as they were in Groningen.

In the end I would like to thank my very good friend Sergii and his wife Katya for all the professional and friendly support you've had for me. The thesis cover design by Katya is totally awesome.

Lan, can you check my English? I think it is ready.

Oh, and mum... and sister, of course. I also used to have a dog Tuzik.

Curriculum Vitae

Maksym SLADKOV

10-09-1982	Born in Uzhgorod, Ukraine.

Education

1996–1999	Polythechnical liceum, Uzhgorod
1999–2004	B.Sc. in physics and applied physics, Faculty of Radiophysics, Taras Shevchenko University of Kiev, Ukraine
2004–2006	M.Sc. Top master program in nanoscience, University of Groningen, The Netherlands
2006–2010	PhD research at the University of Groningen in the group of prof. dr. ir. B. J. van Wees and prof. dr. ir. C. H. van der Wal, under supervision of prof. C. H. van der Wal. Sublect: Coherent optical manipulation of electron spins ensembles in semiconductor.

List of Publications

8. *Ultrafast preparation and detection of arbitrary coherent dark states with donor-bound electrons in GaAs*
   S. Z. Denega, M. Sladkov, D. Reuter, A. D. Wieck, and C. H. van der Wal,
   in preparation.

7. *Polarization-preserving confocal microscope for optical experiments in a dilution refrigerator with high magnetic field*
   M. Sladkov, M. P. Bakker, A. U. Chaubal, D. Reuter, A. D. Wieck, and C. H. van der Wal,
   provisionally accepted for publication in Rev. Sci. Instr. (2010); arXiv:1010.1849.

6. *Electromagnetically Induced Transparency in low-doped n-GaAs*
   C. H. van der Wal, M. Sladkov, A. U. Chaubal, M. P. Bakker, A. R. Onur, D. Reuter, and A. D. Wieck,
   to appear in AIP Conference Proceedings (2010).

5. *Electromagnetically Induced Transparency with an Ensemble of Donor-Bound Electron Spins in a Semiconductor*
   Maksym Sladkov, A. U. Chaubal, M. P. Bakker, A. R. Onur, D. Reuter, A. D. Wieck, and C. H. van der Wal,
   Phys. Rev. B. **82**, 121308(R) (2010).

4. *Towards quantum optics and entanglement with electron spin ensembles in semiconductors*
   Caspar H. van der Wal and Maksym Sladkov,
   Solid State Sciences **11**, 935-941 (2009).

3. *Electrical detection of spin pumping due to the precessing magnetization of a single ferromagnet*
   M. V. Costache, M. Sladkov, S. M. Watts, C. H. van der Wal, and B. J. van Wees,
   Phys. Rev. Lett. **97**, 216603 (2006).

2. *Large cone angle magnetization precession of an individual nanopatterned ferromagnet with dc electrical detection*
   M. V. Costache, S. M. Watts, M. Sladkov, C. H. van der Wal, and B. J. van Wees,
   Appl. Phys. Lett. **89**, 232115 (2006).

1. *On-chip detection of ferromagnetic resonance of a single submicron Permalloy strip*
   M. V. Costache, M. Sladkov, C. H. van der Wal, and B. J. van Wees,
   Appl. Phys. Lett. **89**, 192506 (2006).